NUMERICAL SIMULATIONS of TWO - PHASE FLOWS USING TWO - FLUID APPROACH

İKİ FAZLI AKIŞLARIN İKİ AKIŞKAN YAKLAŞIMI İLE SAYISAL MODELLEMESİ

BUĞRA KILINÇ

Submitted to

HACETTEPE UNIVERSITY

THE INSTITUTE OF GRADUATE STUDIES

IN SCIENCE AND ENGINEERING

in partial fulfillment of the requirements for the degree of

MASTER OF SCIENCE

in

NUCLEAR ENGINEERING

2011

To the Institute for Graduate Studies in Science and Engineering,

This work has been approved by the Graduate Committee as partial fulfillment of the requirements for the degree of **MASTER OF SCIENCE** in the field of **NUCLEAR ENGINEERING**.

Head	:….. Assoc. Prof. Dr. Ayhan YILMAZER
Member (Advisor)	:……. Assoc. Prof. Dr. C. Niyazi SÖKMEN
Member	:….. Assoc. Prof. Dr. S. Sinan KESKİN
Member	:….. Assist. Prof. Dr. Şule ERGÜN
Member	:….. Assist. Prof. Dr. Cemil KOÇER

APPROVED

This thesis has been approved on .....//...../2011 by the Graduate Committee established by the Board of the Institute.

Prof.Dr. Adil DENİZLİ

HEAD OF THE INSTITUTE FOR GRADUATE

STUDIES IN SCIENCE AND ENGINEERING

NUMERICAL SIMULATIONS OF TWO-PHASE FLOWS USING TWO - FLUID APPROACH

Buğra Kılınç

ABSTRACT

This study is performed to gain an understanding of the capabilities of computational fluid dynamic codes in modeling of two phase flows and show their potential. It focuses on two-phase isothermal pipe flows in divergent and convergent channels. Relevant flow regime is “Bubbly Flow Regime” in which void fraction is changed between 5% and 20%.

Two - Fluid” approach of Euler - Euler multiphase model is chosen as a mathematical tool for numerical modeling of two-phase flow systems in the study.

First objectives of the study is to investigate the relationship between pressure drop and flow parameters like void fraction, mass flow rate and bubble diameter in a divergent/convergent pipe. Study also deals with the validation of two - fluid approach by comparing experimental profiles with the results of numerical calculations. Different types of boundary conditions, turbulence models, and bubble interaction models are investigated and compared in the study.

In the study it is concluded that two – fluid approach is an advance and powerful numerical tool in modeling of two phase flows and it can predict void fraction and pressure change in good level of accuracy. But the approach still needs to development.

Keywords: Two phase, two fluid approach, euler euler model, pipe flow, numerical modeling

Advisor: Assoc. Prof. Dr. C. Niyazi SÖKMEN, Hacettepe University, Department of Nuclear Engineering

İKİ FAZLI AKIŞLARIN İKİ AKIŞKAN YAKLAŞIMI İLE SAYISAL MODELLEMESİ

Buğra Kılınç

ÖZ

Bu çalışma hesaplamalı akışkan dinamiği yazılımlarının iki fazlı akışların modellenmesindeki kapasitelerini anlamak ve potansiyellerini göstermek adına yapılmıştır. Çalışma, izotermal koşullarda genişleyen ve daralan kanallarda iki fazlı boru içi akışlara odaklanmıştır. İlgilenilen akış rejimi, boşluk oranının yüzde 5 ila 20 arasında değiştiği "bubbly flow – kabarcıklı akış" rejimidir.

Çalışmada iki fazlı akışların sayısal modellemesi için kullanılan matematiksel araç olarak "Euler – Euler" modelinin "İki – Akışkan" yaklaşımı seçilmiştir.

Çalışmada öncelikle basınç ile boşluk oranı, akış debisi ve kabarcık çapı gibi akış parametreleri arasındaki ilişki genişleyen ve daralan borularda incelenmektedir. Çalışma ayrıca, deneysel verilerin sayısal hesaplama sonuçları ile karşılaştırılması yolu ile iki – akışkan yaklaşımının doğrulaması üzerinde de durmuştur. Çalışma boyunca farklı türbülans modelleri, farklı sınır şartları ve farklı kabarcık etkileşimi modelleri kullanılmış ve aralarında karşılaştırmalar yapılmıştır.

Çalışma sonunda iki akışkan yaklaşımının iki fazlı akışların sayısal modellemesinde güçlü ve ileri bir araç olduğu ve boşluk oranı, basınç değişimi gibi parametreleri iyi bir doğruluk payı ile tahmin edebildiği gözlemlenmiştir. Ancak yaklaşımın hala geliştirilmesine ihtiyaç vardır.

Anahtar Kelimeler: İki fazlı akış, iki akışkan yaklaşımı, boru içi akış, sayısal modelleme

Danışman: Doç. Dr. C. Niyazi SÖKMEN, Hacettepe Üniversitesi, Nükleer Enerji Mühendisliği Bölümü

ACKNOWLEDGEMENTS

I would like to express my sincere gratitude to my supervisor Assoc. Prof. Dr.Cemal Niyazi Sökmen for his guidance and patience during this study and my all education. I am also grateful to Assits. Prof. Dr. Şule Ergün for her support on revision works of this thesis.

I would also like to express my deepest gratitude to my parents.

TABLE of CONTENTS

Page

LIST OF FIGURES

LIST OF FIGURES (Cont'd)

Page

LIST OF FIGURES (Cont'd)

Page

LIST OF TABLES

Page

LIST OF SYMBOLS AND ABBREVIATIONS

A	Area
d_b	Bubble diameter
λ	Darcy friction factor
ρ	Density
D	Diameter
C_D	Drag coefficient
f	Drag function
μ	Dynamic viscosity
x	Flow quality
G, g	Gas
ν	Kinematic viscosity
L	Length
L, l	Liquid
$\dot{m}$	Mass flow rate
G_l	Mass flux
ρ_m	Mixture density
ϵ	Nominal roughness
τ_p	Particulate relaxation time
α_k	Phase density function
Re	Reynolds number
P	Pressure
f_{sp}	Single phase friction factor
S	Slip ratio
σ	Surface tension
f_{tp}	Two phase friction factor
U,v	Velocity
α	Void fraction
V	Volume
θ	Volumetric flow rate
$J_{l,g}$	Volumetric flux
CFD	Computational Fluid Dynamics

IAC	Interfacial area concentration
M-N	Martinelli – Nelson
VOF	Volume of fluid
VKI	Von Karman Institute for Fluid Dynamics
UDF	User Defined Function

1. INTRODUCTION

In industry, there are several applications having flows with two different fluid phases. These types of flows are called two-phase flows in fluid mechanics. These flows generally occur in a system containing gas and liquid phases. Some examples of such flows are often observed in mechanical, chemical and nuclear engineering fields. In this study, two phase flows in nuclear engineering field is the main interest.

Since the mechanic behavior of these flows depends on many parameters, it is difficult and complicated to find any analytical solution to model the two phase flow. Therefore, for the modeling, initial studies were experimental where limited ranges of flow parameters and simple geometries were studied. Especially, two-phase simple pipe flows have been investigated since the beginning of the nuclear industry for its safe operation. However, the two phase flow applications in nuclear industry are observed in more complex geometries and different flow conditions. Most common examples are pumps and safety valves which are important in terms of safety and efficient operation.

The present experimental studies are still in progress and they are not sufficiently diverse to cover these types of important geometries and flow conditions. A solution to these problems may be found in numerical approach. After development of the fast and efficient computers, numerical tools have been getting popular in research of two-phase flows. They are cheaper than experimental studies but they are still in progress.

This study deals with modeling of two-phase flows in complex geometries using numerical tools called computational fluid dynamic (CFD) codes. General aim of the study is assessing capability of these codes in modeling two phase flows in complex geometries and to validate the results of the modeling studies using experimental data. Present study has been started in “Von Karman Institute for Fluid Dynamics (VKI)” as research project for Diploma Course [1]. Some parts of this thesis include findings and results from that study. Building on these

findings, the study has been expanded using additional two-phase modeling options of the CFD and different boundary conditions. Experimental data used for comparison were obtained at VKI.

In literature, there are two main models which are being used for numerical modeling of two phase flows. These are “Euler-Lagrange” and “Euler-Euler” approaches. In this study, two – fluid (Euler-Euler) approach is chosen for the modeling.

1.1. Statement of the Problem

Several industrial equipments may have different flow areas along flow axis and geometry that differ from a simple pipe. The variation of the area may be a sudden expansion or contraction or it could be observed as progressive expansion or contraction. To model the two phase flows in these types of geometries, the experimental and numerical investigations are still needed.

In this study, a simple horizontal pipe which has a divergence/convergence section is analyzed by using numerical tools in isothermal conditions. Therefore any type of energy transfer between phases was ignored. For the modeling, two different pipe geometries are used.

The fluid is a mixture of water-liquid and air bubbles with different void fractions (mixing ratio). Main flow regime of the study is “bubbly flow” which has void fractions between 5% and 20%. Different bubble diameters are also used for the modeling in the study.

Simple sketch of the geometry is shown in Figures 1.1. It is a simple divergent pipe which has a progressive expansion.

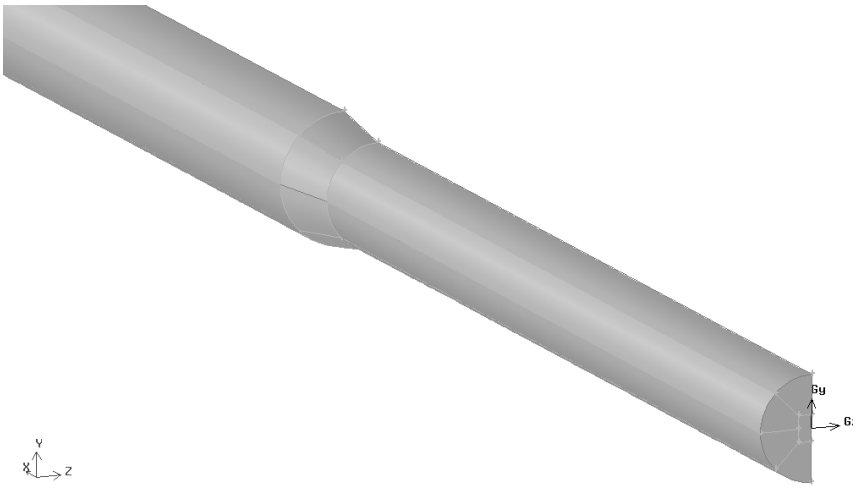

Figure 1.1. Simple sketch of the geometry

Figure 1.2 presents a simple application of the mentioned geometries using in the industry. It is an image of single stage pumps which is used in reactor and steam generator feed applications in the nuclear power plants.

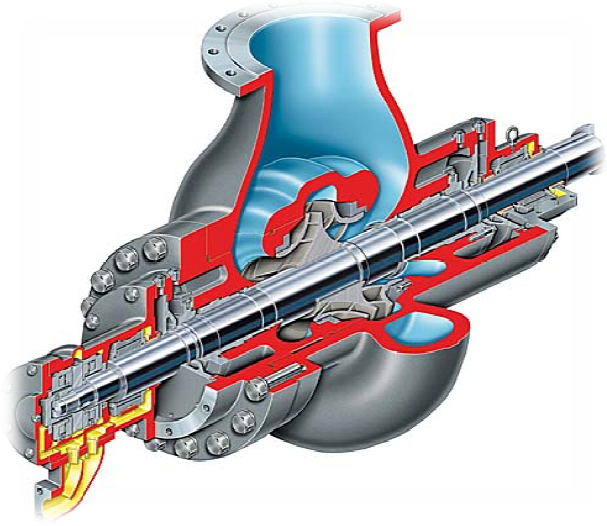

Figure 1.2. A sample application of the geometry in the industry [2]

1.2. Fundamental Physical and Mathematical Parameters of Two-Phase Flows

Two-phase flows show fluctuating character and their nature is generally described by the averaged quantities both in space and time. Therefore, mathematical operators that are used for averaging are defined [3; 4].

The averaging process for fundamental two phase flow parameters are described in below sections.

a) Phase Density Function

This function describes presence or absence of a phase at a certain time. If a phase (*k*) is present at a point $\vec{r}$, phase density function (α_k) can be defined as follows [3; 4]:

$$\alpha_k(\vec{r},t) = \begin{cases} 1 & if\ the\ point\ is\ occupied\ by\ phase\ k \\ 0 & if\ the\ point\ is\ not\ occupied\ by\ phase\ k \end{cases} \quad (1.1)$$

b) Space Averaging Operators and Quantities

In order to define the instantaneous distribution of two-phases, the phase density function can be averaged over a line, an area or a volume. A volume can be divided into two domains which are instantaneous volumes ($V_{k=g,l}$) where “g” and “l” represent gas and liquid respectively. Each domain of the volume is occupied by each one of the two-phases. For any parameter (c), instantaneous volume averaging can be integrated over different volumes. The averaging over the entire volume (V) is defined as follows:

$$\langle c \rangle = \frac{1}{V} \iiint_V c dV \quad (1.2)$$

The averaging over the volume occupied by the phase *k* is defined as follows:

$$\langle c \rangle_k = \frac{1}{V_k} \iiint_{V_k} c dV \tag{1.3}$$

The averaging could be presented over the entire volume by using phase density function as follows:

$$\langle c \rangle_k = \frac{1}{V_k} \iiint_{V} c \alpha_k dV \tag{1.4}$$

If describing the flow conditions at the boundary of a control volume is required, the space and time averaged values of the property must be defined on the surface area (A) surrounding the control volume. This description can be formulated as follows:

$$\{c\} = \frac{1}{A} \iint_{A} c dA \tag{1.5}$$

Similar to the volumetric averaging, phase density function can be used in the Eq. 1.5 as follows:

$$\{c\}_k = \frac{1}{A_k} \iint_{A_k} c dA = \frac{1}{A_k} \iint_{A} c \alpha_k dA \tag{1.6}$$

In two-phase flow calculations, there are important quantities which determine and represent conditions of the flow. Many of them are defined by volume or area averaging, are introduced in the following section [3; 4].

Volume Fraction

This parameter is defined by the volume ratio of phase k and total volume. Flow regimes observed in the two-phase flows depend on this parameter. It is the most basic and most widely used two-phase flow parameter. The formulation of the volume fraction is as follows:

$$\langle \alpha_k \rangle = \frac{1}{V} \iiint_V \alpha_k dV = \frac{V_k}{V} = \frac{V_k}{\sum_{k=1}^{n} V_k} \quad (1.7)$$

Volume fraction of the gas phase is generally called the "*void fraction"* and it is represented simply by sign letter " α " as follows:

$$\langle \alpha \rangle = \langle \alpha_g \rangle \quad (1.8)$$

The instantaneous fraction of an area occupied by phase *k* is defined similarly as follows [3; 4]:

$$\{\alpha_k\} = \frac{1}{A} \iint_A \alpha_k dA = \frac{A_k}{A} = \frac{A_k}{\sum_{k=1}^{n} A_k} \quad (1.9)$$

Flow Quality

Another important two phase flow parameter is mass flow rate fraction of gas phase in the total flow rate. It is defined as follows [3; 4]:

$$x = \frac{\dot{m}_g}{\dot{m}_g + \dot{m}_l} \quad (1.10)$$

Mixture Density

In several two-phase flow models, the mixture density is used and it is calculated as below [3; 4]:

$$\langle \rho \rangle = \frac{m_g + m_l}{V} \quad (1.11)$$

Mass Flow Rate

Mass flow rate is basically defined as the mass quantity which passes through a cross-section per unit time and it is formulized for a mixture as follows:

$$\dot{m} = \rho \, \mathrm{v} \, A \quad (1.12)$$

v is the velocity. For any phase *k* in a flow through the z-direction, mass flow rate is formulized as [3; 4]:

$$\dot{m}_k = \iiint_A \rho \mathrm{v}_{kz} \alpha_k \vec{n}\, dA \tag{1.13}$$

Mass Flux

Mass flux is defined as the phase (mass) flow rate per unit cross-sectional area. As an example, it is expressed for the liquid phase as follows [3; 4]:

$$G_l = \frac{\dot{m}_l}{A} = \frac{\dot{m}(1-x)}{A} \tag{1.14}$$

Volumetric Flow Rate

It is the volume of flow which passes through the given surface per unit time. It is defined for a flow through the z-direction as follows [3; 4]:

$$\theta = \mathrm{v}_z A \tag{1.15}$$

Volumetric Flux

It is defined as the rate of volume flow across a unit area. Its formulation is presented as follows [3; 4]:

$$J_{l,g} = \frac{\theta_{l,g}}{A} \tag{1.15}$$

Slip ratio

It represents the velocity ratio of the phases. It is defined as in Eqn. 1.16. In homogeneous two phase flows, phases are in mechanical equilibrium. Therefore this ratio is equal to 1 [3; 4].

$$S = \frac{v_g}{v_l} \tag{1.16}$$

This ratio is not meaningful in three – dimensional flows. Generally it is an area averaged one dimensional parameter[4].

c) Time Averaging Operators

Since it is very difficult to obtain the instantaneous flow properties over a defined volume in two-phase flows, time averaging is also used very often. The averaging can be defined as follows:

$$\tilde{c} = \frac{1}{\Delta t^*} \int_{t-\Delta t^*/2}^{t+\Delta t^*/2} c dt \tag{1.17}$$

For the observations, Δt^* must be chosen large enough to resolve flow conditions and short enough that flow conditions do not changed significantly. In this case a time average *Δt* value of c could be defined as follows [3; 4]:

$$\bar{c} = \frac{1}{\Delta t} \int_{t-\Delta t/2}^{t+\Delta t/2} c dt \tag{1.18}$$

1.3 Flow Regimes in Horizontal Pipes

The number of two-phase flow regimes observed in horizontal flows is more than the one observed in vertical flows. Reason of this increased number of regimes is the gravity and it plays an important role in the flow mechanics. General affect of the gravity is to separate the phases along the flow direction and to create horizontal stratification. In literature, horizontal two-phase flow patterns are established experimentally, by visualization methods in transparent channels collecting a significant number of data. There are many studies that show flow regime on a map relating the flow parameters with the developed flow pattern. However, attention must be given to a point that each map was created on different experimental setup. Thus each map is unique and they

cannot be used for all cases of similar flows accurately. Therefore, there is not any solid recommendation concerning the choice of the appropriate flow map for different cases. There is not any mechanistic model for the flow regime maps which have been proved entirely accurate. Different maps use different coordinate systems and there is not any consensus about which one is the most suitable system.

The flow patterns described here are related with only the case of a simple horizontal pipe flow without any restrictions. If there is a change in area as modeled in this study, new experiments should be conducted in order to observe the flow patterns and define important parameters of the flow. The flow patterns observed for the simple horizontal channels are introduced in this section.

For the horizontal pipes that are simulated in this study, Alves has proposed the classification of flow regimes [5], as presented in Figure 1.3. There are other versions of this kind of classification and one such classification could be found in [6].

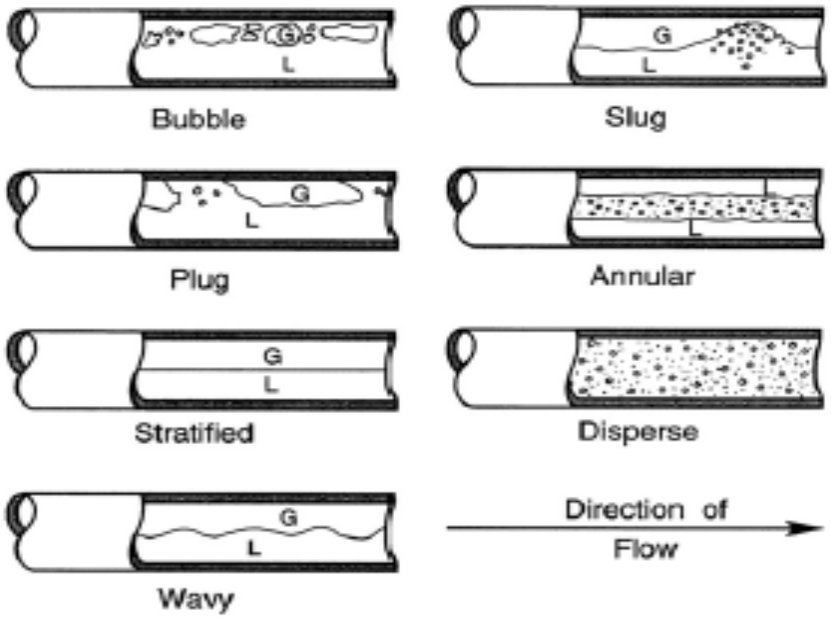

Figure 1.3. Flow patterns in a horizontal pipe. (Alves, 1954) [5]

In the following sections, above mentioned regimes are described.

Bubbly Flow (Bubble Flow)

In this flow regime, bubbles are dispersed in the liquid and they move to the upper part of the pipe. [4; 5; and 6] This is because of the buoyancy effect which is the difference in densities of the liquid and gas phases. Dispersion of the bubbles throughout the tube cross-section depends on the shear force and the liquid velocity. This regime could be observed especially at high flow rates. In this study, the flow regime that is modeled is the bubbly flow.

Plug Flow

Plug flow is observed as the flow rate of gas phase increases. Bubbles that are in shapes of bullets are called gas plugs. This regime consists of gas plugs and coalesced bubbles [4; 5; 6].

Coalescence of bubbles is an important physical phenomenon in two-phase flow dynamics. In this study, for some of the analysis, it is examined in a limited range [4; 5; and 6].

Stratified Flow

In this flow regime, low liquid and gas velocities cause complete separation of the two-phases. The difference in phase density leads gas phase to the upper part of the pipe. Interface is smooth and both phases are continuous [4; 5; 6].

Wavy Flow

In wavy flow regime, for a constant flow rate of liquid, increase in the gas flow rate create waves and these waves propagate along the interface between two phases [4; 5; 6].

Slug Flow

If the gas flow rate in the wavy regime of flow increases, waves could reach to the top wall of the pipe and create slug flow regime. This flow regime is similar to the plug flow regime, however gas bubbles are larger. The gas phase which is moving faster picks up the periodic roll waves and forms slugs that pass

through the pipe at a much greater velocity than the average liquid velocity. Slug and plug flow can be considered as intermittent regimes [4; 5; and 6].

Annular Flow

If liquid flow rate is low enough, then annular regime is observed in the pipe. Liquid forms a thin film along the wall of the pipe. At the same time, gas flows as a core with higher velocity. Because of the gravity, the liquid flow rate is higher at the bottom of the pipe than the one at the top of the pipe. The gas core contains dispersed liquid droplets [4; 5; 6].

Dispersed Flow

At very high gas flow rates liquid droplets are dispersed in the gas phase and the dispersed flow regime is formed in the pipe [4;5; 6].

1.4 Flow Maps

As mentioned earlier, there are many studies that show flow regimes on a map using different properties of the flow, and each map is unique and they cannot be used for all cases of similar flows with utmost accuracy. In this section, Baker's diagram [7] which is the most common flow regime map for the horizontal co-current flows is presented Figure 1.4 shows Baker's flow map.

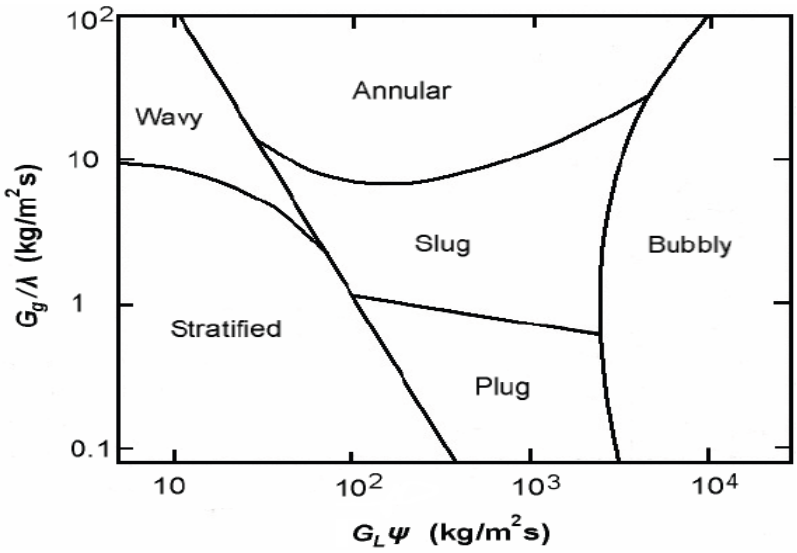

Figure 1.4. Horizontal flow map of Baker (1954) [7]

This map was prepared for the mixture of air and water. Axis of the map presents the superficial mass velocities of gas and liquid (or mass fluxes of the phases). As mentioned in section 1.2, these parameters are defined as follows:

$$G_l = \frac{\dot{m}_l}{A} \quad \text{and} \quad G_g = \frac{\dot{m}_g}{A} \tag{1.19}$$

The generation of the flow regime map is also depends on other parameters which are ψ and λ. These parameters depend on the fluid properties and they are defined by:

$$\lambda \cong \left(\frac{\rho_G}{\rho_{air}} \frac{\rho_L}{\rho_{water}}\right)^{1/2} \tag{1.20}$$

$$\psi \cong \frac{\sigma_{water}}{\sigma} \left[\frac{\mu_L}{\mu_{water}} \left(\frac{\rho_{water}}{\rho_L}\right)^2\right]^{(1/3)} \tag{1.21}$$

In the notation, subscripts μ, σ, G and L refer to dynamic viscosity, surface tension, gas and liquid respectively. To generate the map, the physical properties of air and water at 1 bar pressure and 20° C temperature were used. Thus, λ = 1 and ψ = 1 for air and water mixture for the reference conditions of this study.

1.5 Pressure Drop in Pipes

Pressure drop is a phenomenon which depends on many flow parameters and conditions. The main cause of the pressure drop in a pipe is friction but there are two other different contributors to the process. In most basic and general case, the total pressure drop in pipes is given by:

$$\frac{dP}{dz} = \left(\frac{dP}{dz}\right)_g^1 + \left(\frac{dP}{dz}\right)_a^2 + \left(\frac{dP}{dz}\right)_f^3 \tag{1.22}$$

In this equation, there are three different terms which compose the total pressure drop. These are (1) gravity term, (2) acceleration term and (3) frictional term. Gravity term indicates the effect of the gravity on the pressure which is caused by an inclination on the pipe. For a horizontal pipe, it is equal to zero. Second term comes from the acceleration of the fluid and it indicates the dynamic pressure change. Last term is caused by friction between fluids and walls of the duct [1, 3].

1.5.1 Single Phase Pressure Drop

As indicated before, contribution of the gravity and acceleration terms to the pressure drop could be neglected for a horizontal pipe which has high L/D ratio. Thus, the only term taken into account for this study is the friction term. In single phase laminar and turbulent flows, the friction term of the pressure drop is given as follows [8]:

$$\Delta P = \lambda \frac{L}{D} \rho \frac{U^2}{2} \tag{1.23}$$

In the Eqn. 1.23 "λ" is a non dimensional parameter which is called *friction factor* or the *Darcy friction factor*. *L* and *D* are the length and the inner diameter of the pipe respectively, ρ is the density of the fluid and *U* the average flow velocity in the flow cross section. *U* can be determined using the definition of the flow rate (*Q*) through a constant cross-section (*A*):

$$U = \frac{Q}{A} \tag{1.24}$$

Average velocity can be calculated by using Eqn. 1.24 since flow rate can be measured and the cross-section area is known. The only unknown parameter is the Darcy friction factor and it depends on the flow regime and the roughness of the pipe. The dependence of Darcy factor on flow regime is represented by using Reynolds number (Re):

$$Re = \frac{UD}{\nu} \tag{1.25}$$

where ν is the kinematic viscosity of the fluid. In literature, single phase flows are classified by using this dimensionless number as follows:

$for\ Re < 2300 \rightarrow$ Flow is ***"Laminar"***

$for\ 4000 < Re < 10^5 \rightarrow$ Flow is ***"Turbulent"***

For laminar flows, Darcy friction factor is:

$$\lambda = \frac{64}{Re} \tag{1.26}$$

For turbulent flows, there are two different approaches to present Darcy friction factor in literature. Among them, most widely used correlations are presented below [8]:

For $30000 < \mathrm{Re} < 10^6 \rightarrow$ McAdams relation

$$\lambda = \frac{0.184}{Re^{0.2}} \tag{1.27}$$

For $\mathrm{Re} < 30000 \rightarrow$ Blasius relation

$$\lambda = \frac{0.316}{Re^{0.25}} \tag{1.28}$$

without the roughness. On the other hand Colebrook – White suggested that [8]:

$$Colebrook - White: \ \frac{1}{\sqrt{\lambda}} = \ -2\log\left(\frac{2.51}{Re\sqrt{\lambda}} + \frac{\epsilon/D}{3.715}\right) \qquad (1.29)$$

where ϵ is the nominal roughness of the pipe or duct. This formulation depends on two different variables (Reynolds number and roughness). It is an implicit formulation and cannot be solved explicitly for λ.

In order to determine the friction factor, the chart derived by Moody [9] can also be used. The map represents the friction factor in terms of two non-dimensional parameters (Re and relative roughness) as presented in Figure 1.5. In this figure, friction factors for laminar and turbulent flows are presented.

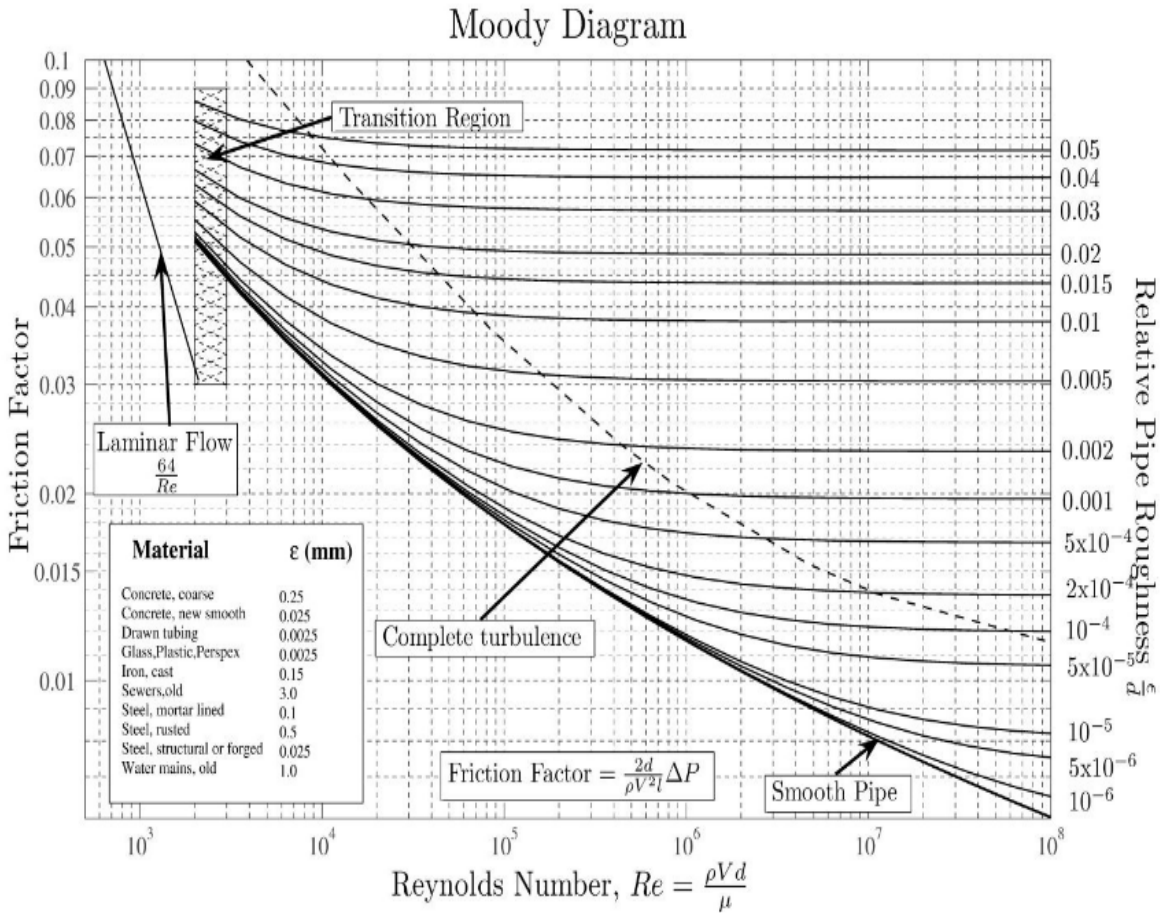

Figure 1.5. Moody diagram [9]

1.5.2 Two-Phase Pressure Drop

Two-phase pressure drop is an important design parameter for many applications of the nuclear, chemical and mechanical engineering fields. This topic has been investigated for many years, especially in the nuclear industry. Because of its non-linear momentum characteristics at the phase interfaces, calculation of pressure drop for two phase flows is more difficult than the single phase calculations. Determination of the pressure drop in two-phase flow systems is a problem that can hardly be solved on a theoretical basis. The only practical solution has been the application of some correlations based on the experimental data.

In this section of the introduction, the description of the gravity and the acceleration terms of the pressure drop in Eqn. 1.22 are omitted. Therefore, the pressure drop due only to friction in a horizontal pipe is discussed in this section.

The two-phase frictional pressure drop can be formulated as similar to single phase frictional pressure drop as follows [4]:

$$\left(\frac{dP}{dz}\right)_f = f_{TP}\,\frac{{G_m}^2}{2\rho_m\,D_e} \tag{1.30}$$

In this formula, ρ_m and D_e are mixture density and the hydraulic diameter respectively. They are defined as follow [4]:

$$\rho_m = \rho_l\,(1-\alpha) + \rho_g\,\alpha \tag{1.31}$$

$$D_e = \frac{4A}{P_w} \tag{1.32}$$

In Eqn. 1.32, P_w is wetted perimeter and *A* is the flow area of the pipe channel.

Experiments have indicated that for any given mass flow rate in any channel geometry, two phase frictional pressure drop is higher than the frictional pressure drop for the single-phase liquid having the same total mass flow rate. Therefore two phase frictional pressure drop is generally related with single phase frictional pressure drop and a correction multiplier as follows:

$$\left(\frac{dP_f}{dz}\right)_{tp} = \left(\frac{dP_f}{dz}\right)_{sp} * \emptyset_{lo}^2 \quad (1.33)$$

Where $\emptyset_{lo}^2$ is the above mentioned correction factor. In literature, different approaches suggest different assumptions for the multiplier. In a chronological order, there were two main models, namely the homogeneous and the separated flow assumptions.

Homogeneous Model

A simple method of estimating the two-phase frictional pressure drop is to use the friction factor of a single phase flow at the same mass flux. Since mechanic equilibrium is assumed, an average two-phase flow mixture density is used in calculating the pressure drop [4]:

$$\left(\frac{dP}{dz}\right)_f = f_{sp} \frac{G^2}{2\rho_m D_e} \quad (1.34)$$

in which f_{sp} is the ordinary single-phase flow friction factor for liquid flow.

$$\frac{1}{\rho_m} = \frac{x}{\rho_g} + \frac{1-x}{\rho_l} \quad (1.35)$$

Eqn. 1.35 is a sort of defining an average specific volume that is calculated with the assumption of mechanical equilibrium in between the phases (Slip ratio, S=1). In most cases the average specific volume calculated according to Eqn. 1.35 is larger than the actual specific volume that will depend on the true void

fraction with S > 1. Hence a part of the error introduced by using a single-phase friction factor will be compensated for by using a somewhat higher value of the specific volume [3].

Separated Flow Model

The mechanical equilibrium as in homogeneous model is not preserved in this approach. Separated flow model is based on introducing a two-phase friction factor. Several investigators have suggested correlations to calculate the two-phase friction multipliers to be used in Eqn. 1.33.

Among them, the study of Martinelli and Nelson (M-N) is the most widely preferred correlation in the literature.

Martinelli-Nelson (M-N) Correlations

Martinelli and Nelson suggested (1948) an approach and empirical correlation for two-phase frictional pressure drop. Their correlation is by far the most widely used one in modeling two phase flows. The only shortcoming of this correlation is that it does not include the effect of mass velocity that has been observed experimentally. This correlation was based on the work of Lockhart and Martinelli [4]. In the M-N approach, the single phase frictional pressure drop is calculated for the given geometry and the total mass flow rate and then calculated single phase flow pressure drop is multiplied with a two-phase correction factor. This factor depends on steam quality and pressure. Martinelli and Nelson employed extensive experimental data to correlate $\emptyset_{lo}^2$ in terms of the following (for turbulent flows of vapor and liquid):

$$X_{tt} = \left(\frac{\mu_l}{\mu_v}\right)^{0.1} * \left(\frac{\rho_v}{\rho_l}\right)^{0.5} * \left(\frac{1-x}{x}\right)^{0.9} \quad (1.36)$$

This is known as the Lockhart - Martinelli parameter, and for any single substance is a function of pressure and steam quality. The $\emptyset_{lo}^2$ can be plotted directly as a function of "*X* "for different pressures.

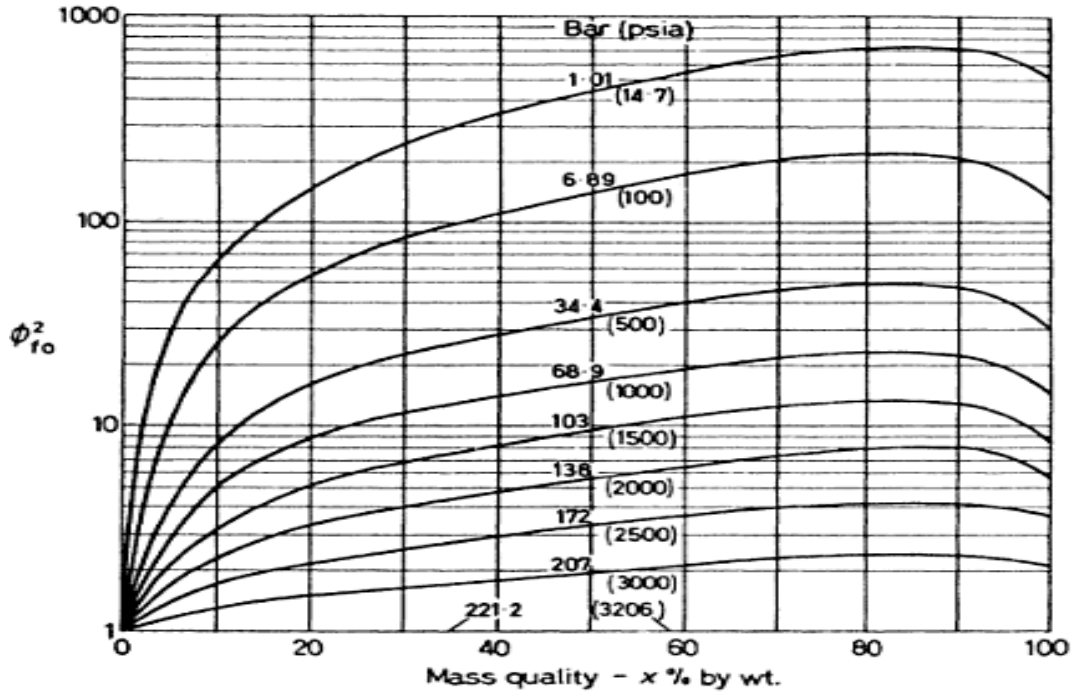

Figure 1.6. Martinelli - Nelson two - phase multiplier for steam-water mixture [4]

1.5. 3 Pressure Drop for Contractions or Expansions

The geometry modeled in this study is a pipe which has area changes along the flow direction. Correlations developed to represent the pressure drop in this type of geometries with contractions and expansions were proposed by Hewitt and Hall- Taylor [3] for two phase flows. The correlations presented simple corrections to the single-phase flow models developed for sudden area changes.

With subscripts 1 and 2 referring to inlet and outlet respectively, for homogeneous flow, the pressure loss is simply given by the Eqns. 1.37 and 1.38. Static pressure change in sudden contraction

$$\Delta P = \frac{G_2^2}{2\rho_L}\left[\left(\frac{1}{C_c} - 1\right)^2 + 1 - \frac{1}{s^2}\right]\left[1 + x\left(\frac{\rho_L}{\rho_G} - 1\right)\right] \qquad (1.37)$$

The contraction coefficient Cc is defined as the area in the vena contracta and the area in the mid-plane of the blockage ratio and s the ratio between inlet and outlet cross-section. Static pressure change in sudden expansion

$$\Delta P = -\frac{G_1^2}{2\rho_L}(1-s)^2\left[1 + x\left(\frac{\rho_L}{\rho_G} - 1\right)\right] \quad (1.38)$$

Following sections consist of the description of the specific literature and procedures of two-fluid modeling approach and results. Chapter 2 introduces numerical modeling of two phase flows. Chapter 3 deals the of numerical modeling which this study is based on. Grid generation, establishment of numerical model by using a computational fluid dynamics (CFD) software are discussed. Chapter 4 shows the results of simulations. Finally, general discussion about the study and conclusions are presented in Chapter 5.

2. NUMERICAL MODELING OF TWO-PHASE FLOWS

General View

Numerical modeling in the fluid dynamics is placed between experimental and theoretical approach. Section of the fluid mechanics which is responsible for the numerical modeling is called computational fluid dynamics (CFD). Since 1950s, CFD tools have been developed with faster and efficient computers.

In background, these tools solve partial differential equations which describe conservation of mass, momentum and energy in specific points of domain. Finite difference method (FDM) and finite volume method (FVM) are basic methods in solution of mentioned equations. In this study, FLUENT is chosen as commercial software. FLUENT is a numerical tool which uses FVM for the solution. It is assessed as the most capable commercial CFD package in numerical modeling of two phase flows currently.

In literature, there are two main methods for numerical modeling of two phase flows. These are “Euler – Lagrange” approach and “Euler – Euler” approach. Following sections describe the methods. Moreover, their advantages and disadvantages depending on flow parameters are discussed below.

2.1 Euler – Lagrange Approach

Euler – Lagrange approach solves the Navier - Stokes equations for continuous phase independent of the discrete phase and tracks the dispersed particles through the calculated flow field. Trajectories of the discrete phase are computed individually at specified intervals for the continuous phase calculation. Exchange of momentum, mass, and energy between the continuous and dispersed phase can be taken into account. Assumption based on the approach is that the dispersed second phase has low volume fraction. When the number of particles is high, the approach will be expensive in terms of computational time. The volume fraction generally should be lower than 10 – 12 %. Euler-

Lagrange approach is also not efficient for the case of big bubbles. It is suitable for the modeling of spray dryers, coal and liquid fuel combustion. Fluidized beds and liquid-liquid mixtures are in this class of two-phase flow systems.

2.2 Euler – Euler Approach

Euler-Euler approach takes phases into account indivually. In mathematical point of view it assumes that phases are interpenetrating continua. Volume of a phase cannot be occupied by the other phases naturally. From this phenomena FLUENT defines a concept for phasic volume fraction in this model. In this concept, the volume fractions of the phases are assumed to be continuous functions of space and time and their sum is equal to one. A set of conservation equations is derived for each phase. These equations are closed by using constitutive relations that are obtained from empirical information.

Approach has superior to Euler-Lagrange in where high void fractions and high particle concentration.

FLUENT has both of these approaches. It also divided the Euler-Euler approach into three categories. These are discussed in the following section briefly [10].

2.2.1 The VOF Model

The VOF model is based on the surface-tracking. It tracks the interface between two or more immiscible fluids. A single set of momentum equations is shared by the fluids, and the volume fraction of each of the fluids is tracked in each computational cell throughout the domain. VOF model is generally used in modeling of stratified flows, free-surface flows, large bubbles in a liquid, the motion of liquid after a dam break or the prediction of jet breakup (surface tension).Another example of its applications is the steady or transient tracking of any liquid-gas interface.[10]

2.2.2 The Mixture Model

The mixture model is designed for two or more phases (fluid or particulate). The mixture model solves the momentum equation for mixture and prescribes relative velocities to describe the dispersed phases. This model is generally used in modeling of particle-laden flows with low concentrations, bubbly flows, sedimentation, and cyclone separators. To model homogeneous multiphase flows, the mixture model is used without relative velocities of the dispersed phases.[10]

2.2.3 The Two – Fluid Model (Eulerian Model)

The two-fluid model seems as the most advance numerical model of the multiphase models in the literature. It is an effective model in terms of accuracy. It is more convenient than the other models in case of flows in where there is high concentration of particles or where the void fraction of the discrete phase is high enough to dominate flow. The model uses two sets of balance equations separately for each phase in conjunction with a set of empirical relationships for the interfacial mass, momentum transport and wall-to-fluid heat transport. Therefore in this approach, there are several parameters which must be satisfied. These are mainly concern about interfacial momentum and mass interactions between two-phases (because of the slip velocity and etc.) and turbulence parameters.

As summarized in [11], the model has been investigated by several authors and its development is connected with the studies of Ishii (1975), Ishii-Mishina (1984), Bouré (1975), Drew-Lahey (1979) [12], Lahey-Drew (2001) [13], Delhaye - Achard (1976). Applications of the Eulerian model include bubble columns, risers, particle suspension, and fluidized beds.

In this study, this multiphase model is used to obtain more realistic results using a commercial CFD code. FLUENT is selected as the most proper code for this study [10].

Following sections include the description of conservation equations which must be satisfied when two-fluid model is used. General terminology and definitions are quoted from “Theoretical Guide of Fluent” [10].

2.2.3.1 Conservation Equations of the Two-Fluid Model

As described in the previous section, each phase has a set of balance equations separately in two – fluid approach. FLUENT solves momentum and continuity equations for each phase and the solution is based on single pressure assumption. All phases have same pressure at the computation nodes. Conservation of mass and momentum are described below.

Conservation of Mass

As an example for our case, the continuity equation for liquid phase is:

$$\frac{\partial(\alpha_l \rho_l)}{\partial t} + \nabla.(\alpha_l \rho_l \overrightarrow{u_l}) = \dot{m}_{gl} - \dot{m}_{lg} + S_l \qquad (2.1)$$

Where $\overrightarrow{u_l}$ is the velocity of liquid phase and $\dot{m}_{gl}$ characterizes the mass transfer from the gas phase to liquid phase, and $\dot{m}_{lg}$ characterizes the mass transfer from liquid phase to gas phase, and S_l is the source term for the mass. If there is this source term in the model, similar term appears in the momentum equation. In case of isothermal conditions like the ones modeled in this study, there is not a mass transfer between phases and there is not any source term as well. Thus right side of the Eqn. 2.1 is equal to zero.

Conservation of Momentum

The momentum balance for liquid phase:

$$\frac{\partial(\alpha_l \rho_l \overrightarrow{u_l})}{\partial t} + \nabla.(\alpha_l \rho_l \overrightarrow{u_l}\,\overrightarrow{u_l}) = -\alpha_l \nabla p + \nabla.\overline{\overline{\tau}}_l + \alpha_l \rho_l \vec{g} +$$

$$\vec{R}_{gl} + \dot{m}_{gl}\overrightarrow{u_l} - \dot{m}_{lg}\overrightarrow{u_l} + \overrightarrow{F_l} + \overrightarrow{F}_{lift,l} + \overrightarrow{F}_{vm,l} \qquad (2.2)$$

In the equation, $\overline{\overline{\tau_l}}$, $\overrightarrow{F_l}$, $\overrightarrow{F}_{lift,l}$, $\overrightarrow{F}_{vm,l}$ are the stress-strain tensor for liquid phase, external body force, lift force and virtual mass force respectively. "$\vec{R}_{gl}$" is interaction force between bubbles and liquid, "p" is the pressure and it shared by both phases. To close Eqn. 2.2, term of inter-phase force $\vec{R}_{gl}$ must be defined by using appropriate expressions. This force depends on the friction and pressure as well as other effects. In the case modeled in this study, code uses a simple form of this interaction term as follow:

$$\vec{R}_{gl} = \vec{K}\left(\overrightarrow{u_g} - \overrightarrow{u_l}\right) \qquad (2.3)$$

$\vec{K}$ is inter-phase momentum exchange coefficient. This coefficient can be written for liquid-gas mixture which is the case modeled in this study as follows:

$$K = \frac{\alpha_l \alpha_g \rho_g f}{\tau_p} \qquad (2.4)$$

Here, *f* is described as drag function. It has different formulations. However, it is described in a general form as follow:

$$f = \frac{C_D Re}{24} \qquad (2.5)$$

Nearly all definitions of *f* include a drag coefficient (C_D) that is based on the relative Reynolds number (Re). For the primary phase liquid and secondary phase gas, this number is obtained from

$$Re = \frac{\rho_l |\vec{u}_g - \vec{u}_l| d_b}{\mu_l} \qquad (2.6)$$

Models for the drag function generally propose different approximations to drag coefficient C_D. Most famous drag coefficient models are “Schiller and Naumann”, “Morsi and Alexander” and “Universal” models. FLUENT has all these models currently [10].

As last term of Eqn. 2.4, τ_p represents the “particulate relaxation time”. It is defined as;

$$\tau_p = \frac{\rho_g d_b^2}{18\mu_l} \tag{2.5}$$

where d_b is the diameter of the bubbles.

For all these situations, K should approaches to zero whenever the primary phase is not present within the domain. To enforce this, the drag function *f* is always multiplied by the volume fraction of the liquid phase, as is shown in Eqn. 2.4.

As pointed at the beginning of the section, there are other force terms in the momentum equation. One of them is the “lift-force” which exerts on the bubbles in this study. Existence of velocity gradient in liquid phase is driving force for the lift force. The lift force acting on a gas phase g in a liquid phase l is computed from,

$$\overrightarrow{F}_{lift} = -0.5\,\rho_l \alpha_g \left(\vec{u}_l - \vec{u}_g\right) \mathrm{x} (\nabla \mathrm{x}\, \vec{u}_l) \tag{2.8}$$

In most cases, the lift force is not significantly high compared to the drag force. However, if the phases separate quickly, the magnitude of lift force is in order of the drag force and it should be taken into account during the solutions. FLUENT does not include this term by default.

Another force term in the Eqn. 2.2 is the virtual mass force “$\overrightarrow{F}_{vm}$”. This force is significant if the bubbles accelerate relative to the liquid phase. The inertia exerts a “virtual mass force” on the bubbles. The effect is important when the

density of the bubbles is much smaller than the liquid phase density (for example, transient bubble column). The virtual mass force is calculated as follows:

$$\vec{F}_{vm} = 0.5\ \alpha_g \rho_l \left(\frac{d_l \vec{u}_l}{dt} - \frac{d_g \vec{u}_g}{dt} \right) \tag{2.9}$$

In the general form of the Two-Fluid Model, there is also another equation derived for the conservation of energy but in this study, since isothermal conditions are modeled, the energy equation is not described here [10].

2.3 Turbulence Modeling of the Two – Phase Flows

The flows modeled in this study have highly fluctuating velocity fields and these fluctuations describe characteristics of turbulence in the model. Transported quantities between phases such as momentum are also mixed by these fluctuations, and fluctuate as well. Because of the fact that they can be of small scale and high frequency, direct simulation of these fluctuations is computationally expensive. In practical engineering calculations the instantaneous (exact) governing equations can be time -averaged, ensemble-averaged, or otherwise manipulated to remove the resolution of these small scales, resulting in a modified set of equations that are computationally less expensive to solve. However, the modified equations have additional unknown variables, and turbulence models are needed to determine these variables in terms of known quantities. In present literature, there is not any single turbulence model which is universally accepted as accurate or well-suited for all types of problems. The choice of the model depends on the physics of the flow and the level of accuracy wanted. On the other hand the available computational resources and the amount of time available for the simulations are important in terms of efficiency.

Basically, condition of turbulence is described by Navier-Stokes equation. The simple way to derive an equation for numerical modeling of turbulence is applying of Reynolds decomposition method on Navier-Stokes equations. After this mathematical manipulation, one could mention about two different classes of the turbulence modeling. These are *"Reynolds – Averaged Approach"* and "*Reynolds Stress Transport Models".* Turbulent flows in two-phase flow systems have anisotropic turbulence conditions. Typically two equation models are based on isotropic conditions and single-phase models. Therefore they cannot capture the physics accurately. Useful way is to combine the Reynolds stress model with the multiphase algorithm in order to capture reality for turbulence and the Eulerian multiphase formulation.

FLUENT defines Reynolds Stress Model transport equations as follows [10]:

$$\frac{\partial(\overline{\alpha_c}\rho_c)}{\partial t} + \nabla\left(\overline{\alpha_c}\rho_c\widetilde{U_c}\right) = 0 \tag{2.10}$$

$$\frac{\partial(\overline{\alpha_c}\rho_{rmc}\widetilde{U_c})}{\partial t} + \nabla\left(\overline{\alpha_c}\rho_{rmc}\widetilde{U_c}\otimes\widetilde{U_c}\right) = -\overline{\alpha_c}\,\nabla\,\tilde{p} + \nabla.\tilde{\tau}_c^t + F_{DC} \tag{2.11}$$

$$F_{DC} = K_{dc}\left[\left(\widetilde{U_d} - \widetilde{U_c}\right) - \left(\frac{\overline{\alpha_d u_d'}}{\overline{\alpha_d}} - \frac{\overline{\alpha_c u_c'}}{\overline{\alpha_c}}\right)\right] \tag{2.12}$$

$$\tilde{\tau}_k^t = \overline{\alpha_k}\rho_k\tilde{R}_{k,ij} \tag{2.13}$$

In above equations, Rij is Reynolds stress. FLUENT provides two turbulence options within the context of the Reynolds stress models (RSM). These options are,

- Dispersed Turbulence Model

- Mixture Turbulence Model (the default)

2.3.1 RSM Dispersed Turbulence Model

FLUENT uses dispersed turbulence model if the secondary phase is dilute and the primary phase turbulence is dominant in the flow. Turbulence quantities are only solved for the primary (continuous) phase, while the predictions of turbulence quantities for dispersed phases are obtained using the "Tchen" theory. The model defines the transport equation for the primary phase as follows [10]:

$$\frac{\partial(\bar{\alpha}_\rho \tilde{R}_{ij})}{\partial t} + \frac{\partial(\bar{\alpha}_\rho \tilde{U}_k \tilde{R}_{ij})}{\partial x_k} = -\bar{\alpha}_\rho \left(\tilde{R}_{ik} \frac{\partial \tilde{U}_j}{\partial x_k} + \tilde{R}_{jk} \frac{\partial \tilde{U}_i}{\partial x_k}\right) + \ldots\ldots \quad (2.14)$$

$$\frac{\partial}{\partial x_k}\left[\bar{\alpha}\mu \frac{\partial}{\partial x_k}\left(\tilde{R}_{ij}\right)\right] - \frac{\partial}{\partial x_k}\left[\bar{\alpha}\, \rho \overline{u_i' u_j' u_k'}\right] + \bar{\alpha} p \overline{\left(\frac{\partial u_i'}{\partial x_j} + \frac{\partial u_j'}{\partial x_i}\right)} - \bar{\alpha}\rho\tilde{\epsilon}_{ij} + \prod R, ij$$

Last term of Eqn. 2.14 $\prod R, ij$ takes into account the interaction between the continuous and the dispersed phase turbulence. A general simplified model for this term can be defined as follows:

$$\prod R, ij = \frac{2}{3}\delta_{ij} \prod_k \quad (2.15)$$

where $\delta_{ij}$is the Kronecker delta, and $\prod_k$ represents the modified version of the original "Simonin" model.

$$\prod_{kp} = K_{sp}\left(\tilde{k}_{sp} - \widetilde{2k}_p + \tilde{V}_{rel}.\tilde{V}_{drift}\right) \quad (2.16)$$

where K_{sp} represents the turbulent kinetic energy of the primary phase, $\tilde{k}_{sp}$ is the primary-secondary phase velocity covariance. $\tilde{V}_{rel}$ and $\tilde{V}_{drift}$ are the relative and the drift velocities, respectively.

To closure the equation, the transport equation for the turbulent kinetic energy dissipation rate $(\tilde{\epsilon})$ is needed as well.

2.3.2 RSM Mixture Turbulence Model

In the mixture model all phases share the same turbulence field which consequently means that the term $\prod_R$ in the Reynolds stress transport equations Eqn. 2.14 is neglected. Apart from that, the equations maintain the same form but with phase properties and phase velocities being replaced with the mixture properties and mixture velocities. The mixture density, for example, can be expressed as

$$\rho_m = \sum_{i=1}^{N} \bar{\alpha}_i \rho_i \tag{2.17}$$

while mixture velocities can be expressed as

$$\widetilde{U}_m = \frac{\sum_{i=1}^{N} \bar{\alpha}_i \rho_i \widetilde{U}_i}{\sum_{i=1}^{N} \bar{\alpha}_i \rho_i} \tag{2.18}$$

where N is the number of species [10].

2.4 Interfacial Area Concentration (IAC) Model

Interfacial area is where mass, momentum and energy transfers are carried out. Therefore these transferred terms depend on this parameter. In addition, its concentration (IAC) is described as the interfacial area between two – phases per unit mixture volume (m^2/m^3). Mathematically it can be formulated as follow [10]:

$$a_i\,(x, V, t) = \int_{V_{min}}^{V_{max}} f(x, V, t) A_i(V)\, dV \tag{2.19}$$

In the equation, *f* is distribution function of discrete particle number density. In addition, V_{max} , V_{min} and $A_{\mathrm{i}}(V)$ are maximum, minimum volumes of all discrete particles and averaged interfacial area of the discrete phase having a volume of V respectively.

Simple calculation for interfacial area could be formulated as follows:
For a constant diameter of bubble “db“and n bubbles in a sphere with diameter D:

$$IAC = \frac{n * \pi * db^2}{\frac{\pi * D^3}{6}} \tag{2.20}$$

In Eqn. 2.20, number of bubbles “n” could be represented in terms of void fraction and bubble diameter as follows:

$$n = \frac{\alpha * D^3}{db^3} \tag{2.21}$$

Finally, the version of IAC which is used in initial calculations of the simulations can be formulated as follows:

$$IAC = \frac{6 * \alpha}{db} \tag{2.22}$$

Prediction of this concentration parameter is an important issue in modeling of two – phase flow systems by using two – fluid approach. As it can be observed from Eqn. 2.19, it depends on size and distribution of the discrete phase in the mixture. These two terms, size and distribution, are changed by growth, expansion, coalescence, breakage and nucleation mechanisms in the flow. In literature most popular model is “Population Balance Model” in simulation of these mechanisms. However it solves several transport equations. Therefore, it is a computationally expansive method. On the other hand, FLUENT has another option which is called interfacial area concentration model. It uses IAC as a correction factor on calculation of interfacial transfer mechanisms. In the model, a single transport equation is solved for the secondary phase. The model is specific for bubbly flows currently.

The transport equation for the interfacial area concentration is described in the code as follow:

$$\frac{\partial(p_g a_p)}{\partial t} + \nabla.\left(\rho_g \vec{u}_g a_p\right) = \frac{1}{3}\frac{D\rho_g}{Dt}\, a_p + \frac{2}{3}\frac{\dot{m}_g}{\alpha_g}\, a_p + \rho_g(S_{RC} + S_{WE} + S_{TI}) \quad (2.23)$$

a_p is the interfacial area concentration and α_g is the gas volume fraction. There are terms in Eqn. 2.23 due to gas bubble expansion, compressibility and mass transfer (phase change). $\dot{m}_g$ is the mass transfer rate into the gas phase per unit mixture volume ($kg/m^3/s$). S_{RC} and S_{WE} are sink terms for the coalescence due to random collision and wake entrainment, respectively. S_{TI} is a source term for the breakage due to turbulent impact.

As parallel to the literature, FLUENT has two combination sets of models for those source and sink terms in the transport equation. These two sets are Hibiki-Ishii model [14] and the Ishii-Kim model [15, 16]. They are based on the works of Ishii et al. [14, 15].

In these studies, the coalescence mechanism consists of:

- Coalescence due to random collision driven by turbulence.
- Coalescence due to wake entrainment

The breakage mechanism consists of:

- Breakage due to the impact of turbulent eddies.
- Breakage of large cap bubbles due to flow instability on the bubble surface.

In FLUENT, only the first three effects, random collisions, turbulent eddies and wake entrainment, are considered. More detailed information can be found in the Theory Guide of ANSYS FLUENT 12 [10].

3. ESTABLISHMENT OF THE NUMERICAL MODEL

3.1 Grid Generation

In the study, two different geometries (32/40 and 65/80) are used to model different experimental setups. Thus, two different sets of grids are created in accordance with the flow conditions and geometries. Dimensions of these geometries are listed in Table 3.1. Table 1 also shows two different version of the geometry-I in terms of dimensions. Longer version of this type geometry is generated to use proper boundary condition type at the outlet. In Results chapter, more information is given. On the other hand, geometries I and II are created for the divergent type singularity with a divergence angle 8° . Their proportional dimensions with pipe diameters are same. Both geometries have a 10d/20d length in up-stream section before the singularity and 14D/20D down-stream section after the singularity.

Table 3.1. Dimensions of the generated geometries for the simulations

Parameters	**Geometry I**		**Geometry II**
Diameter Ratios	32/40 - I	32/40 - II	65/80
Length of the pipe	0.905 m	1.625 m	1.772 m
Inlet diameter (d)	0.032 m	0.032 m	0.0627 m
Outlet Diameter (D)	0.040 m	0.040 m	0.078 m
Length of the Singularity	0.025 m	0.025 m	0.0529 m

Generally pipe geometries need special attention to avoid having improper cell shapes and density at the center of the pipe (because of the cylindrical coordinate). One may try several methods for accuracy. In this study, preferred way is generation of rectangular zone in the mid-section of the pipe. In addition, circular shape is created by turning of a plane which is lying on XY plane, around this rectangular volume in the Z – direction. Selected regions from the generated grids are represented in Figures 3.1 through 3.4.

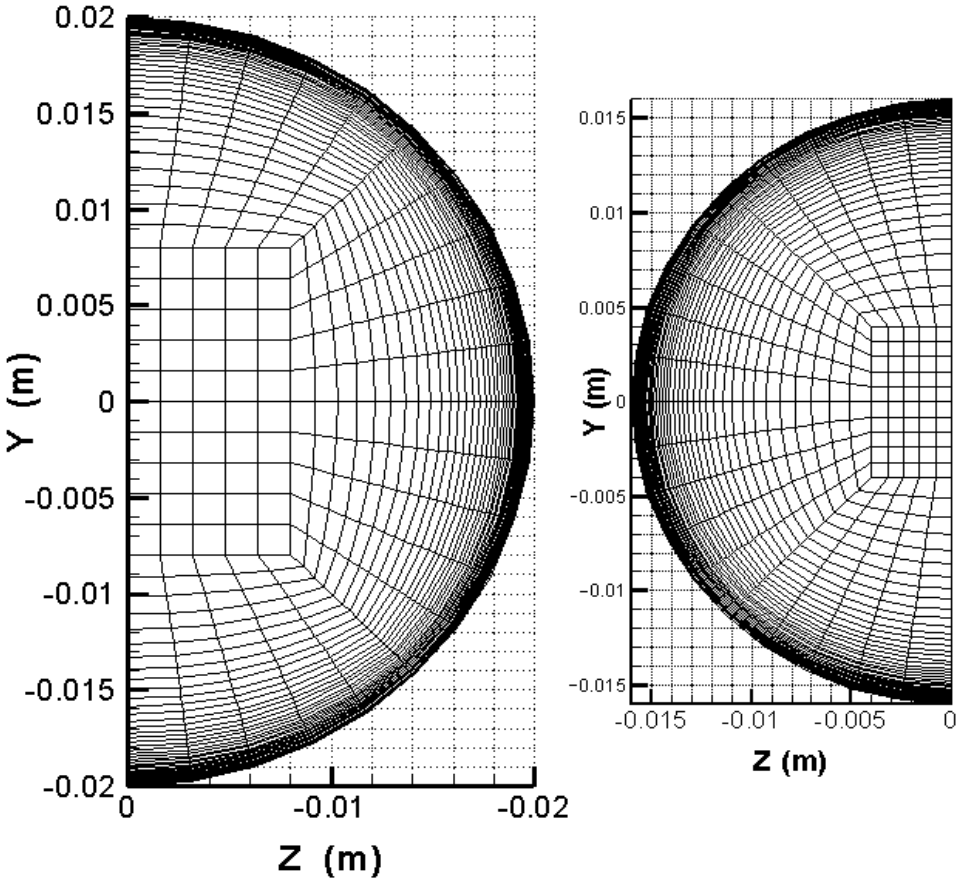

Figure 3.1. Outlet and inlet regions of the 32/40 case, respectively

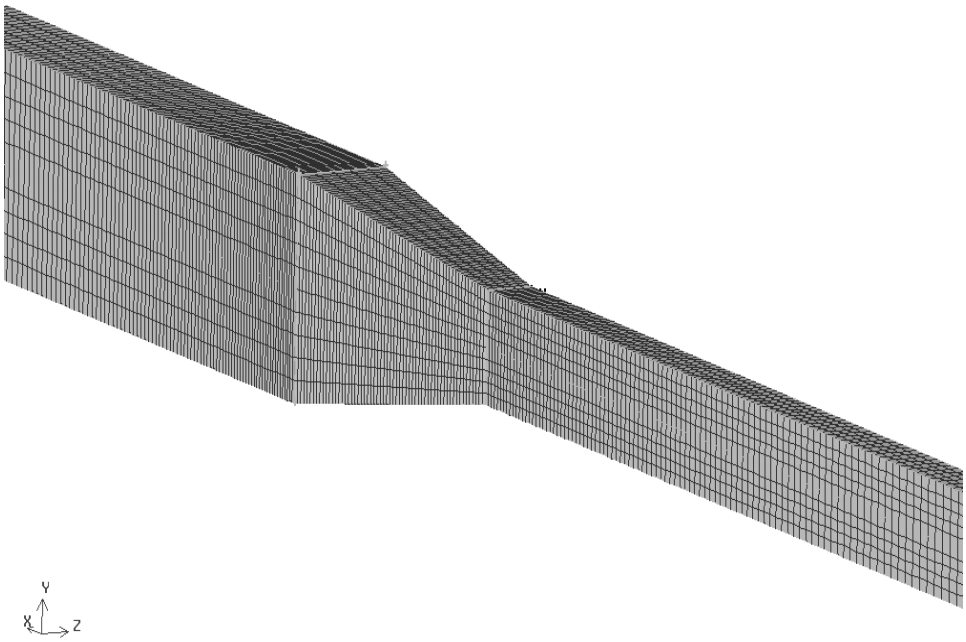

Figure 3.2. Middle channel of the grid / rectangular base

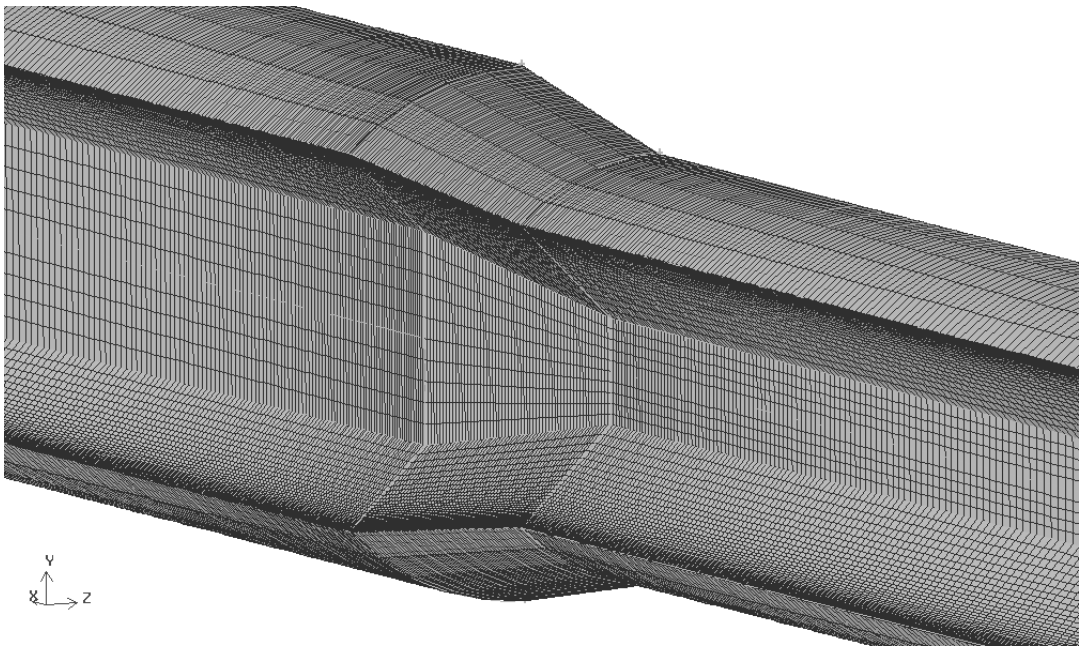

Figure 3.3. Generation of the grid around the rectangular base

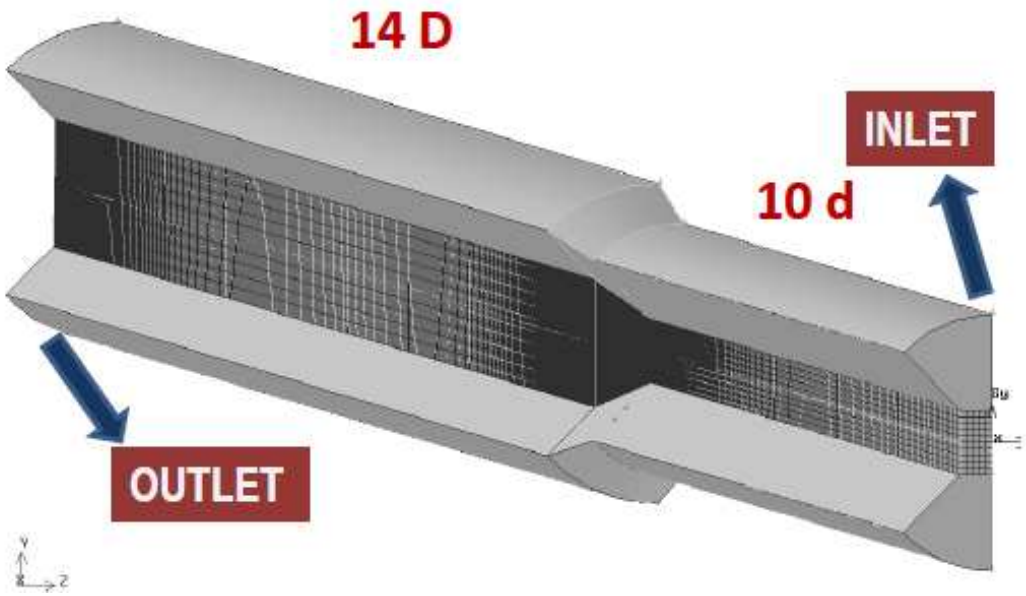

Figure 3.4. Length of the grid (32/40 l)

In grid generation process, some special criteria have been applied to provide sufficient resolution for modeling turbulence characteristics of the viscous sub-layer near the wall. One should have at least one grid point inside this region. In theory, viscous sub-layer corresponds to y^+ values between 0 and 5. y^+ is defined as a non-dimensional wall distance for a wall bounded flow. It is formulated as follows:

$$y^+ = \frac{y_p * \nu}{U_\tau} \tag{3.1}$$

Here, U_τ is "Friction Velocity, ν is kinematic viscosity and y_p is distance to the nearest wall. FLUENT suggests an empirical equation to calculate the friction velocity.

$$U_\tau = U_\infty * \sqrt{0.039 * Re^{-0.2}} \tag{3.2}$$

In Eqn. 3.2, U_∞ is "Bulk Velocity". After calculation of the friction velocity, one can calculate the first grid position as y_p using Eqn. 3.1. In this study, y^+ is

chosen equal to 4. In following section, the grid performance is shown by presenting the y^+ values for the wall adjacent cells. Grids were generated by using GAMBIT 2.4.6. This code has an ability to create special boundary layers on the wall. However in this study, these layers were created by hand using proper cell-size ratio. Generally, this ratio must be around 1.2. This can be observed in Figure 3.1. Above the rectangular base; there are equal numbers of cells at the inlet and outlet region. In the calculation of this number of necessary cells, basic mathematical formulation of the power series, Eqn. 3.3 is used. In the calculation *"(n + 1)"* is equal to number of interval, and "*L"* is the length of the edge that will divide into cells. In addition, "*x*" is the cell size ratio criteria (like 1.2 and etc).

$$\frac{L}{y_p} = \sum_{i=0}^{n} x^i = \frac{(1-x^{n+1})}{(1-x)} \tag{3.3}$$

Another approach of the study, is applying symmetry on the plane at center of the z – coordinate axis. There is gravity force in y – direction and there is not any other body force or source which changes in the z – direction. In this respect, this assumption is reasonable and applicable. This assumption results in obtaining two times more number of cells in the model. In this study the smallest cell number belongs to the 32/40-I case and it is nearly 300000 cells. Other grids have higher cell numbers.

3.1.1. Evaluation of the Grid

As it is stated earlier, all grids were designed to resolve viscous sub-layer in the turbulence conditions. So, the "y^+" values should be in a range between 0-5 for the wall adjacent cells. Figures 3.5 and 3.6 show the y^+ values for the selected simulations. The y^+ values set for all simulations are smaller than 5 on the wall adjacent cells.

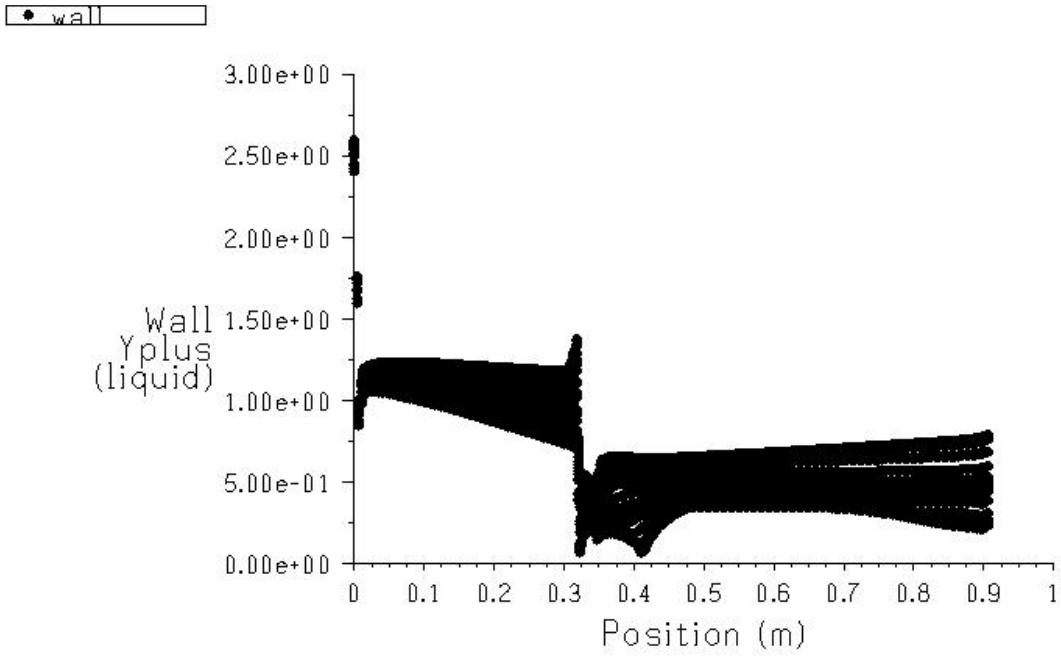

Figure 3.5. y^+values of the wall adjacent cells for primary phase.

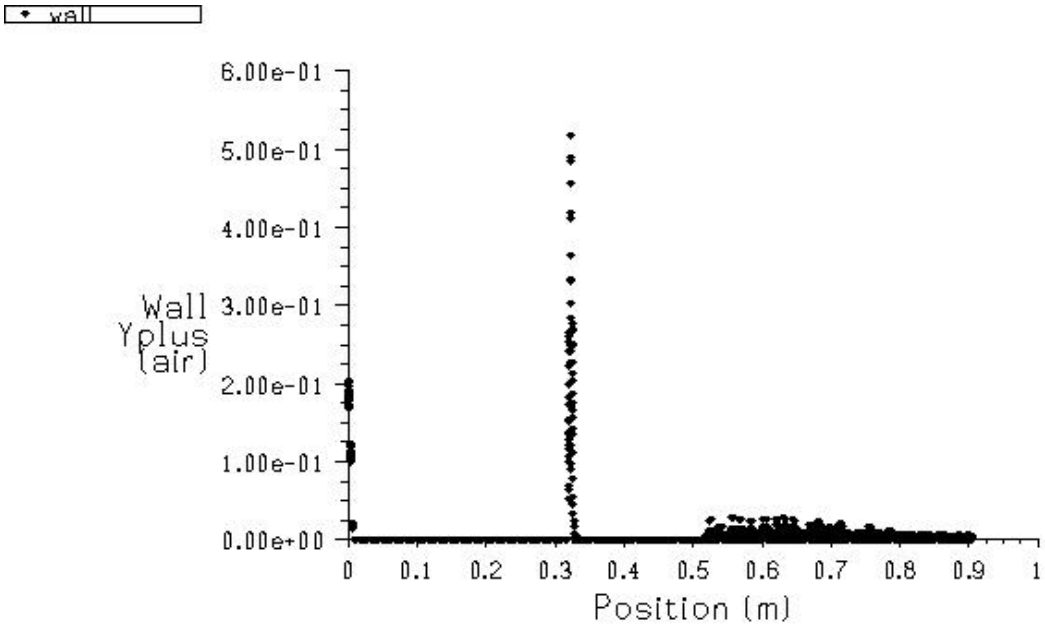

Figure 3.6. y^+ values of the wall adjacent cells for secondary phase.

3.2. Numerical Parameters of the Simulations Used by FLUENT

As mentioned before, FLUENT is the commercial CFD code used in this study. It has all multiphase flow models explained in the previous chapter. In this study "Eulerian Model" is chosen for all cases simulated. The turbulence model option of the code is described in the previous chapter. Because of highly isotropic turbulence conditions of the flow "Reynolds Stress Model (RSM)" is implemented to the model. In the study, "RSM Mixture Turbulence Model" is used for all cases except the case described in section 4.4. In this section is dedicated to show differences between RSM and one of the two-equation turbulence models. Therefore "k-e" turbulence model is used in that part of the study.

Dimensions of the model for the numerical study are shorter than the real experimental setup in the flow direction. In the real case injection of the bubbles were made at least 30d far from the expansion. In addition setup has also longer section after the expansion in a closed loop experimental setup. Therefore, "Turbulence Velocity Profile" is applied at the inlet boundary to get fully developed velocity profile. This velocity profile comes from the "Power Law" and it is calculated by using the Eqn. 3.4.

$$\mathrm{u} = U_{\infty}\left(1 - \frac{\mathrm{r}}{\mathrm{R}}\right)^{1/7} \tag{3.4}$$

The bulk velocity (pick value of the profile) must be calculated directly from the integration of this profile over inlet are in accordance with the mass – flow rate (*Q*) of the phase. Integration is shown in the Eqn. 3.5.

$$Q = \int_0^R U_{\infty}\left(1 - \frac{\mathrm{r}}{\mathrm{R}}\right)^{1/7} 2\pi \mathrm{r}\,\mathrm{dr} \tag{3.5}$$

The term *"r"* can be transformed to "Cartesian coordinates" using $r = \sqrt{y^2 + z^2}$ relationship.

Turbulent velocity profile is generated by using the “User Defined Function (UDF)” option of FLUENT. The generated UDF for the turbulent velocity profile is listed in the Appendix. A simple example of the 2D turbulent velocity profile is presented in Figure 3.7.

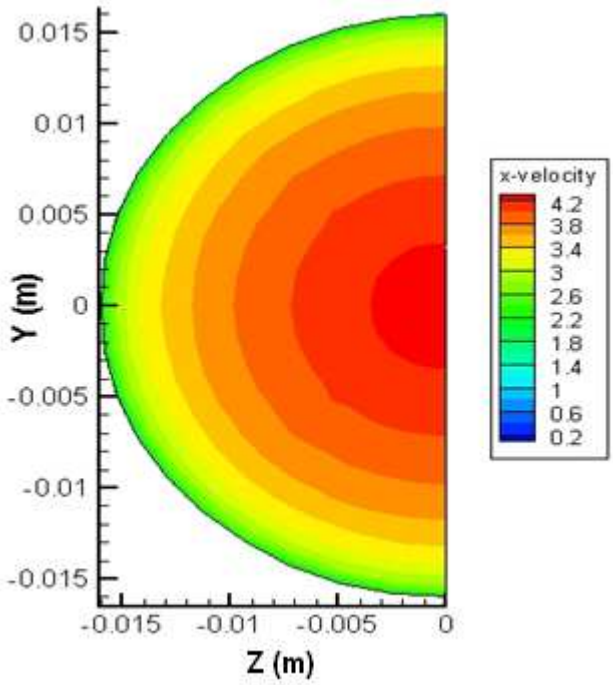

Figure 3.7. Turbulent velocity profile at the inlet boundary

Inlet and Outlet boundary conditions defined are “the Velocity Inlet” and “the Outflow or the Pressure Outlet” conditions respectively. Except for the investigation of the mass flow rate effect part of the study, there is no slip velocity specification at the inlet boundary.

In the simulations, only drag force is taken into account. Material properties are defined in accordance with the experimental data and measurements.

Turbulence specification is made by turbulent length scale and turbulent intensity. For this specification, length scale is calculated using an empirical relationship from Eqn. 3.6. The intensity is chosen as equal to 10 % [17].

$$l = 0.07 * D \tag{3.6}$$

In the study, interfacial area concentration (IAC) is calculated using Eqn. 2.20 over an inlet area as follows:

$$IAC = \frac{4 \times \alpha}{d_{bubble}} \tag{3.7}$$

“Linear – Pressure Strain Model” default option of the Reynolds Stress Turbulence Model is chosen. Moreover, it’s “Enhanced Wall Treatment” is applied in the model for the “Near Wall Treatment”. Performance of the grid with this wall treatment is described in the previous sections in terms of y^+ values.

Operation Conditions

Gravity effect is taken into account in the direction of negative “y” axis for all the simulations. As another important two phase flow parameter, the operating density is set as the lightest density between the phases as suggested by FLUENT.

Solution Procedures

To improve convergence behavior, FLUENT suggests computing an initial solution before solving the complete Eulerian multiphase model. There are three methods one can use to obtain an initial solution for an Eulerian multiphase calculation [17]:

• Set up and solve the problem using the mixture model (with slip velocities) instead of the Eulerian model. One can then enable the Eulerian model, complete the setup, and continue the calculation using the mixture-model solution as a starting point [17].

• Set up the Eulerian multiphase calculation as usual, but compute the flow for only the primary phase. To do this, deselect Volume Fraction in the Equations list in the Equations dialog box. Once an initial solution for the primary phase, turn the volume fraction equations back on and continue the calculation for all phases [17].

• Use the mass flow inlet boundary condition to initialize the flow conditions. It is recommended to set the value of the volume fraction close to the value of the volume fraction at the inlet [17].

In this study, the second solution procedure was applied on simulations.

The performance of the procedure is discussed on the preceding sections using “Residual graphs” and order of the mass-imbalance between inlet and outlet boundary.

4. RESULTS of SIMULATIONS

At the initial stage of the study two phase bubbly flow in a simple pipe has been studied. In this part, pipe length has been controlled and verified in terms of the stratification of the bubbles. Following section of this chapter consists of parametric studies on the modeled two phase flows. Effects of flow parameters on pressure drop like bubble diameter, void fraction and mass flow rate have been studied for divergent and convergent channel but mainly divergent channel. Next section is devoted to validation of two - fluid approach. Data from void fraction and static pressure experiments are used for the verification. Last two sections of this chapter are about different modeling options and abilities of the CFD code. Different models and boundary condition types are used to improve verification results.

4.1 Two-Phase Flow in a Simple Pipe

As mentioned before in this section, the results of numerical simulations are compared with the experimental data for the two phase flow in a divergent pipe. In the experimental setup, bubbles were injected far from the widening section of the pipe. They are in injected in a uniform profile. For this reason, the effect of the pipe length on void distribution should be investigated. For this purpose a 0.96 m (30d) long straight pipe with channel diameter of 32 mm is used. Bubble diameter is 1 mm in the simulation. Development of the void fraction profiles is studied. Figures 4.1 – 4.3 show change of the void fraction along the pipe. Results show that bubbles stratify fast. Uniform distribution profile is not preserved in the pipe even in the upstream part and bubbles stratified easily. For the later analysis, 0.32m long pipe section is used before widening.

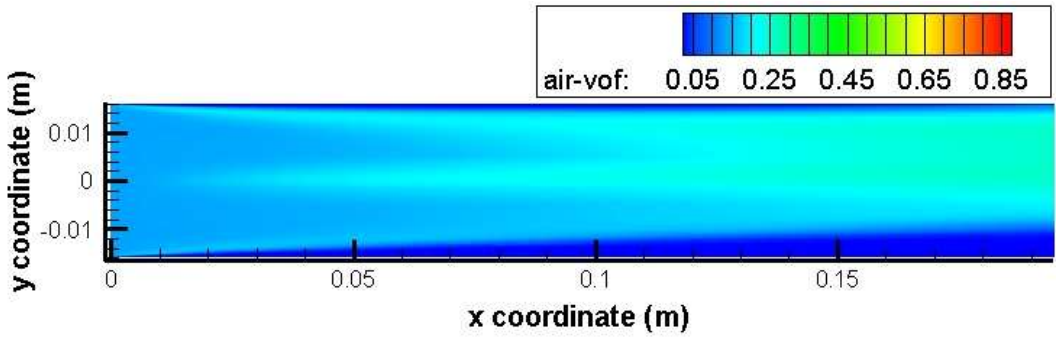

Figure 4.1. Void fraction on the symmetry plane between x = 0 m and 0.2 m

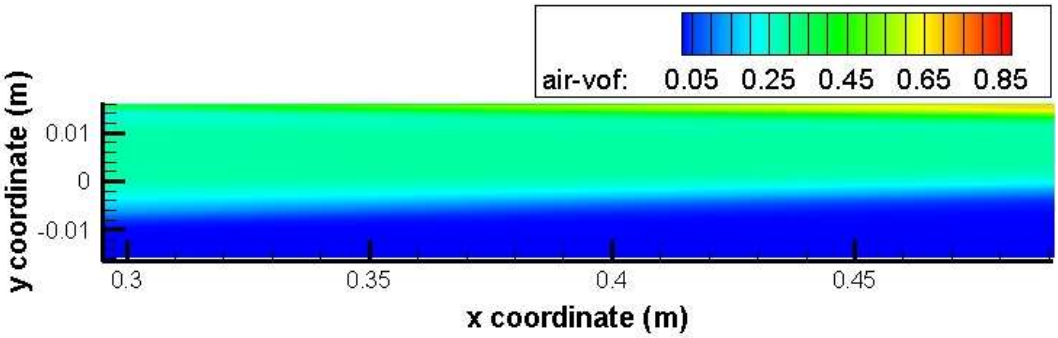

Figure 4.2. Void fraction on the symmetry plane between x = 0.3 m and 0.5 m

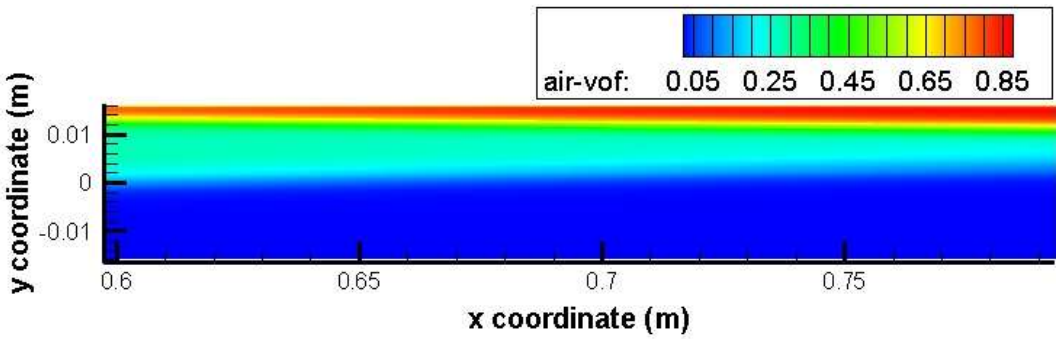

Figure 4.3. Void fraction on the symmetry plane between x = 0.6 m and 0.8 m

Figure 4.4 shows stratification of bubbles more clearly. At the inlet there is uniformity. However, bubbles are stratified easily just after 10d along the flow

direction. Figure shows that the upstream section of the pipe is suitable to observe stratification.

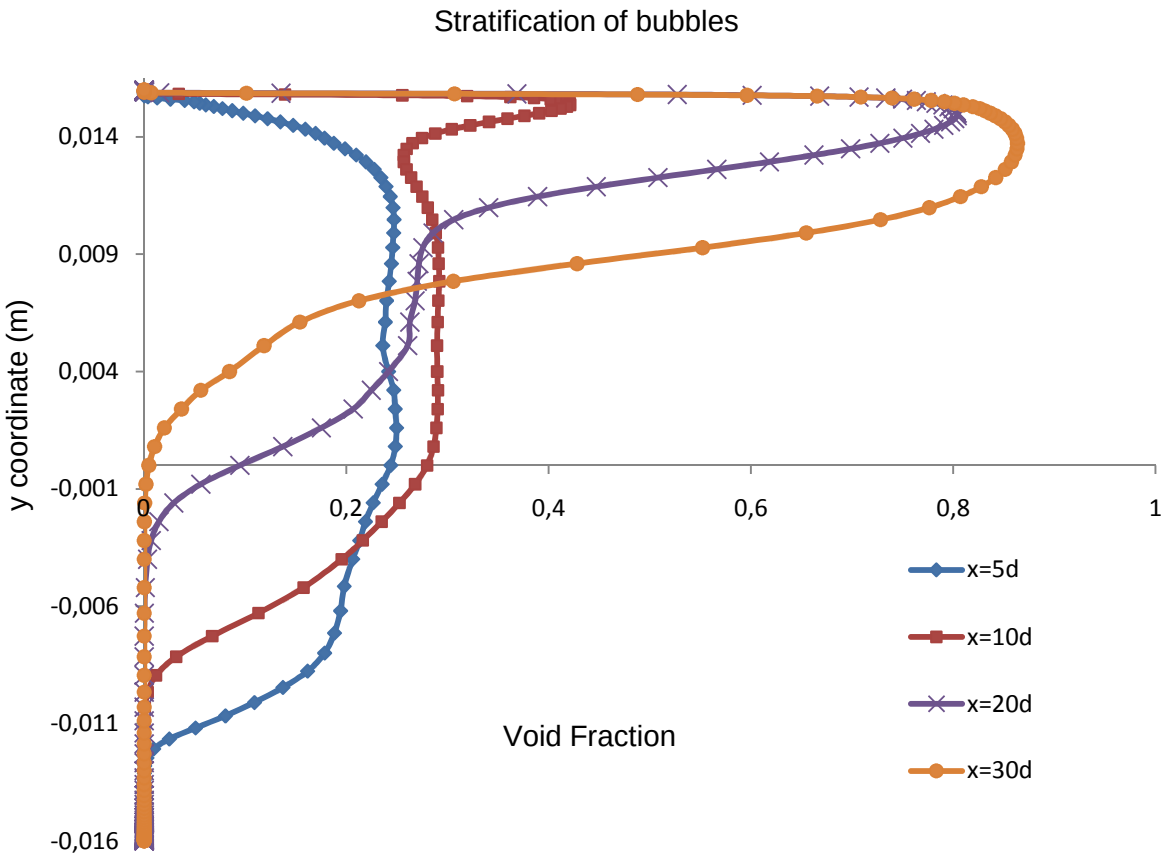

Figure 4.4. Progression of void fraction distribution along the flow direction x.

4.2 Two Phase Flow in Divergent/Convergent Channels

In this study, two phase pipe flows has been studied in two main parts. This first part is dedicated to investigate the effect of the flow parameters on pressure and velocity profile of the fluid. Therefore, the first part can be called as a parametric study. Studied flow parameters are bubble diameter, void fraction and mass-flow rate. Each of them has a characteristic effect over the velocity profiles and static -

pressure recovery or total pressure drop for the flow. In the following four sub-sections, the results of the analysis showing the effects of these three parameters are described in divergent and convergent channels. For all parts of the parametric study, 32/40 I type of geometry is used. Dimensions of the geometry are presented in Table 3.1. In addition, the flow conditions of the simulations performed for the "parametric study" is presented in Table 4.1. To indicate similar cases, colors are used in the table.

Table 4.1. The flow parameters of the simulations performed for the "parametric study"

Parametric Study	Q_{air}/ Q_{water} m^3/s	2.45 E-3			2 E-3	1.5 E -3	1 E-3	2.45 E-3		Bubble Diameter
Effect of Void Fraction	1.3 E-4									1 mm
	2.7 E-4									
	4.3 E-4									
	6.2 E-4									
Effect of Mass Flow Rate	4.8 E-4									
	3.9 E-4									
	2.9 E-4									
	1.9 E-4									
Effect of Bubble Diameter	4.3 E-4									
	4.3 E-4									0.5 mm
	4.3 E-4									0.1 mm
	Void Fraction %	5	10	13				15	20	

4.2.1 Effect of Bubble Diameter

In this part of the study, effect of bubble diameter on the variation of void fraction and continuous phase velocity are investigated. In the two - fluid (Eulerian) multiphase model, momentum exchange terms depend on bubble diameters. Body forces like "buoyancy" and "drag force" which is the only interaction force considered initially between phases are affected by this

parameter. Results are important for this study especially in terms of the simulation parameters in the validation process.

In the simulations, turbulence velocity profile was applied for both phases and there is no difference between phase velocities at the inlet (no-slip condition). Flow inlet conditions in this part are as follow;

Q water = 2.45 x 10^{-3} m³/s, U_∞ = 4.4 m/s

Q air = 4.3 x 10^{-4} m³/s, α = 15 %

Figures 4.5 through 4.13 show the effect of bubble diameter on velocity, flow streamlines and the void fraction.

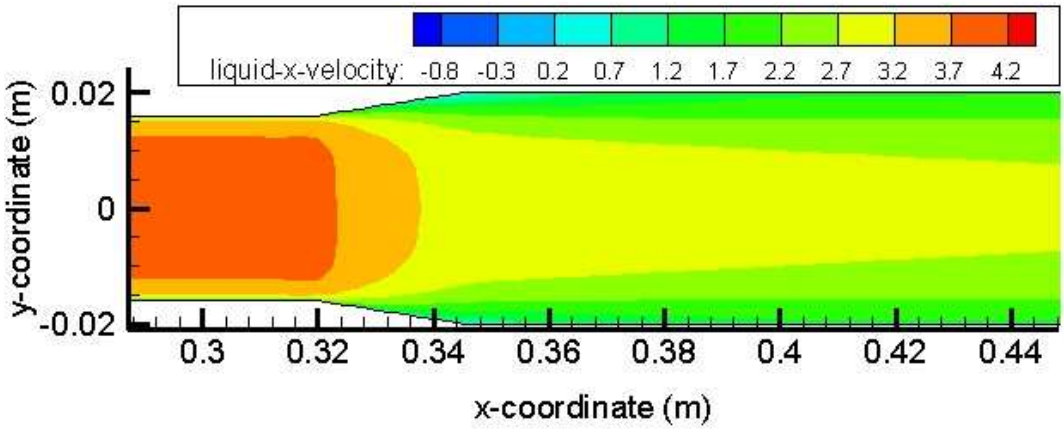

Figure 4.5. U-velocity profile for $\mathbf{d_b}$ = 0.1 mm

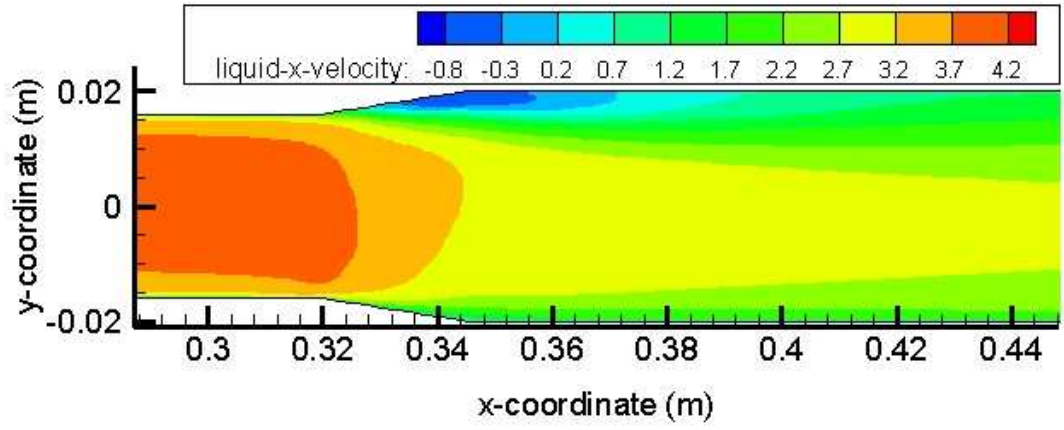

Figure 4.6. U-velocity profile for $\mathbf{d_b}$ = 0.5 mm

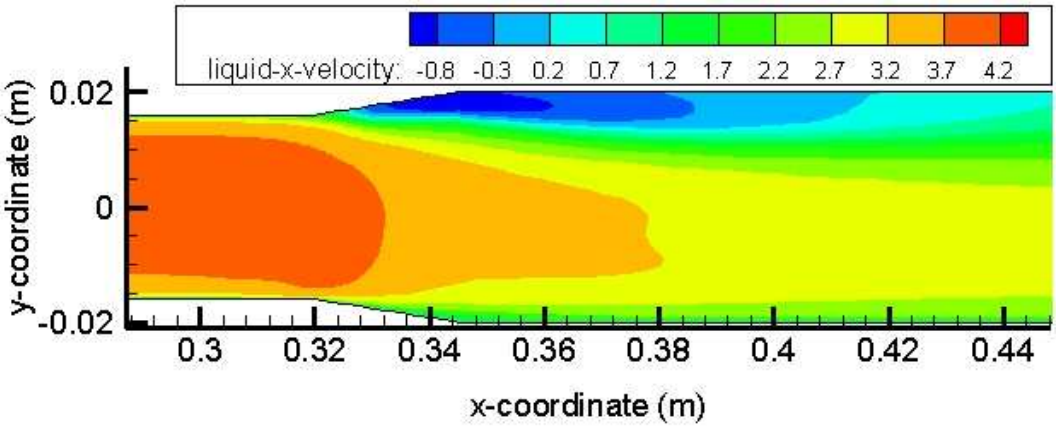

Figure 4.7. U-velocity profile for $\mathbf{d_b}$ = 1.0 mm

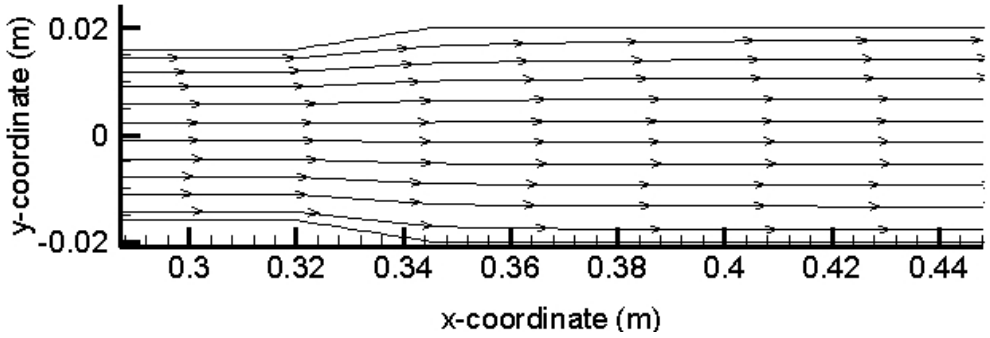

Figure 4.8. Streamlines for $\mathbf{d_b}$ = 0.1 mm

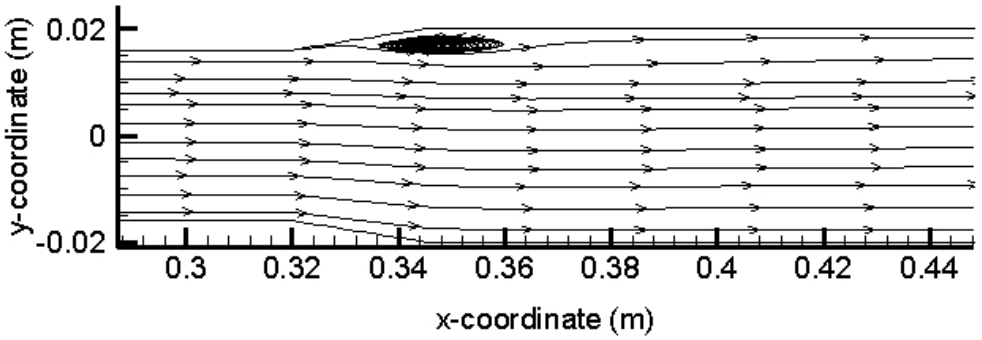

Figure 4.9. Streamlines for $\mathbf{d_b}$ = 0.5 mm

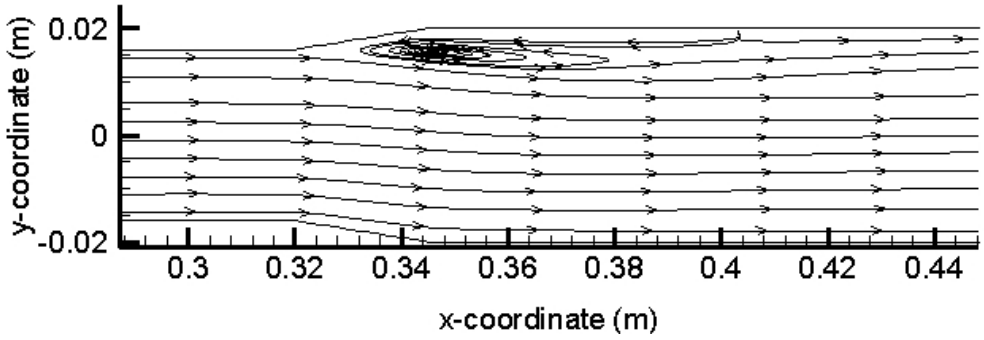

Figure 4.10. Streamlines for $\mathbf{d_b}$ = 1.0 mm

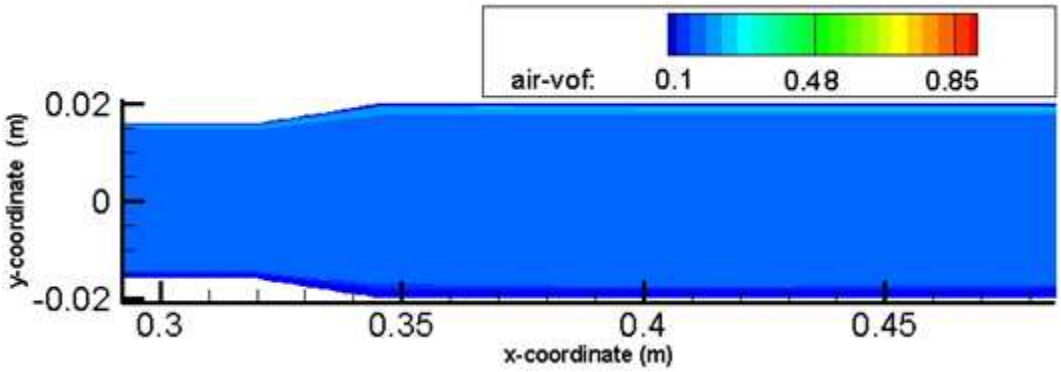

Figure 4.11. Void fraction for $\mathbf{d_b}$ = 0.1 mm

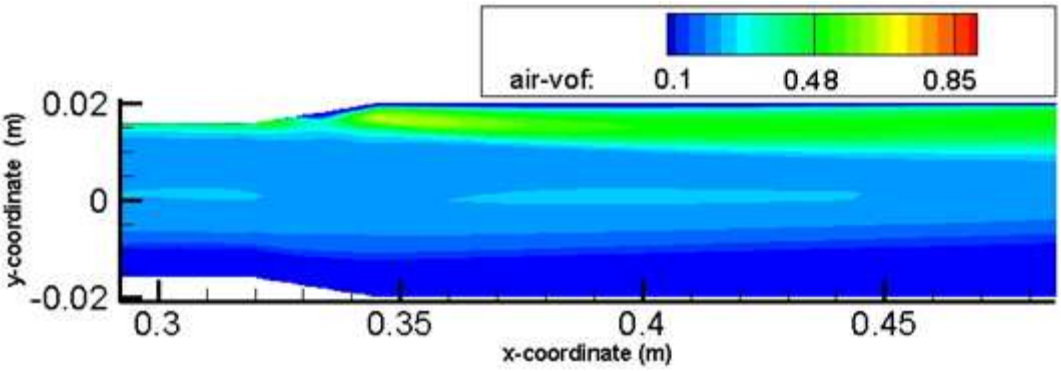

Figure 4.12. Void fraction for $\mathbf{d_b}$ = 0.5 mm

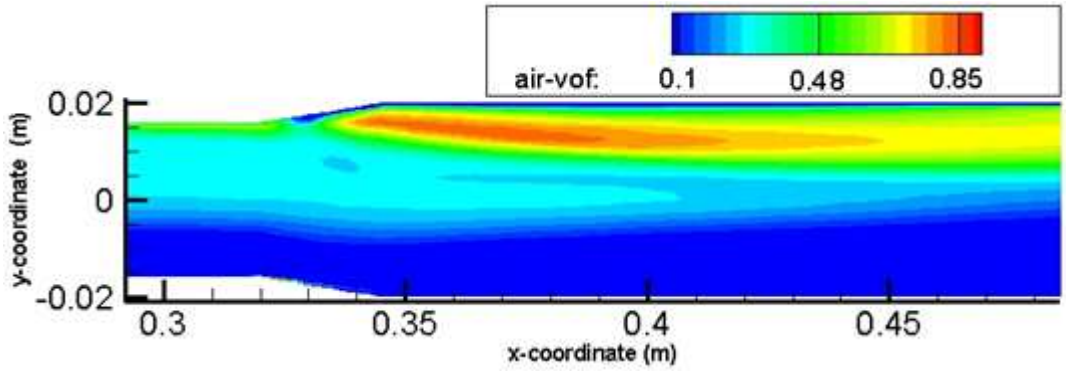

Figure 4.13. Void fraction for $\mathbf{d_b}$ = 1.0 mm

Figures 4.5 through 4.13 present the effect of bubble diameter on stratification. This type of manner is directly related with the “buoyancy” phenomena. In existence of gravity, the bubbles are affected by buoyancy-force in the domain, and this force depends on the bubble diameter:

- Fnet = g x V (bubble) x ρ (liquid) – m x g (4.1)
- Fnet = g x V (bubble) x [ρ (liquid) – ρ(air)] (4.2)

Above equations show that the buoyancy force which is exerted on the biggest bubble in y-direction is 1000 times bigger than the small one. So big bubbles can escape from the gravity easily and collect in the upper-part of the channel.

It is clear that the bubble collection phenomena restricts the flow area and makes the fluid flow at higher velocities. Thus, it is expected that the “static-pressure recovery” is affected by this and lower static-pressure recovery for bigger bubbles is observed. The static pressure changes are shown below in Figure 4.14. In the figure, pressure values taken with two different “average methods” are presented. In the study, area weighted average value of static pressure and mass weighted average value of total pressures are used in comparison.

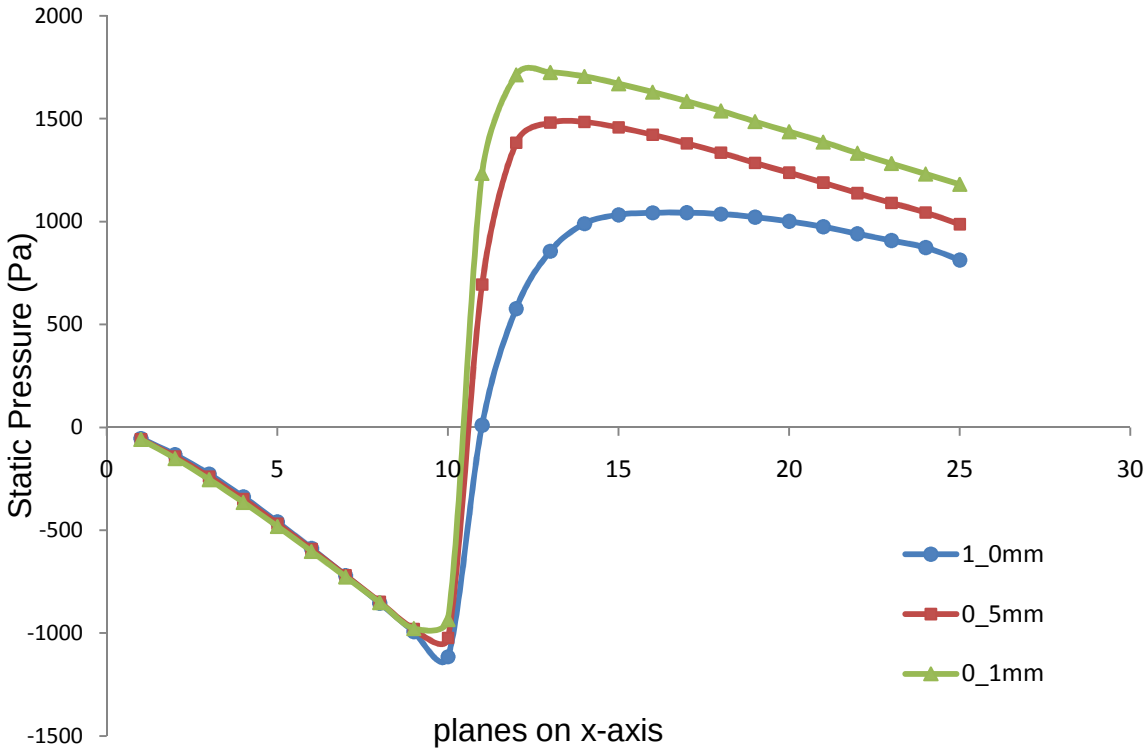

Figure 4.14. Static pressure change (Pa) for different bubble diameter

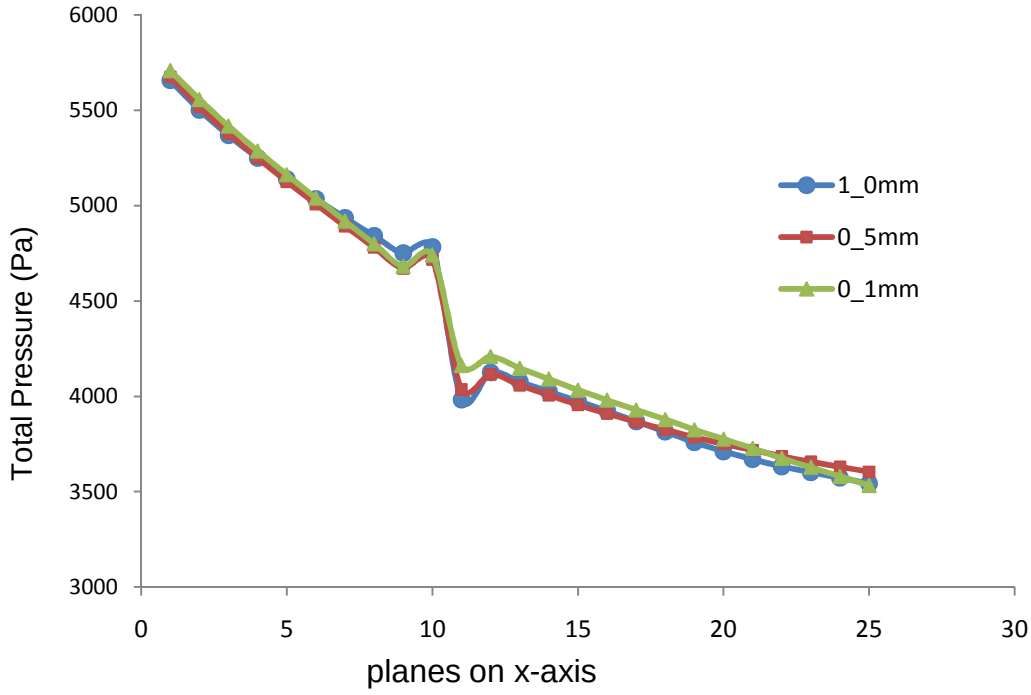

Figure 4.15. Total pressure drop (Pa) for different bubble diameter

Figure 4.15 shows that, total pressure drop is not affected by bubble diameter as much as the static pressure is. It is obvious the bubble diameter is an important parameter for validation part to analyze static pressure recovery accurately.

The results of simulations performed to analyze the bubble diameter effect on flow show that the convergence of the simulations is in order of 1E-3 and mass-imbalance between inlet and outlet is in order of 1E-4. Figure 4.16 shows the residuals.

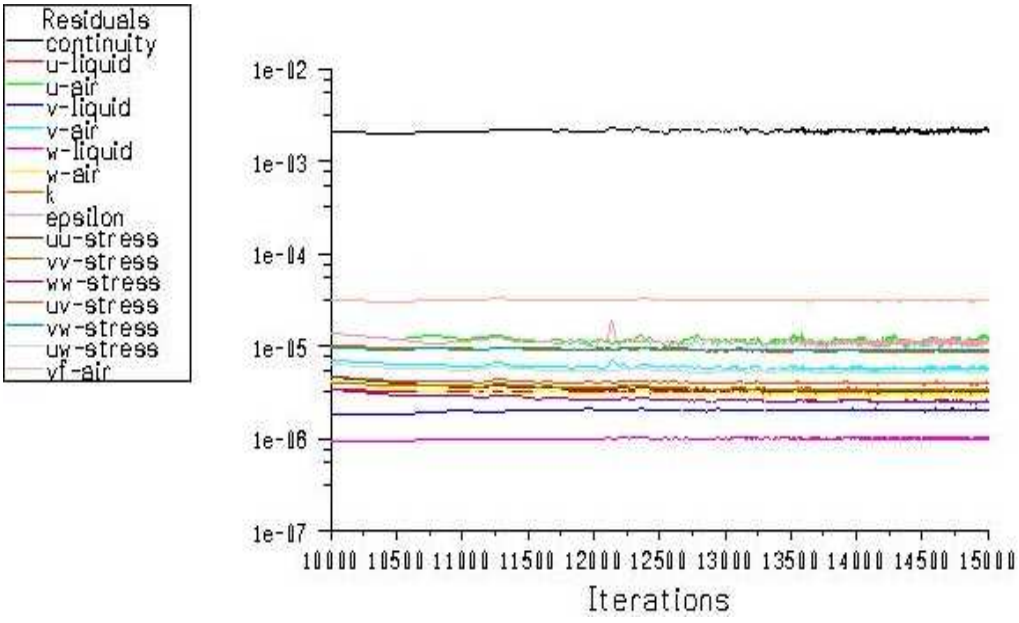

Figure 4.16. Residuals for case of $\mathbf{d_b}$ = 1.0 mm

4.2.2 Effect of Mass-Flow Rate

In this part of the study, the results of the investigating the effect of mass-flow rate on the pressure drop are discussed. Four different mass flow rates (thus four different velocities in a constant void fraction at the inlet) were studied. Basically, it is expected that the total pressure drop decreases with lower mass-flow rates of the mixture. In low velocities there is also another phenomenon; bubbles could collect in the upper part of the pipe easily and continuous phase

has not enough momentum to push them. In the simulations, constant flow parameters are as follows;

Q max, water = 2.45 x 10^{-3} m³/s, $U_{max,\infty}$ = 4.4 m/s

Q max, air = 4.8 x 10^{-4} m³/s, α = 13 %

Bubble diameter = 1 mm

Figures which are below show the results**.**

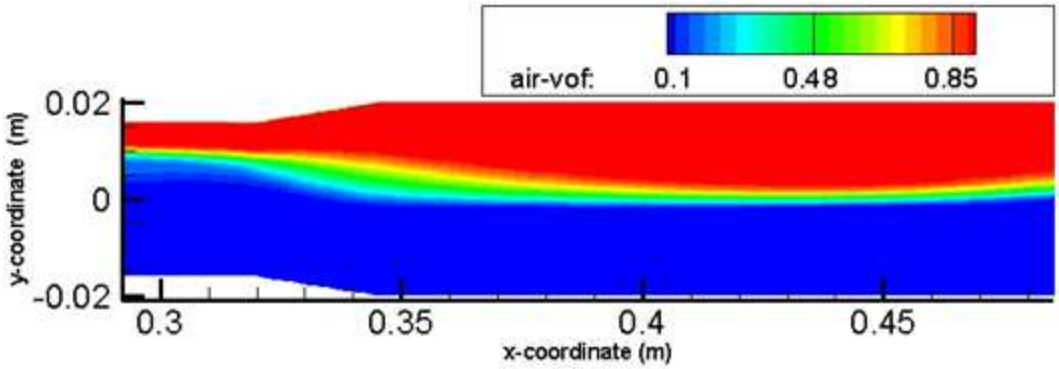

Figure 4.17. Volume fraction of air Q = 0.4Qmax

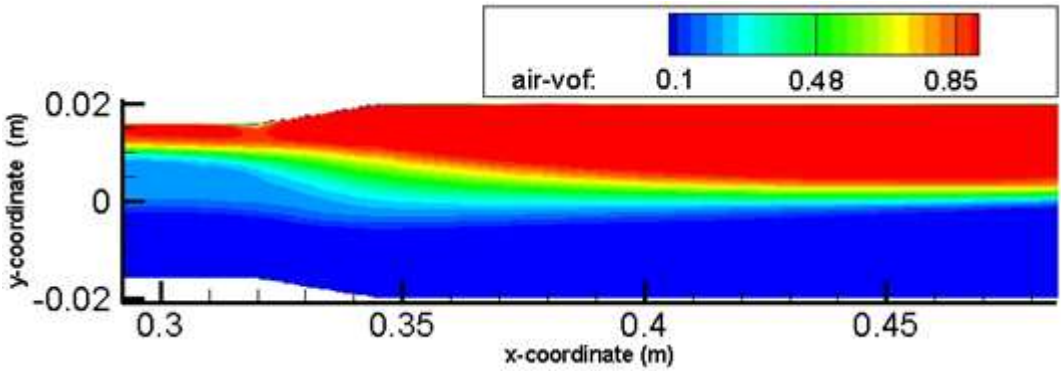

Figure 4.18. Volume fraction of air Q = 0.6Qmax

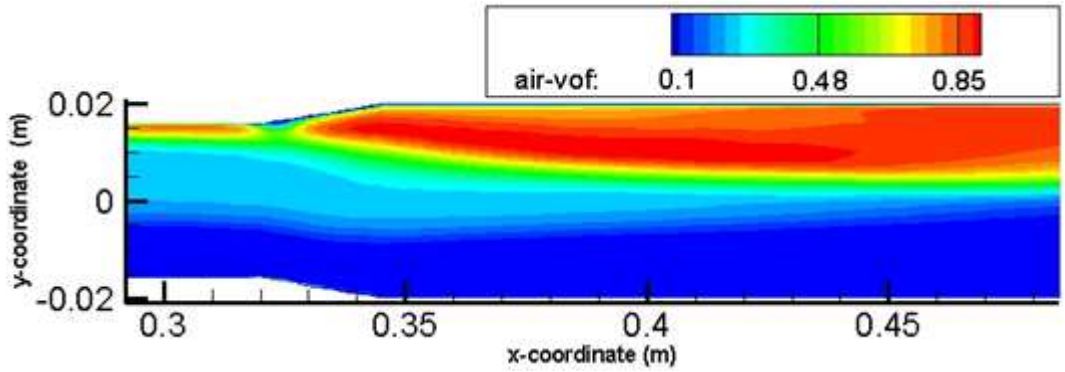

Figure 4.19. Volume fraction of air Q = 0.8Qmax

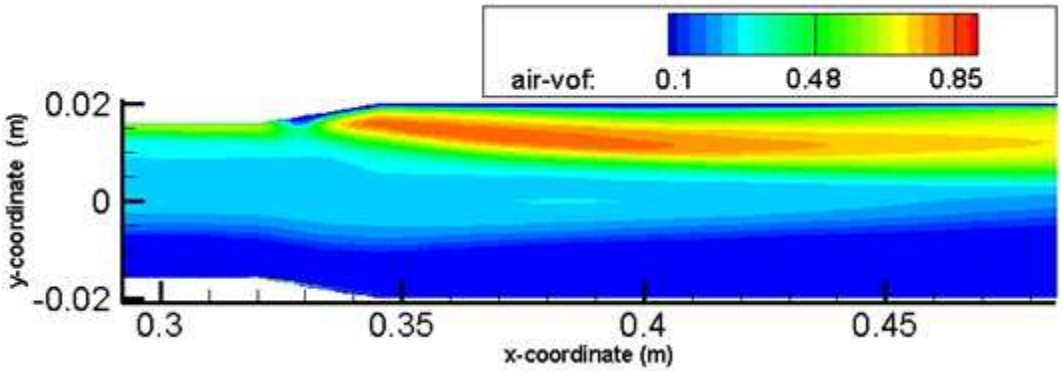

Figure 4.20. Volume fraction of air Q = Q max

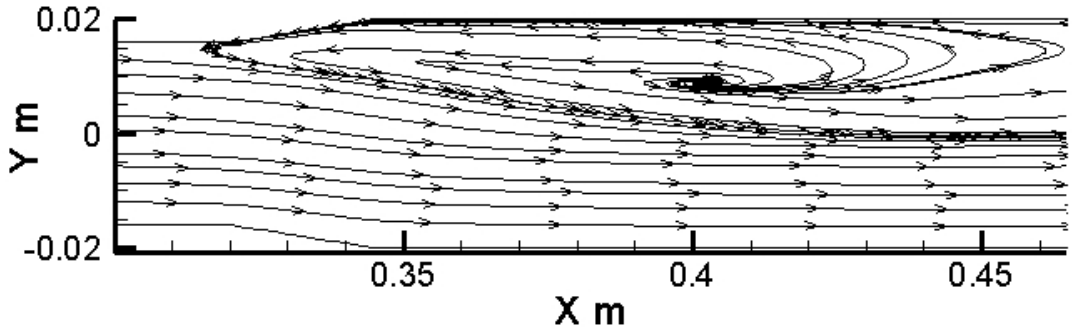

Figure 4.21. Streamlines for Q = 0.4Qmax

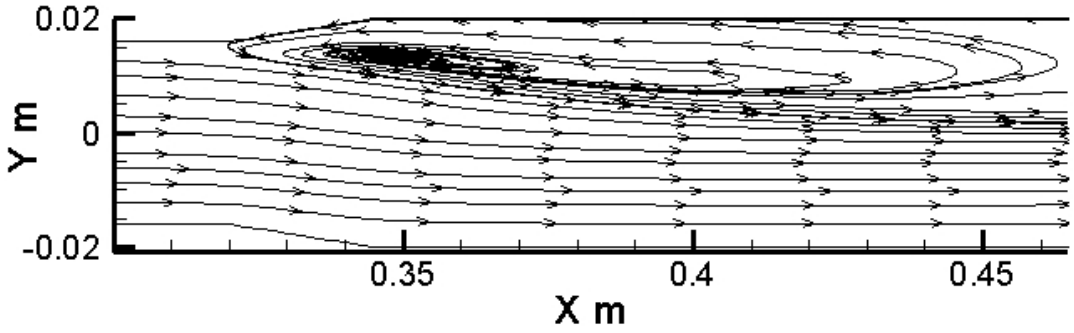

Figure 4.22. Streamlines for Q = 0.6Qmax

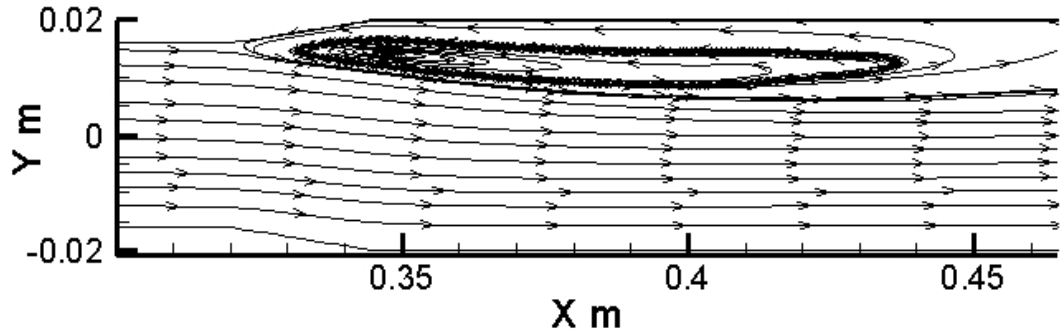

Figure 4.23. Streamlines for Q = 0.8Qmax

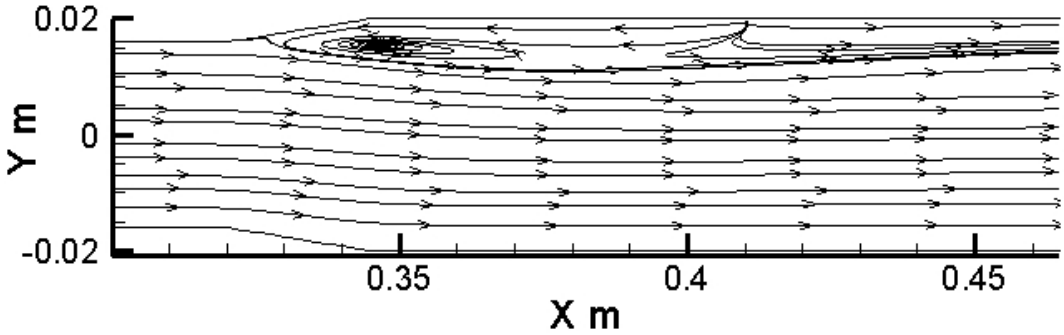

Figure 4.24. Streamlines for Q = Qmax

In Figures presented above, it is seen that for low mass flow rate, phases segregate and void fraction of the air could reach to 100% in certain parts. Streamline of the liquid velocity shows recirculation areas. Big and wide

recirculation areas are created by low-velocities. Existence of such recirculation zones makes numerical convergence difficult. This effect can be observed from Figure 4.25. The residuals for the case of 0.4Qmax are higher than the other cases.

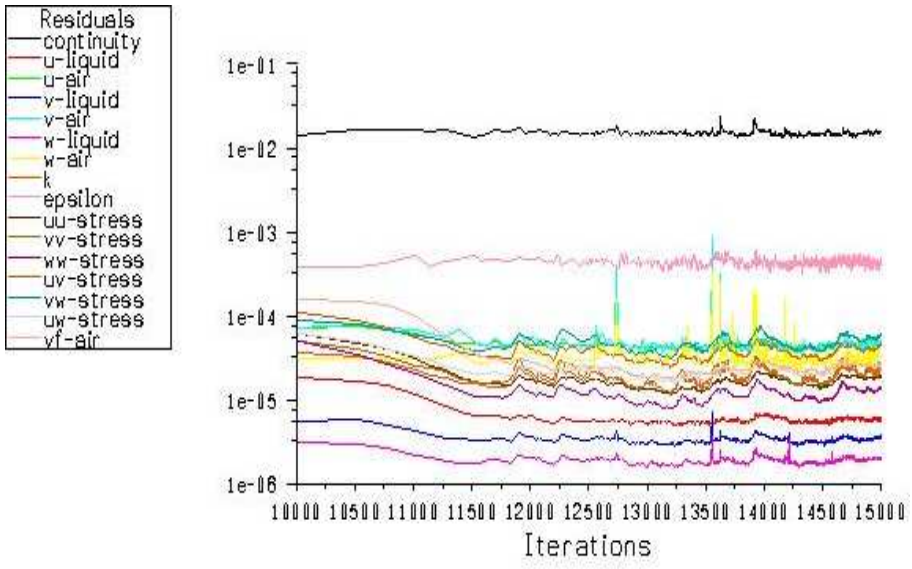

Figure 4.25. Residuals for the case of Q = 0.4Qmax

Pressure drop is directly proportional to the square of the flow rate (see Eqn. 1.29). For this reason, the total pressure-drop along the pipe decreased with the mass-flow rate. Figure 4.26 shows consistent results with this relation.

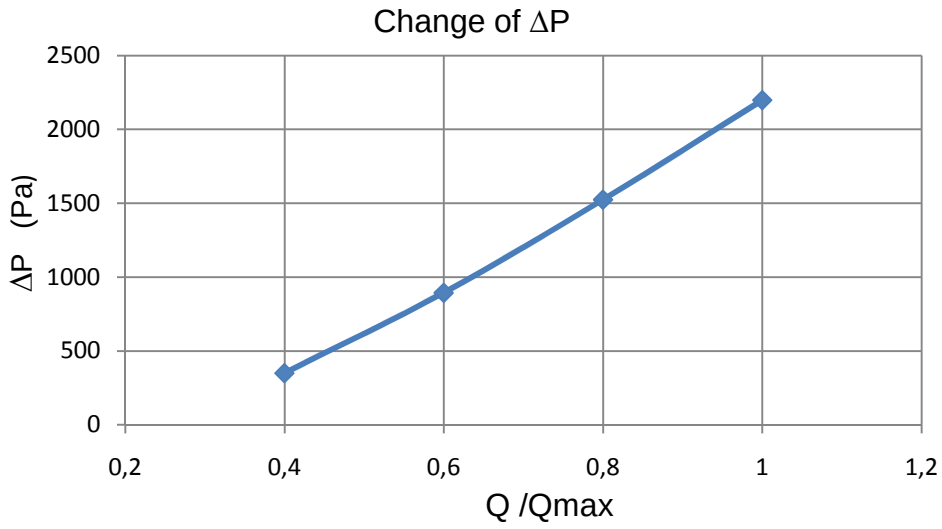

Figure 4.26. Change of ΔP

4.2.3 Effect of Void-Fraction

In this section, the results of analyzing the effect of void fraction on the static-pressure recovery are presented. It must be stated expressly that the inlet flow area is constant. Therefore, the boundary condition for void fraction depends on the air-flow rate directly (thus velocity of air) at the inlet. To see the effect of the void-fraction, mass-flow rate of the water was assumed constant for all simulations of this study. In the simulations, “no-slip velocity” condition at the inlet is assumed. This assumption is reasonable because the air is pumped into the pipe quite far from the singularity and the inlet boundary in the numerical model as well. Thus, for keeping water flow rate constant, the velocity values for the mixture are calculated differently for different cases in accordance with the no-slip condition. Table 4.2 shows the flow parameters of the simulations. Void fraction distributions are shown in Figures 4.27 through 4.34.

Table 4.2. Flow parameters of the simulations in presented in section 4.2.3

Qair (m^3/s)	1.3E-4	2.7E-4	4.3E-4	6.25E-4
Velocity (m /s)	3.9	4.14	4.4	4.67
Void Fraction	5%	10%	15%	20%
Qwater (m^3/s)	2.45E-3	2.45E-3	2.45E-3	2.45E-3

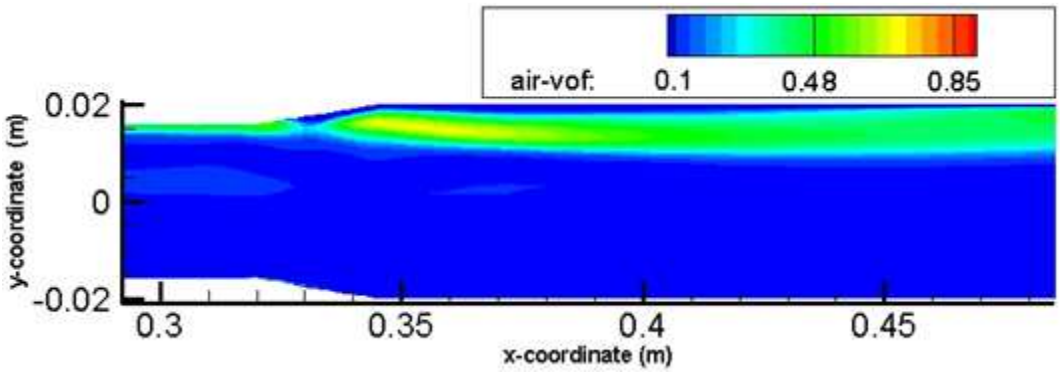

Figure 4.27. Volume fraction of air, α = 5 %

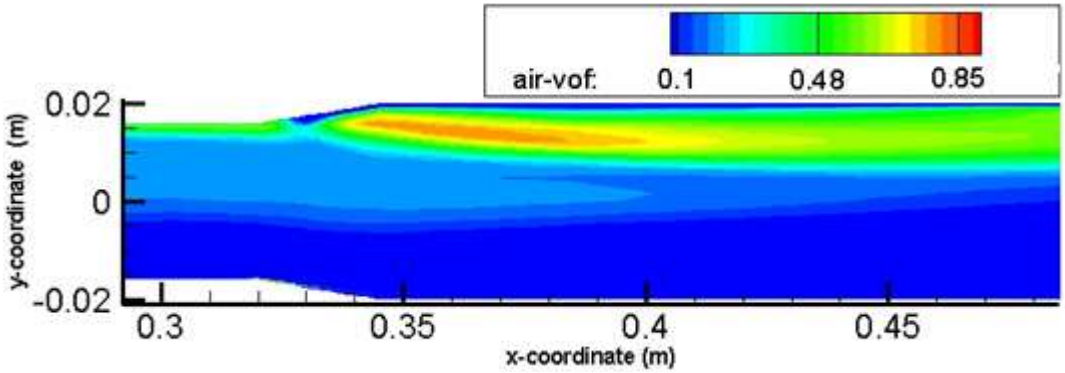

Figure 4.28. Volume fraction of air, α = 10 %

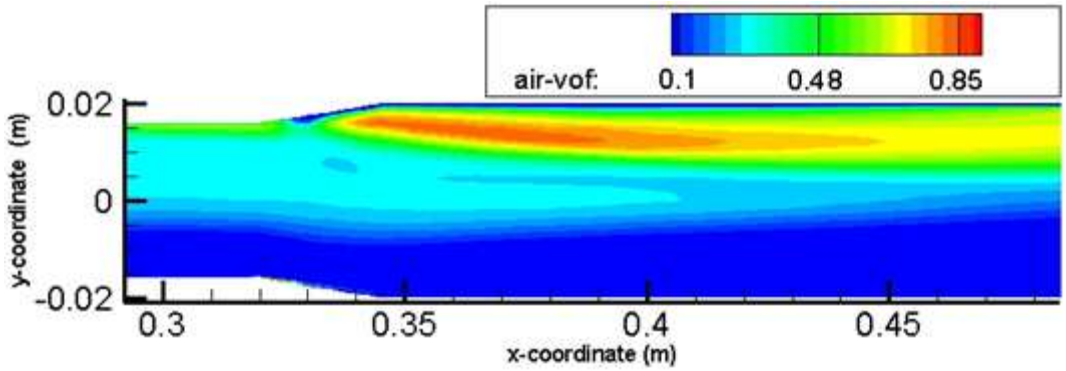

Figure 4.29. Volume fraction of air, α = 15 %

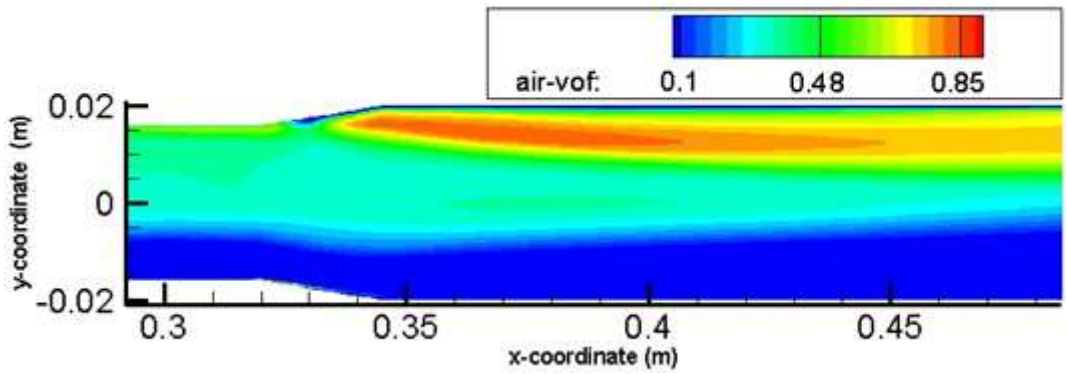

Figure 4.30. Volume fraction of air, α = 20 %

As presented in Figures 4.31 through 4.34, increasing void fraction causes a change of the static – pressure recovery. Difference between regular pressure losses before widening is caused by different velocities of the simulation cases that we indicate at the start. Higher void fraction is applied using higher velocity in the model.

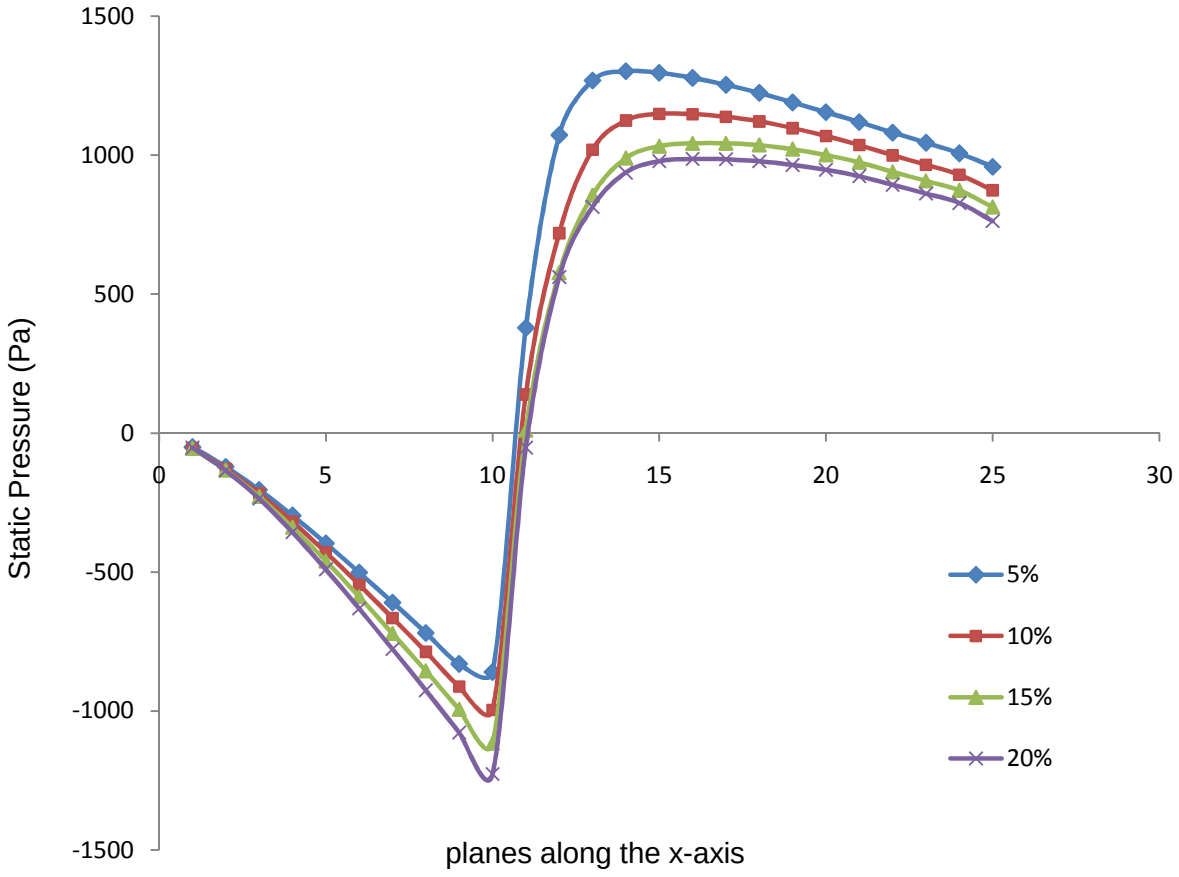

Figure 4.31. Static pressure (Pa)

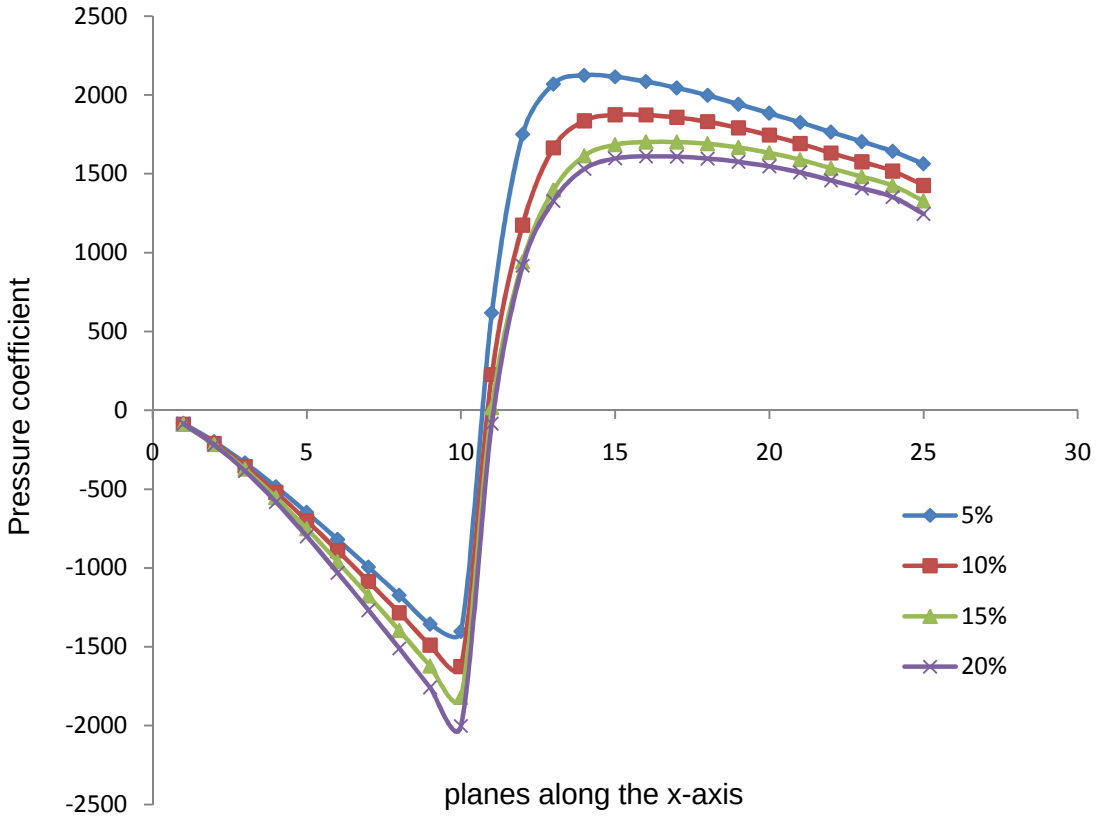

Figure 4.32. Pressure coefficient

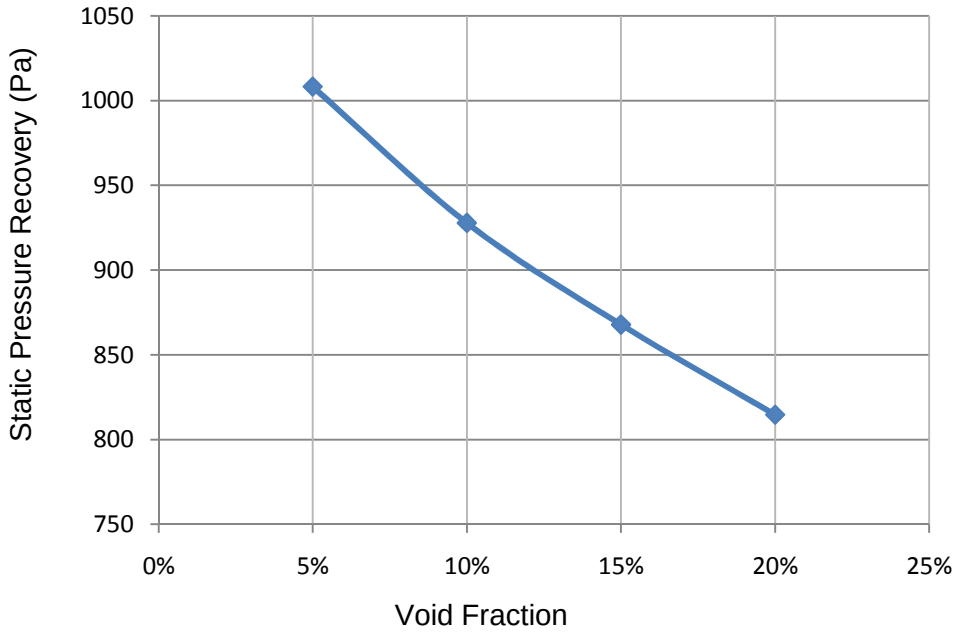

Figure 4.33. Static pressure recovery (Pa)

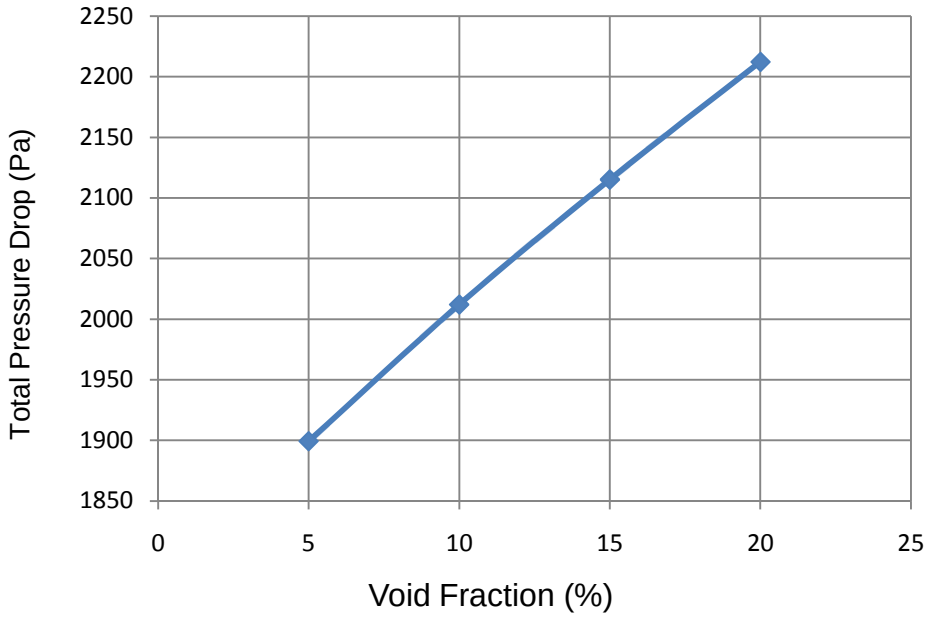

Figure 4.34. Total pressure drop (Pa)

As discussed earlier, results show that bubble diameter effect on the total pressure drop is small and there is no significant difference between the results when bubble diameters are 0.1 mm and 1 mm. On the other hand, results show higher total pressure drop for higher mass flow rate and void fraction.

Effect on static pressure is more complicated than the total pressure. In accordance with the velocity of the primary phase after and before the expansion of pipe, graphs show different recoveries of the static pressure. In the part of bubble diameter effect, same velocity of the primary phase showed same regular pressure loss before the expansion and this velocity changed in the expansion zone of the channel directly proportional with flow area that is left by bubbles. Other static pressure graphs show different regular pressure losses for different liquid velocities. Thus it is more reasonable to take the static pressure recoveries into account for the analysis. Recovering of pressure after the expansion is easy for smaller bubbles at lower void fractions.

4.2.4 Void-Fraction Effect in Convergent Pipe

In this sub-section of the parametric study, the results of void fraction effect analysis for a convergent channel are presented shortly. Table 4.2 shows the operating conditions for this case. In the simulations constant bubble diameter is equal to 1 mm.

Table 4.2. Flow conditions of the simulations performed for the convergent pipe

Velocity (m /s)	3.24	3.4	3.6
Void Fraction	10%	13.88%	20%
Qwater (m^3/s)	2.45E-3	2.45E-3	2.45E-3

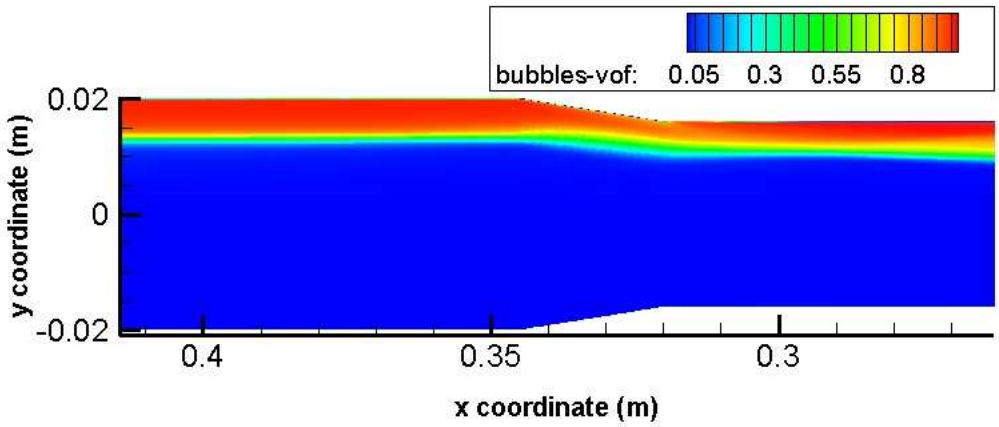

Figure 4.35. Volume fraction of air, α = 10 %

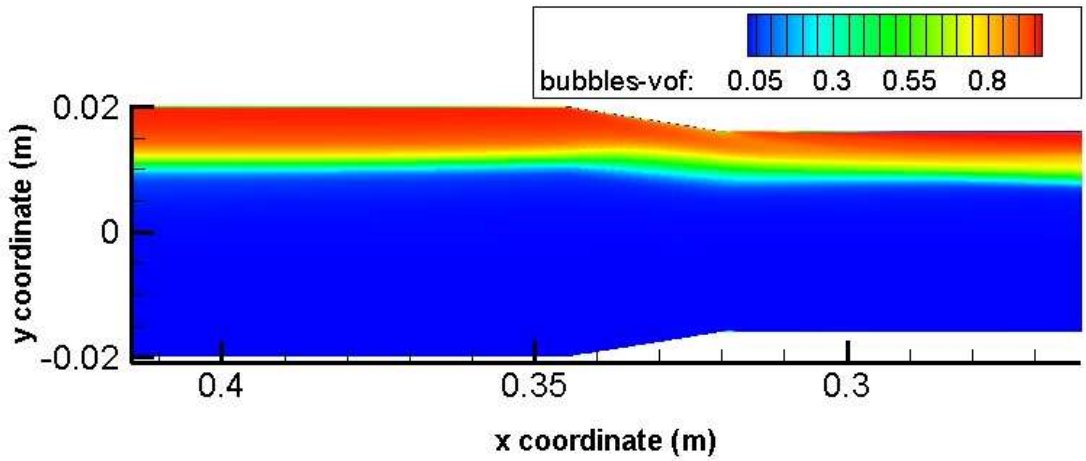

Figure 4.36. Volume fraction of air, α = 13.875 %

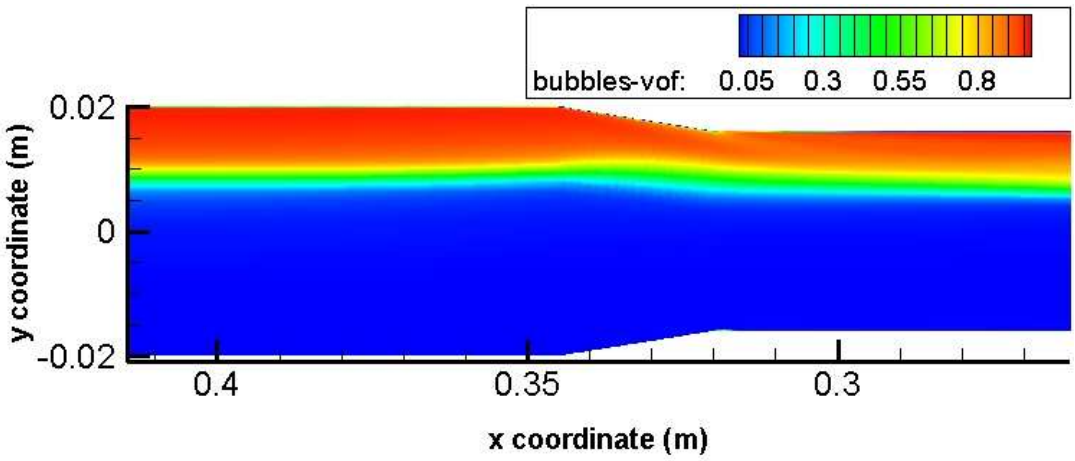

Figure 4.37. Volume fraction of air, α = 20 %

As mentioned before, one of the main focuses on this study is to get experience about how static pressure changes with different flow parameters. In Figure 4.38 static pressure change calculated is seen along the flow direction x. First sharp decrease at point seven is because of starting of contraction. In this convergent pipe case, it can be concluded that void fraction of the mixture does not affect the static pressure significantly.

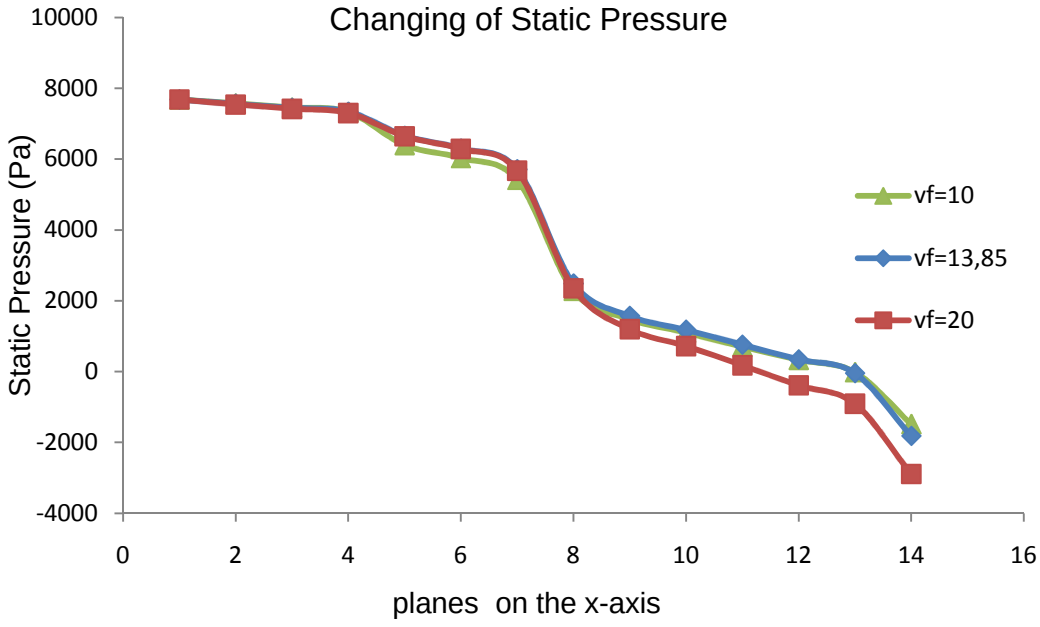

Figure 4.38. Static pressure along the x-axis (Pa)

4.3 Validation of the Two-Fluid (Eulerian) Model

Experimental data used in the validation part is taken from the reference study [1] performed in VKI. Experiments of two phase flows studied in this work were performed in VKI by other researchers listed in the reference work [1]. Among their studies, other experimental data related with the subject of this study could be found in [18] and [19].

In the presented part of the study, validation of “Eulerian Model” using these experimental data is studied. To do this, two different diameter ratios for the pipe are used for two different validation processes in accordance with experiments. First case is used for comparison of void fraction profile on setup of 32/40 type. Second one is used for comparison of static pressure data on setup of 65/80 type. All experiments mentioned here are performed for divergent flow [1].

4.3.1 Validation with Void Fraction Profile

In the analysis presented in previous sections, “Outflow Boundary” condition is used at the outlet boundary. This boundary is restricted by FLUENT in case of Eulerian multiphase models. However, convergence difficulties with low velocities, time problem and existence of a reference case which uses outflow boundary in similar geometries [20] direct the study to prefer this boundary type in the part of parametric study [1]. In this part of the validation work, first attention is given to finding a way to use “Pressure Outlet Boundary” as it is recommended by FLUENT. It is important to see actual capability of the model in accordance with code developer’s instruction.

In previous works, the main difficulty of using “pressure outlet boundary” is reverse flow at the outlet boundary where there should not been any reverse flow. According to FLUENT Manual, there are specific reasons to get “reverse flow” at the outlet if there is not any real flow into the modeled domain. The reason could be grid resolution or setting of correct turbulence parameters. Some of the recommended solutions are about grid resolution near the outlet.

This could be done by generating more cells or make the geometry longer along the axial direction. First option was tried before [1] and it didn't work. In this part of the study 32/40 type geometry is changed along the x-dimension and a longer geometry is created in accordance with new and fast computational system. With this new geometry, "Pressure outlet" boundary condition could be used without getting any reverse flow which is not expected in our model. Dimensions of the geometry can be seen in Table 3.1 as 32/40 II and Figure 4.39 shows new geometry.

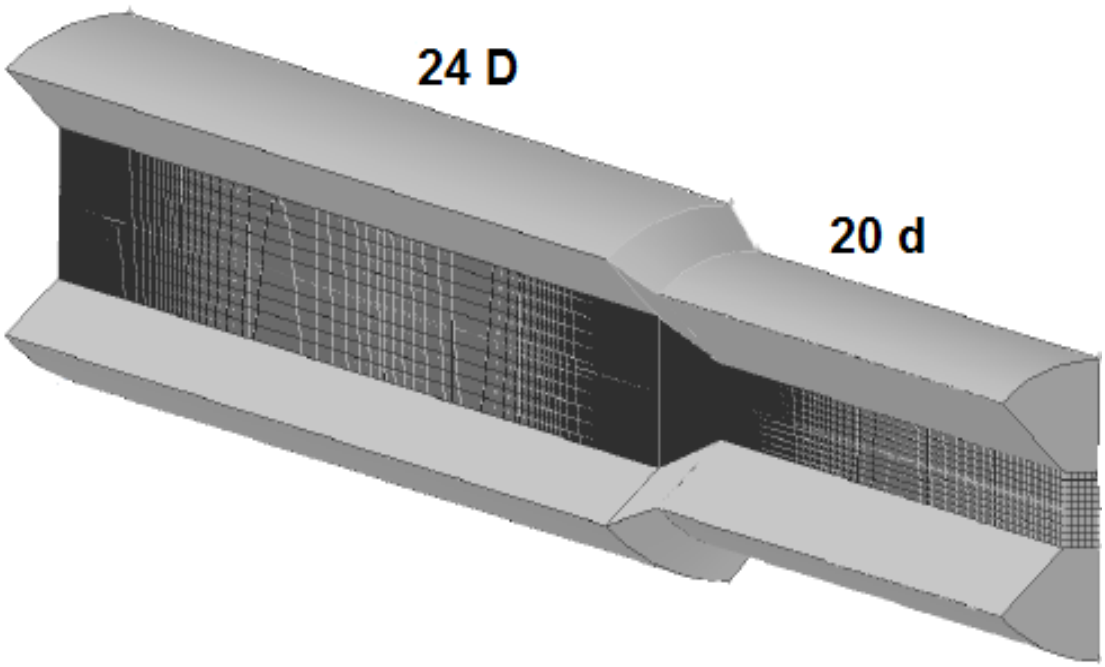

Figure 4.39. New dimensions of the geometry I

In this first part of the validation work for numerical simulations, experimental data for void fraction is studied. The data were taken on 32/40 type experimental setup. Experiment and numerical simulations have been performed in following conditions;

Q_{water} = 3 x 10^{-3} m³/s, U_{∞} = 5.3 m/s

Q_{air} = 4.8 x 10^{-4} m³/s α = 13.88 %

For comparison, three different locations were used [1]. These are position 1 at “- 6d” from inlet of expansion zone at the upstream, and position two at “6d” and position three at ”16d” from outlet of the expansion zone in the downstream. Figure 4.40 shows vertical profile lines on symmetry plane at three different positions.

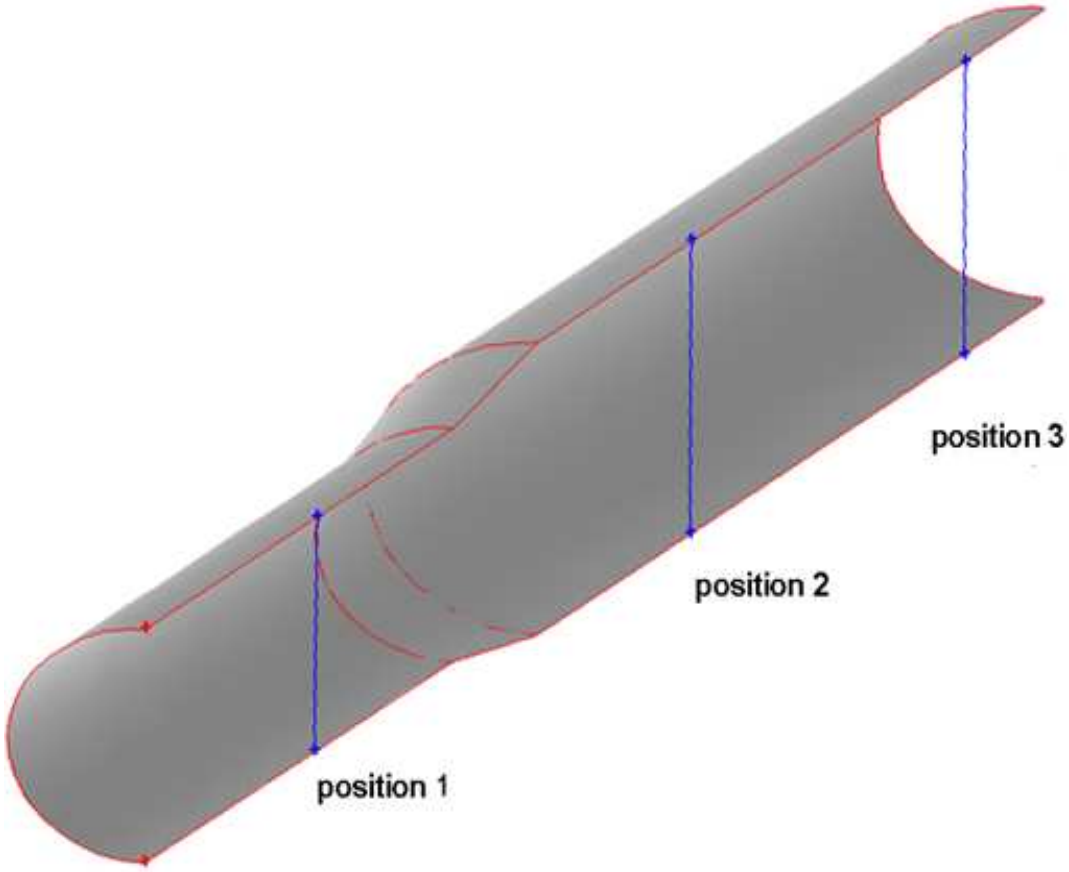

Figure 4.40. Positions of vertical lines for void fraction data in experiment

Figure 4.41 and 4.42 show contour plots of void fraction distribution on symmetry plane with vertical lines for experimental data. Contours show core region for void fraction after the expansion.

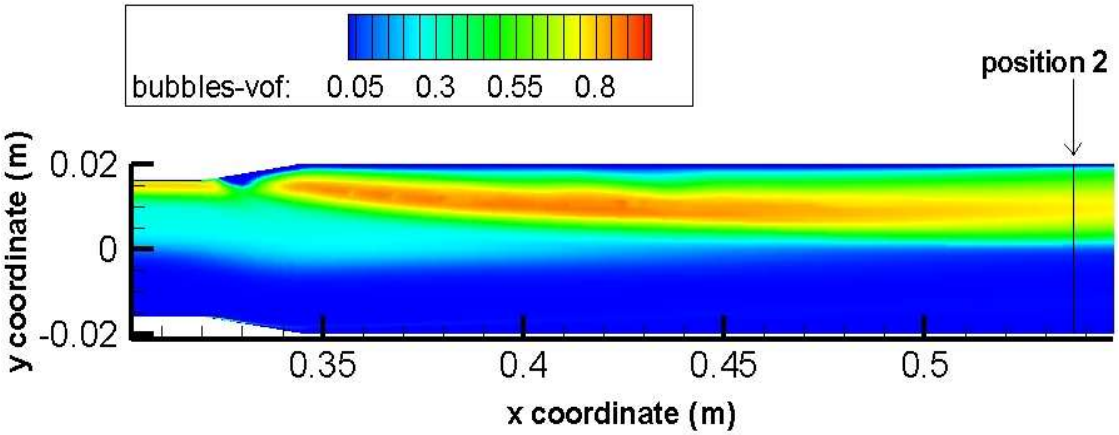

Figure 4.41. Contour plots of void fraction along the symmetry axis

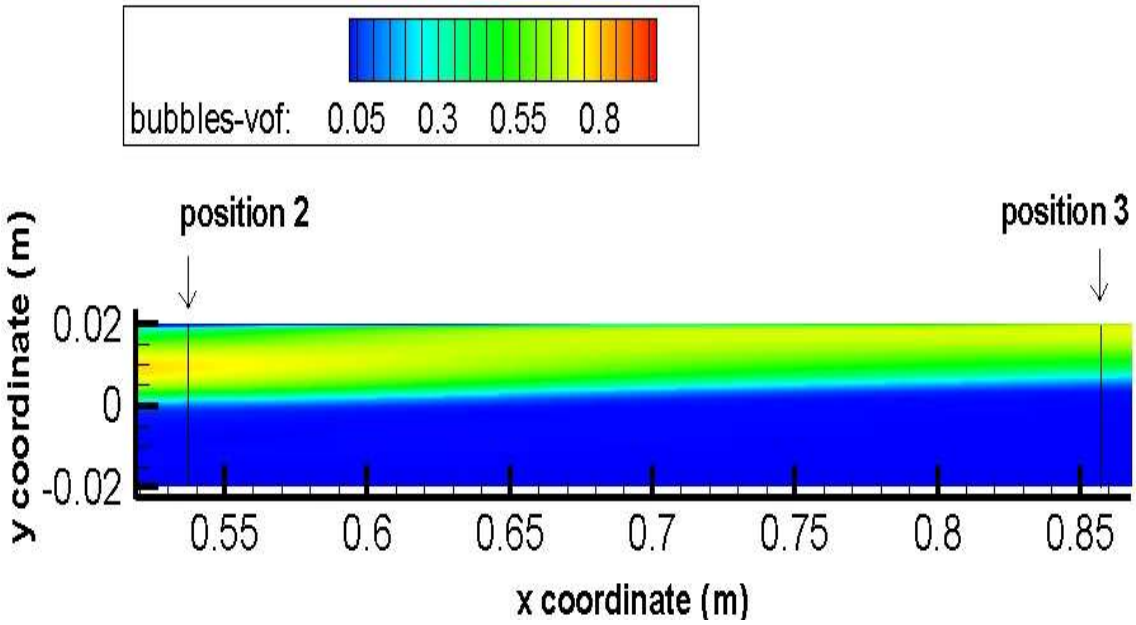

Figure 4.42. Contour plots of void fraction along the symmetry axis

In section 4.2.1, it was stated that bubble diameter has an effect on the void fraction distribution in the pipe. Because of this reason, validation was performed using different bubble diameters. Figure 4.43 and 4.44 show comparison between experimental data and simulation results of different bubble diameters at position 2. According to figures, 1 mm and 0.8 mm are more realistic values for bubble diameter than smaller diameters.

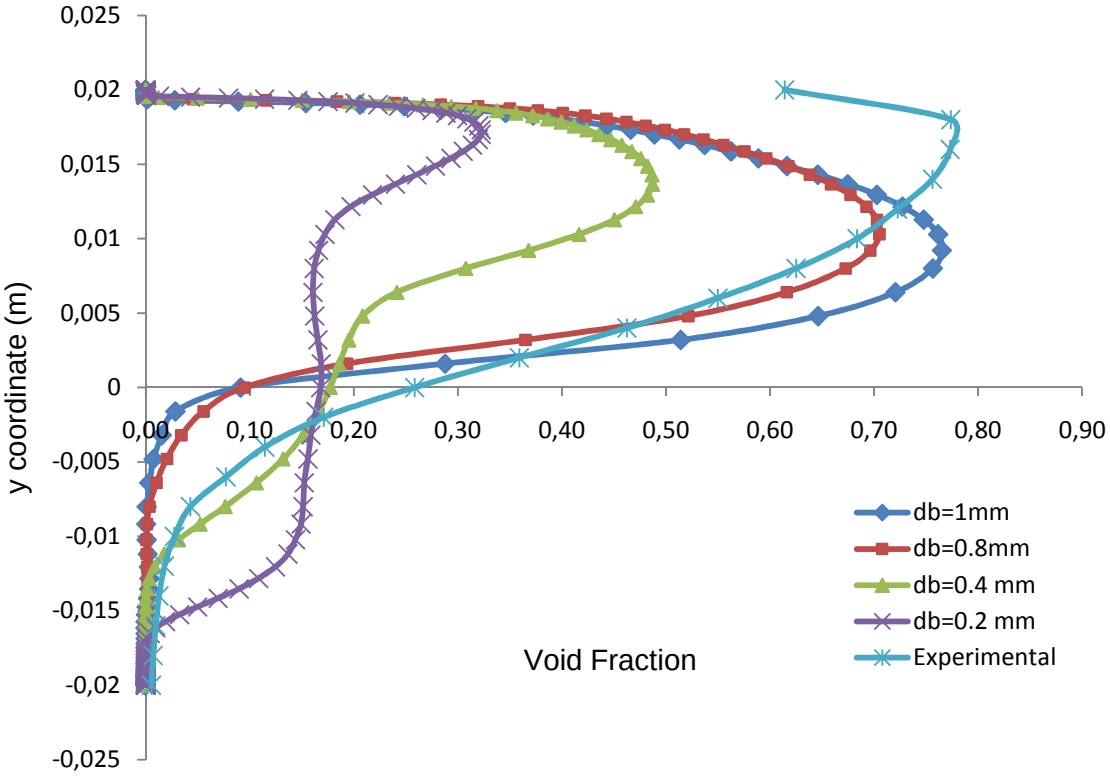

Figure 4.43. Vertical void fraction profiles for different bubble diameters at position 2

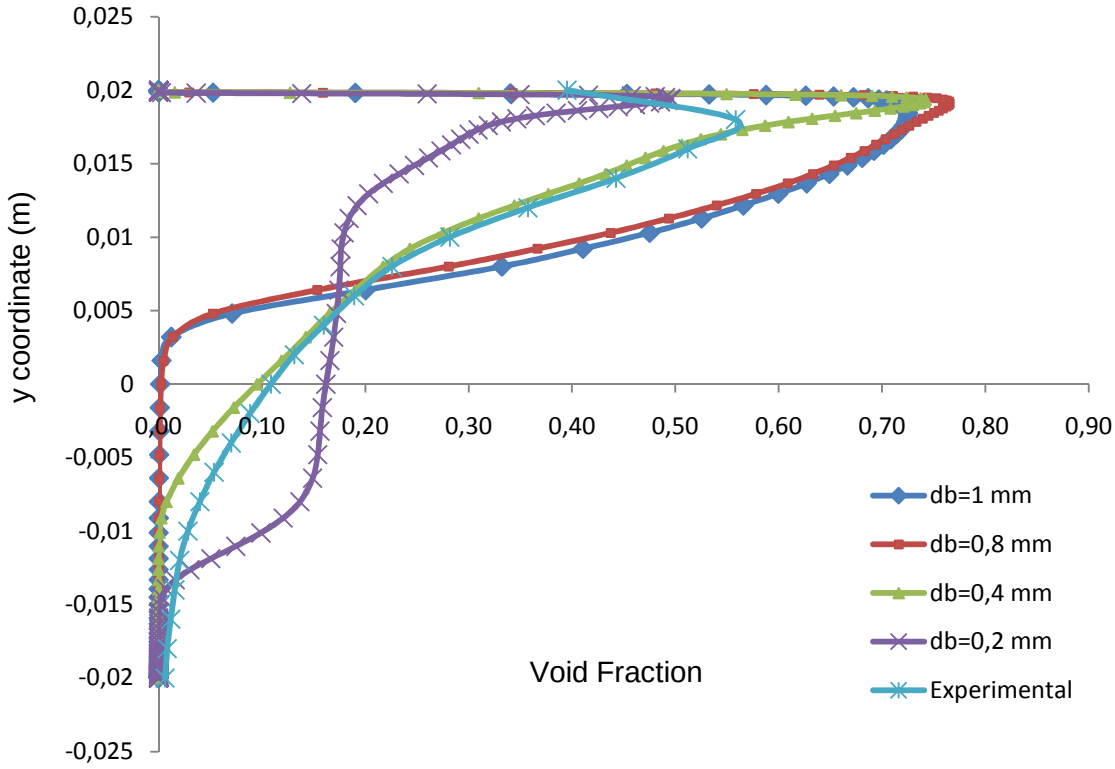

Figure 4.44. Vertical void fraction profiles for different bubble diameters at position 3

Figures show a good agreement between the experimental data and the numeric result at position 2 in terms of the magnitude. However, model under predicted stratification of bubbles. When it is assessed with next position, it can be concluded that model missed the main flow behavior at core region of flow and separation of flow on the wall. Thus, over predicted void fraction profile at position 3 seems expected. The main reason of this could be neglection of lift force in the momentum equation. Lift force generally is smaller than the drag force in terms of magnitude. However, some type of flows like quickly separated flows have lift force as big as the drag force.

During the validation, some horizontal profiles of void fraction along y = 0 axis were also investigated. The best prediction is achieved at position 2. It is shown below in Figure 4.45. Model could predict void fraction at this position successfully. On the contrary of this, other horizontal void fraction profiles show disagreements with experimental data and they are not shown here.

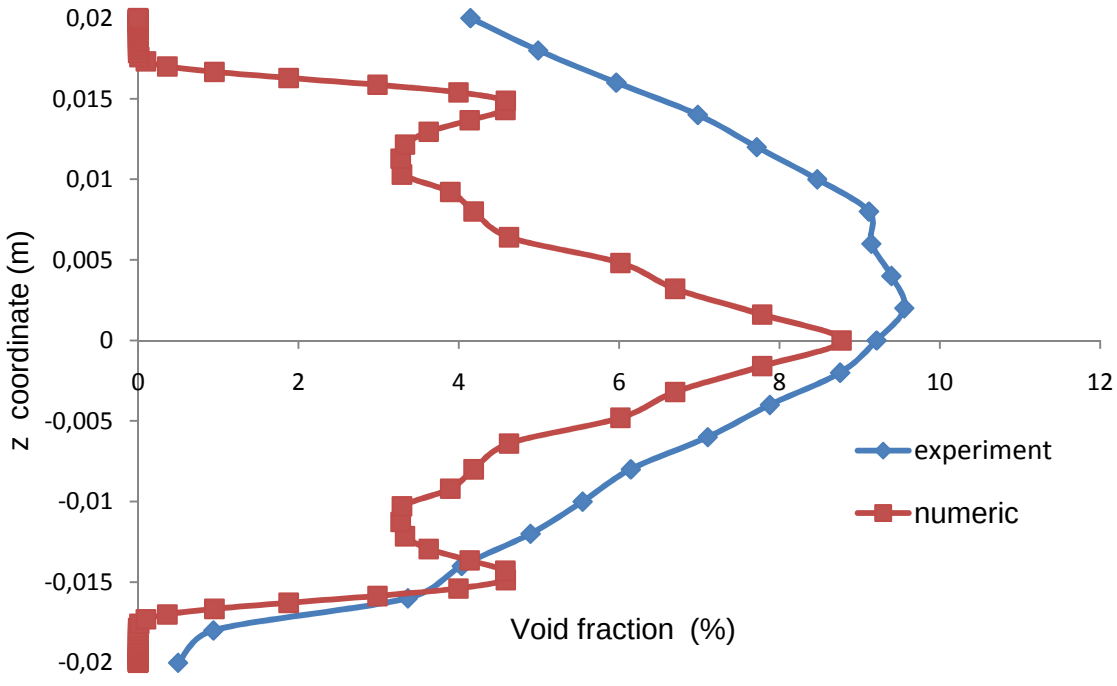

Figure 4.45. Horizontal void fraction profiles at x = 0.537 m / downstream for db = 1mm

Figure 4.46 represents the residuals of the simulation. The model converged good enough for this type of simulations. Mass imbalance between the inlet and outlet after the convergence is in the order of 1/1000.

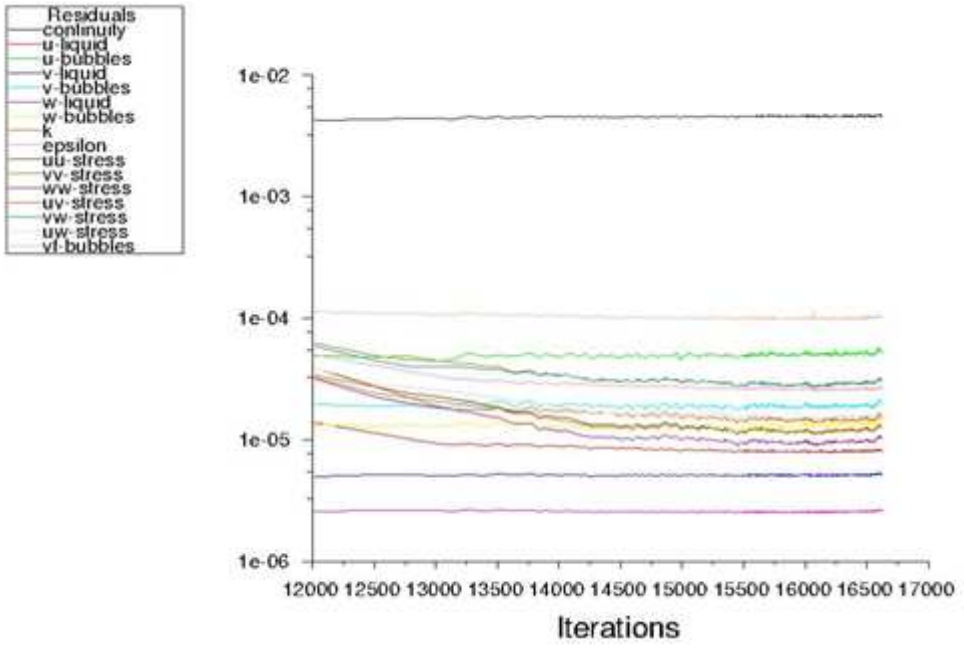

Figure 4.46. Residuals of the simulation for db = 1mm

At the inlet boundary slip ratio is chosen as equal to unity. Figure 4.47 and 4.48 shows that this ratio is preserved in general part of the flow.

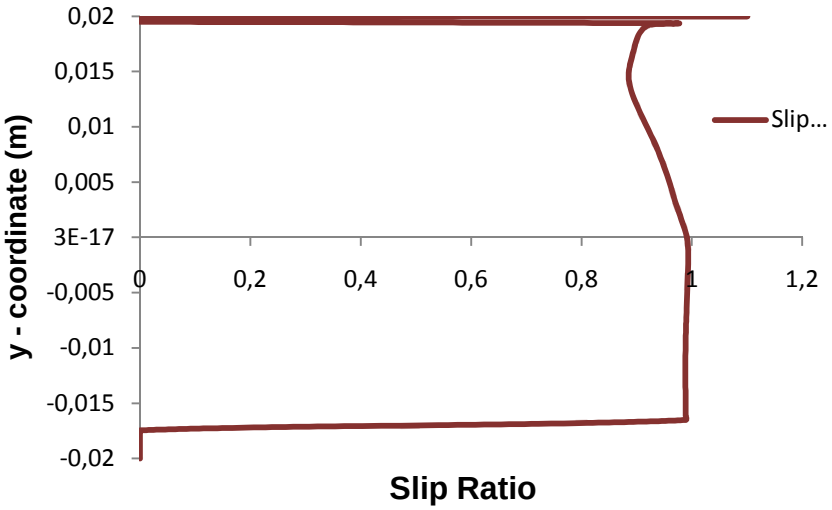

Figure 4.47. Slip ratios at position 2 / downstream

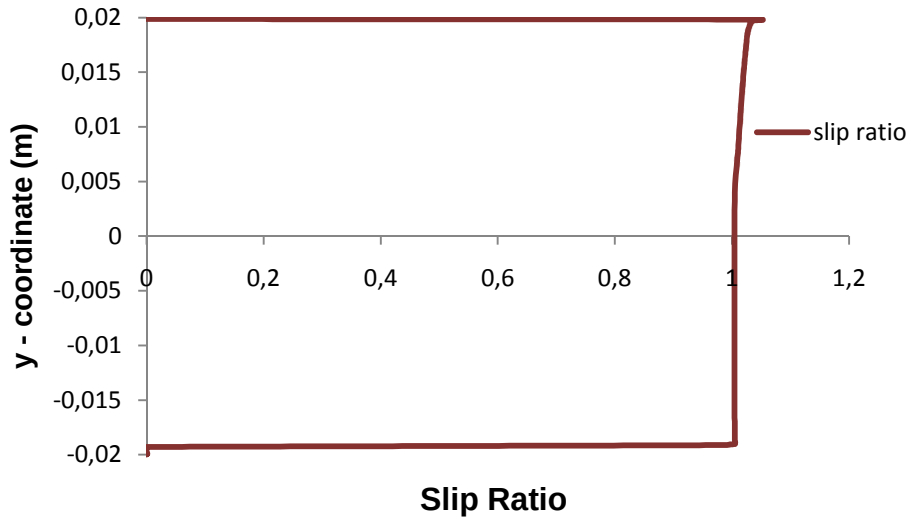

Figure 4.48. Slip ratios at position 3 / downstream

4.3.2 Validation with Static Pressure Data

In this section of the work, “Eulerian two-phase flow model” is tested using static-pressure data [1]. The chosen geometry is experimental setup of 65/80 type. Model parameters are shown below;

Q_{water} = 8.4 x 10^{-3} m³/s, U_∞ = 3.4 m/s

Q_{air} = 5.4 x 10^{-3} m³/s, α = 2.08 %,

Velocity was chosen same for each phase at the inlet boundary like the previous section. Again numerical simulations were performed with different bubble diameters. Figure 4.49 shows comparison between experimental data and the numerical results.

In the Figure 4.49, curves for experimental data represent two different pressure readings from two different locations in the expansion zone. As the figures present, two different bubble diameter cases result in the regular pressure loss in the upstream section in a good agreement with the experimental data. However after the divergence they show different pattern and agreement with experimental data in different locations.

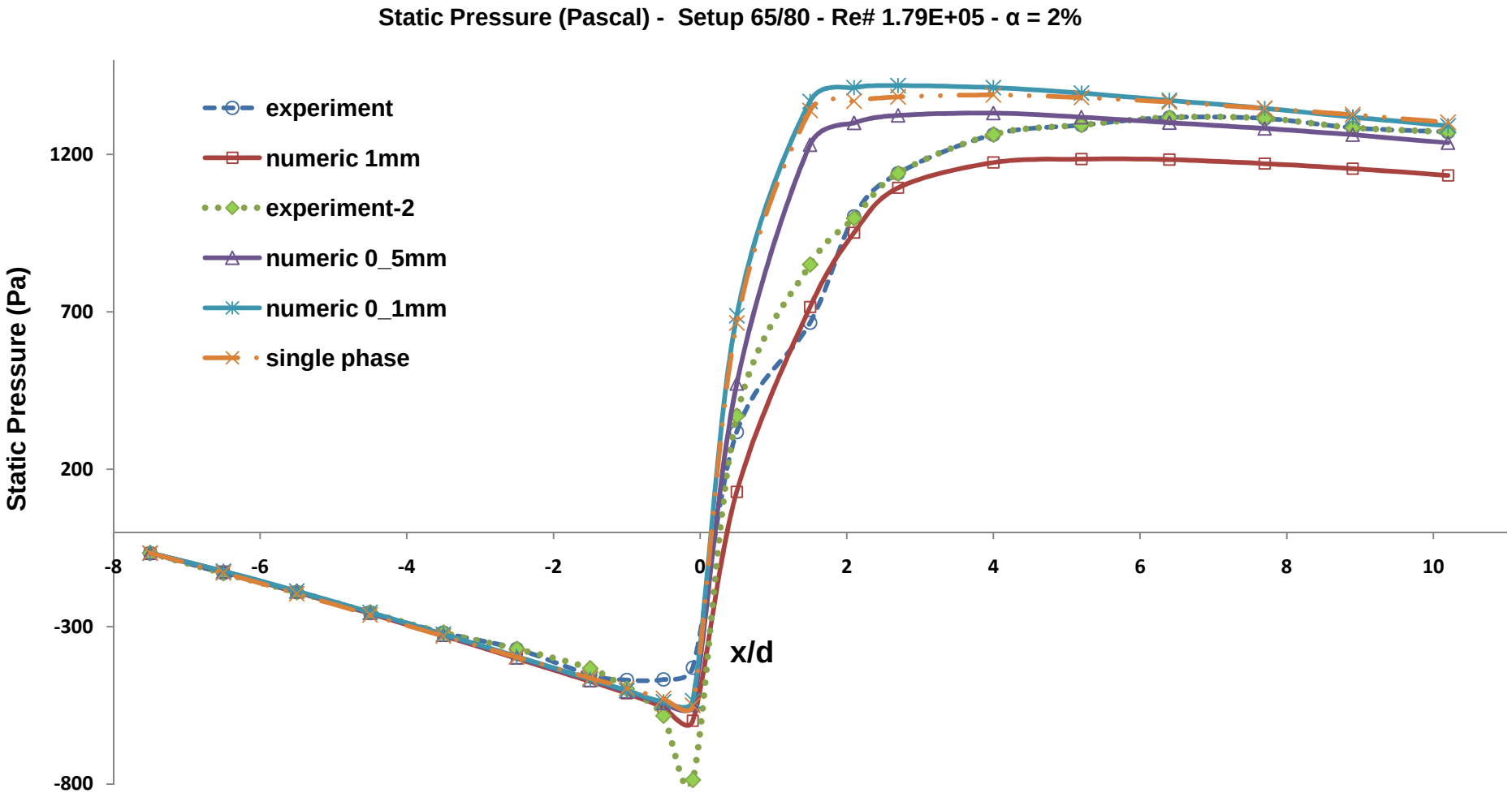

Figure 4.49. Static pressure changes along x axis

For example 1mm bubble diameter case represents the static pressure pattern inside the singularity but it underestimates the total static pressure recovery. On the other hand bubble diameter of 0.5 mm case predicts the order of static pressure value and the regular loss of after the singularity.

It can be concluded that the reasonable bubble diameter is 0.5 mm for this case. Therefore bubble diameter has not an effect on static pressure as much as on the void fraction.

In validation part, two-fluid approach could predict the vertical void fraction profiles with an error between % 1 and % 30 at positions 2 and 3 respectively. In the second part of the analysis, the results show that the static pressure can be predicted with an error range of % 1 for 0.1 mm and 0.5 mm bubble diameters and % 20 for 1 mm bubble diameters.

4.4 Comparison of Different Type of Outlet Boundary Conditions

Section 4.2.1 describes the difficulties and reasons of using “pressure outlet” type boundary at the outlet. On the other hand it is mentioned that some parts of this study used “outflow” type boundary. In the literature there is an example of two-fluid approach with outflow condition and it claims that it works [20]. To overcome this confusion, this section of the study compares these boundary condition types. The geometry is shown in Figure 4.39. Main parameters of the model are as follows:

Q_{water} = 3 x 10^{-3} m³/s, U_{∞} = 5.3 m/s

Q_{air} = 4.8 x 10^{-4} m³/s α = 13.88 %,

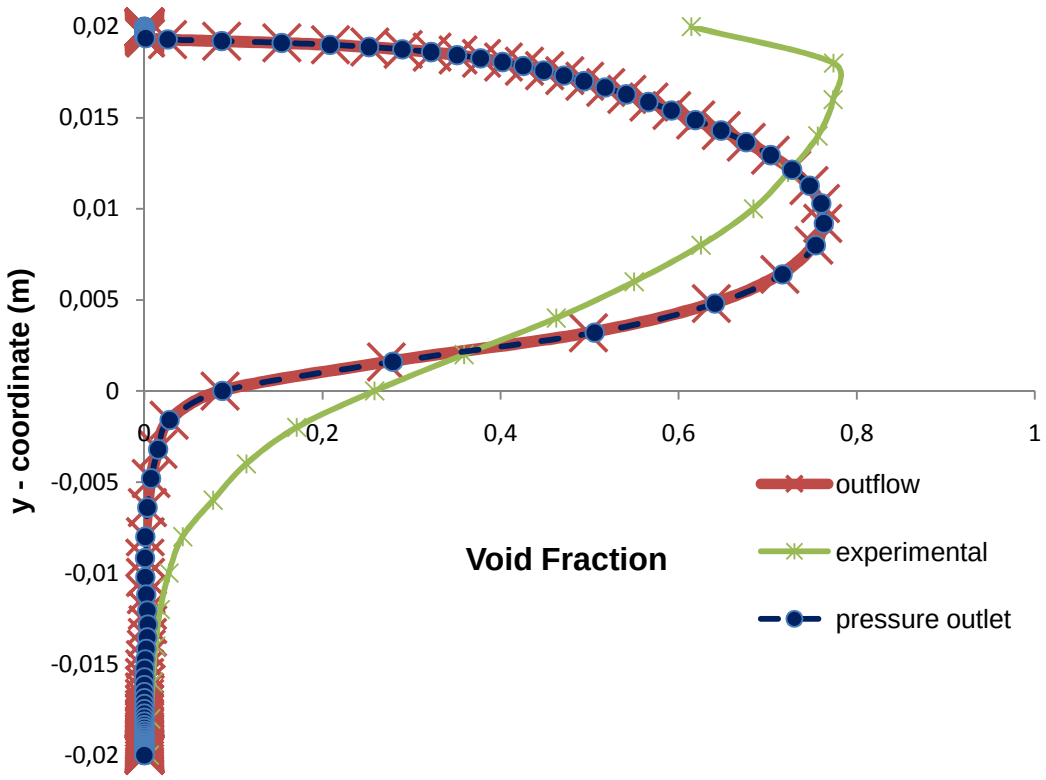

Figure 4.50. Void fraction profile at position 2

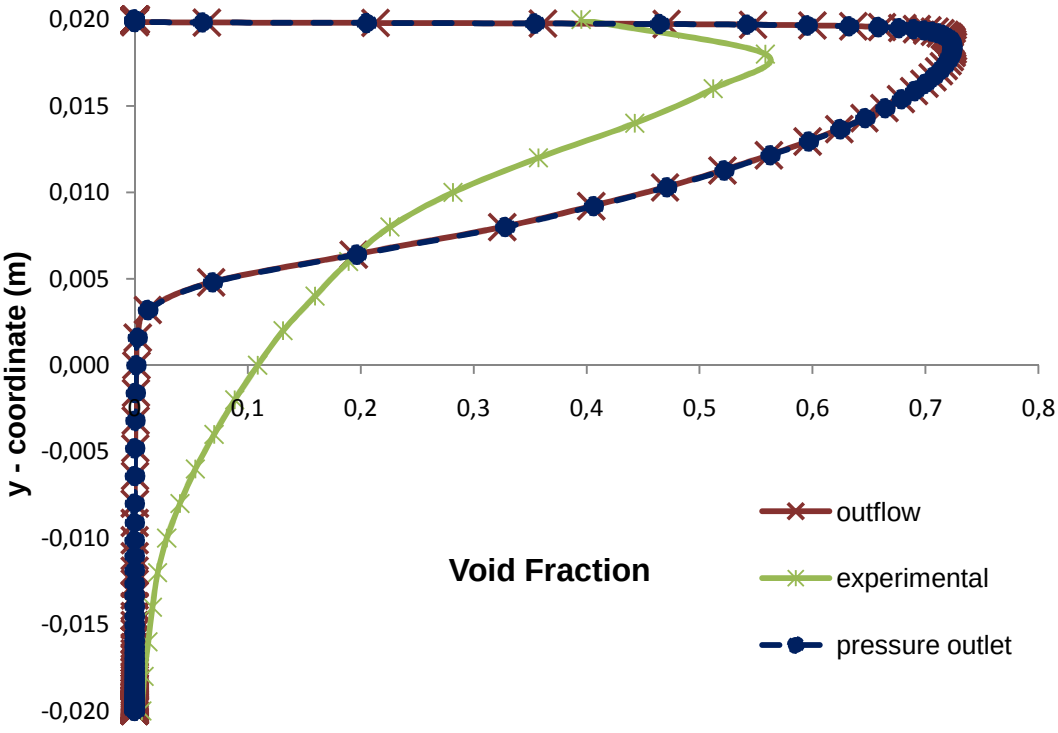

Figure 4.51. Void fraction profile at position 3

Theoretical differences between “outflow” and “pressure outlet” is expected near the outlet boundary. As shown in Figure 4.51, there are not any differences between the models in the region close to outlet. Moreover, results show no difference between predictions of “pressure outlet” and “outflow” boundaries in anywhere. It can be concluded that instead of “pressure boundary condition”, “outflow boundary” could be used properly.

Figure 4.52 shows the residuals of the simulations. If it is compared with Figure 4.46 it can be concluded that convergence of the model using “outflow” type boundary is better than the one with “pressure outlet”.

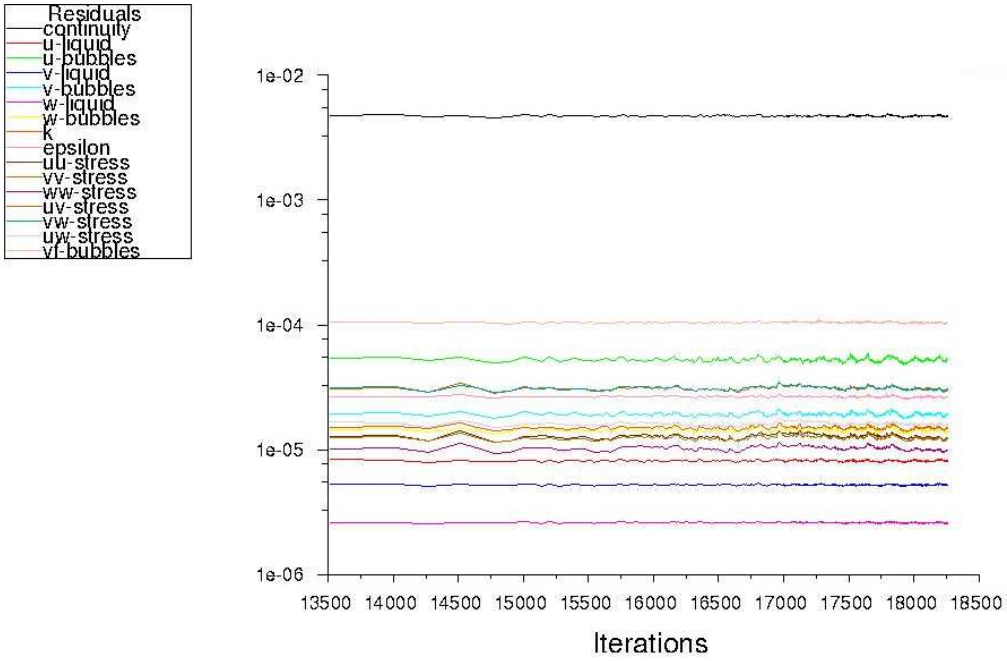

Figure 4.52 Residuals for case of “outflow”

Following parts of the study used “pressure outlet boundary” condition in the simulations in accordance with FLUENT recommendation.

4.5 Comparison of Turbulence Models

As described before, there are not isotropic turbulence conditions in this type of two phase flows and it is not expected that two-equation turbulence models get accurate solutions in these kinds of conditions. However still some attempts were tried and results are shown here to see capabilities of k-e turbulence mixture model in this type of flows. FLUENT has three types of k-e turbulence models. Best fit for the case modeled is the “realizable k-e model”. This model is more powerful in modeling of flow which has recirculation zones and flow separation. Because of the fine grid, “Enhanced wall function” was also used with k-e model. Finally main parameters at the boundaries are same with previous cases. Results are shown below.

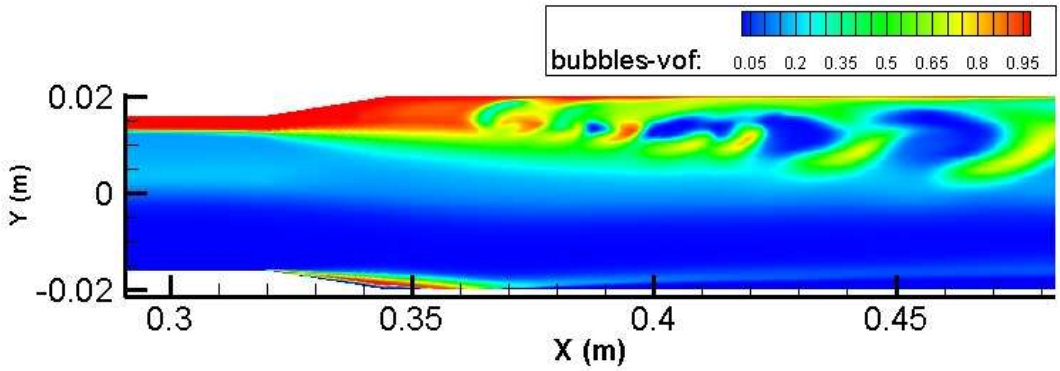

Figure 4.53. Contours of void fraction along the symmetry plane in case of k-e model

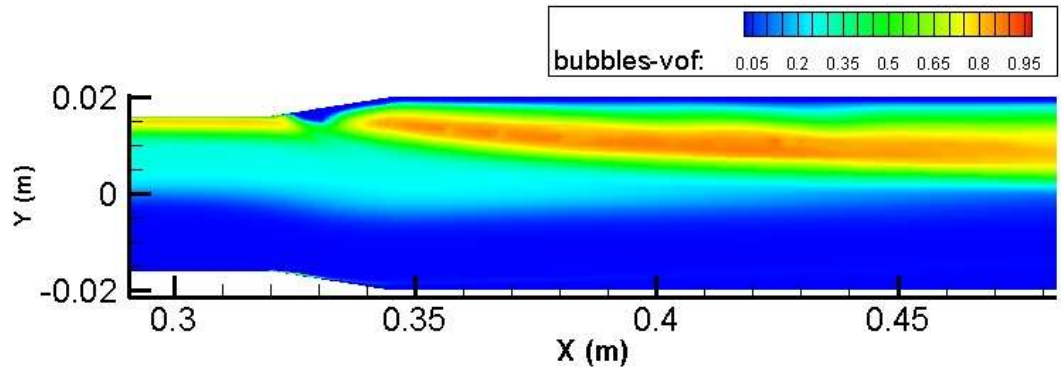

Figure 4.54. Contours of void fraction along the symmetry plane in case of RSM

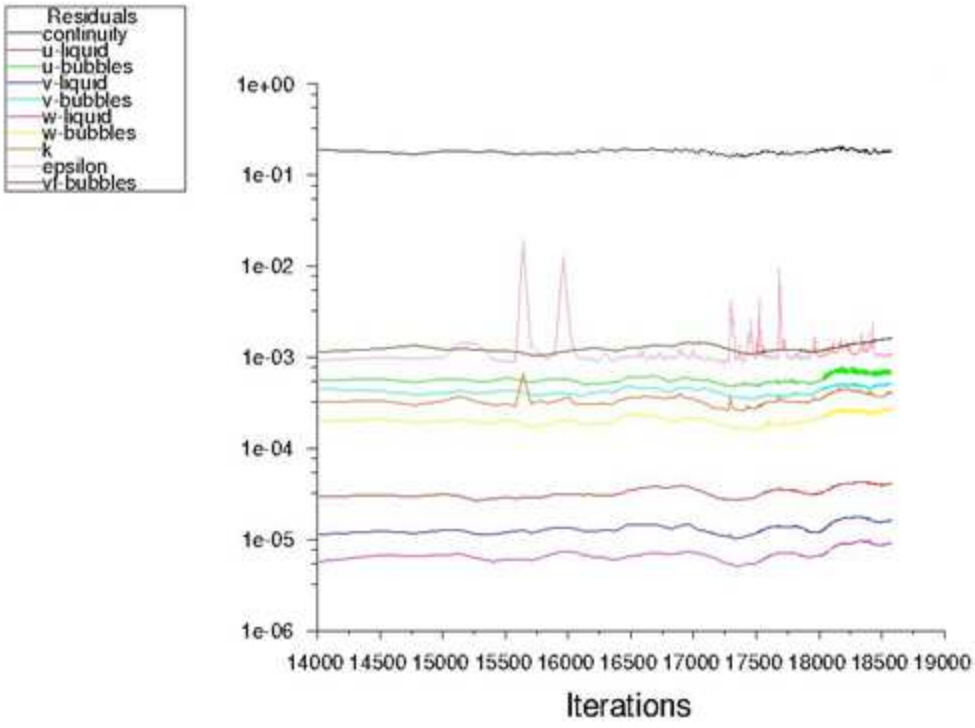

Figure 4.55. Residuals for case of k-e model

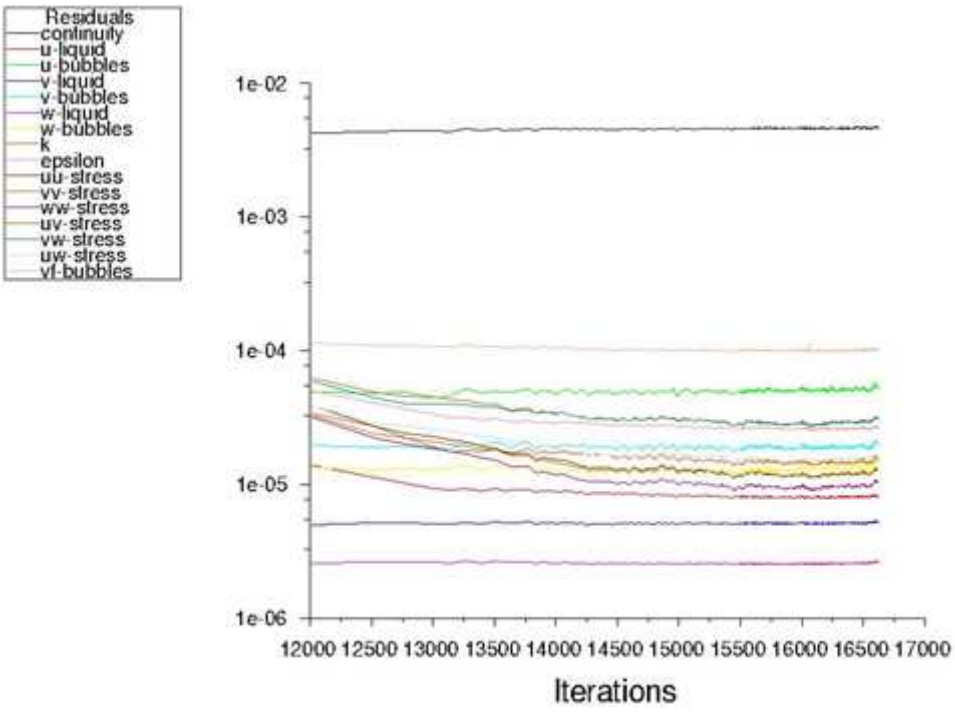

Figure 4.56. Residuals for case of RSM

Two – equation turbulence models can't represent the physics of the flow as it is expected at the beginning. Above Figure 4.55 represents the residuals for the case of k-e. Model did not converge enough. According to the literature, there are some ways to modify two-equation models to use in modeling of this type of two phase flows. However these methods are not applied and discussed here.

4.6 Use of "Interfacial Area Concentration" Model and "Dispersion Effect on Momentum Equation"

As described before, interfacial area concentration (IAC) model is an important parameter for predicting mass and momentum through the interface between phases. On the other hand "dispersion effect" is another option for correction over the momentum equation. In this part of the study, main goal is developing the numerical model results using IAC model on the 32/40 II type geometry. The reference case is the one used for validation work with experimental data of void fraction profiles.

4.6.1 Comparison of IAC Model and "Dispersion Effect" with Reference Case

In this part of the study, these two different modeling options were used to improve numerical results of the two phases modeling in FLUENT. As a reference case to analyze the improvement on the results, the case described in section 4.3 with "pressure outlet" boundary was chosen. Two modeling options were performed on this case which was showed converging. Main parameters and results of the model are shown below:

Q_{water} = 3 x 10^{-3} m³/s, U_{∞} = 5.3 m/s

Q_{air} = 4.8 x 10^{-4} m³/s α = 13.88 %

Moreover, there are other parameters related with interfacial area concentration model. These parameters are as follows:

Inlet IAC concentration = 555 (1/m)

Min. Diameter = 0.0001 m

Max. Diameter = 0.01 m

Coalescence & Breakage Kernel = Ishii – Kim

Diameter = Sauter Mean Diameter

Figures 4.57 and 4.58 show the comparison of the results of different model options with experimental data.

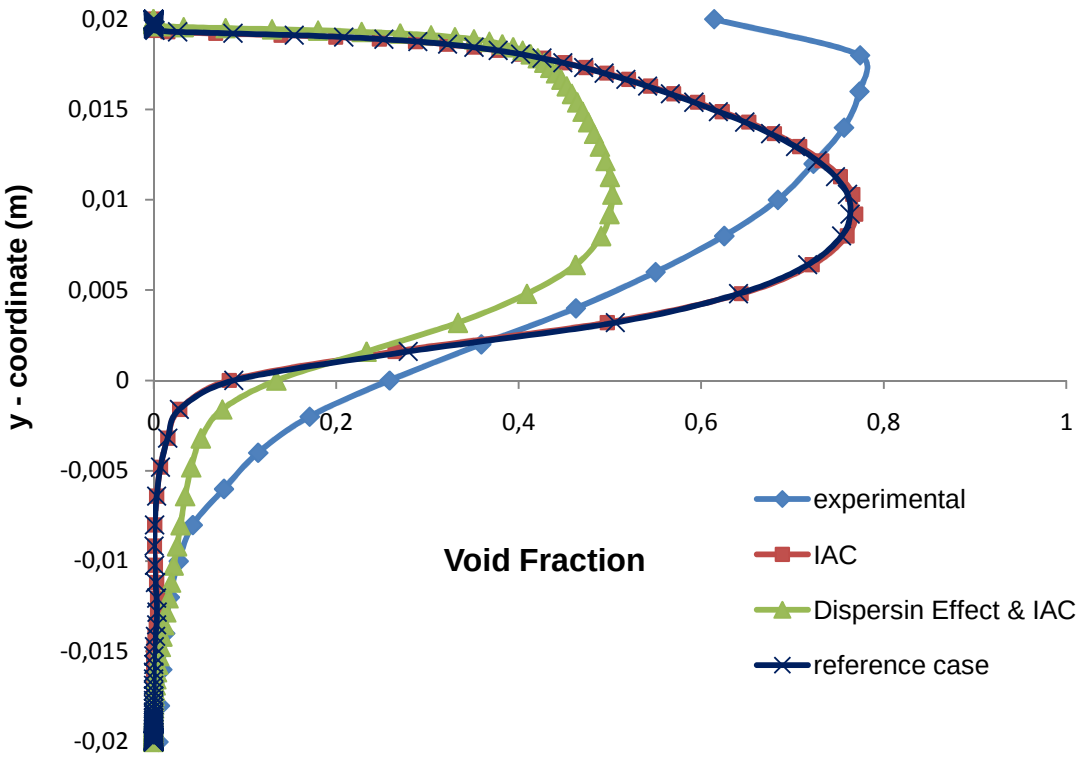

Figure 4.57. Comparison of void fraction profiles in position 2

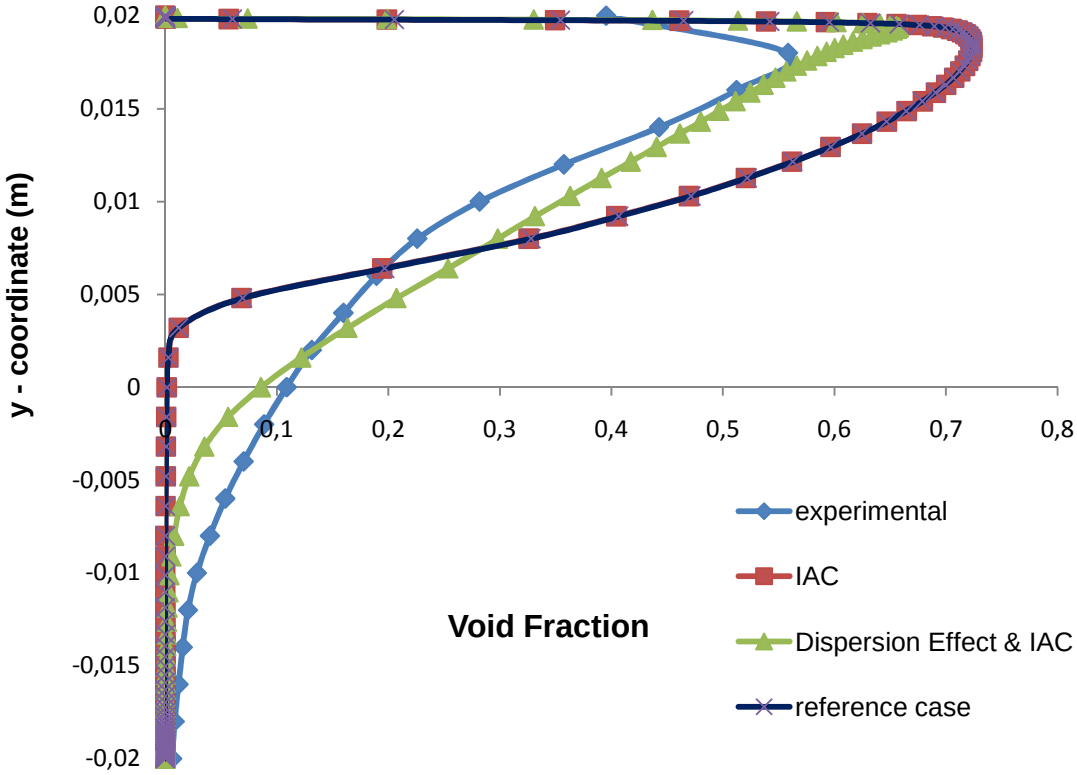

Figure 4.58. Comparison of void fraction profiles in position 3

First of all, as one can see from the figures, there are not any differences between reference case and IAC model only. On the other hand, IAC model with "momentum dispersion effect" predicted more accurate results in terms of bubble stratification. Figure 5.48 shows almost perfect match. However the case under estimated the void profile at position 2.

4.6.2 Comparison of Different IAC Models

FLUENT has different options for coalescence and break-up kernel in the IAC model. As mentioned before, these are "Hibiki-Ishii" and "Ishii-Kim" models. In this part of the study, main objective is investigate to effect of different IAC kernel options on void fraction profile and predicted bubble diameter. There are three different cases modeled. Main parameters and choose of different kernel are shown below:

Q_{water} = 3 x 10^{-3} m³/s, U_{∞} = 5.3 m/s

Q_{air} = 4.8 x 10^{-4} m³/s α = 13.88 %

Inlet IAC concentration = 555 (1/m)

IAC Parameters are;

Min. Diameter = 0.0001 m

Max. Diameter = 0.01 and

Case 1 / Ishi-Kim: Both kernel were chosen as Ishii & Kim assumption

Case 2 / Hibiki-Ishii-Kim: Coalescence kernel was chosen as Hibiki & Ishii. Break-up kernel was chosen as Ishii & Kim.

Case 3 / Hibiki – Ishii: Both kernel were chosen as Ishii & Kim assumption

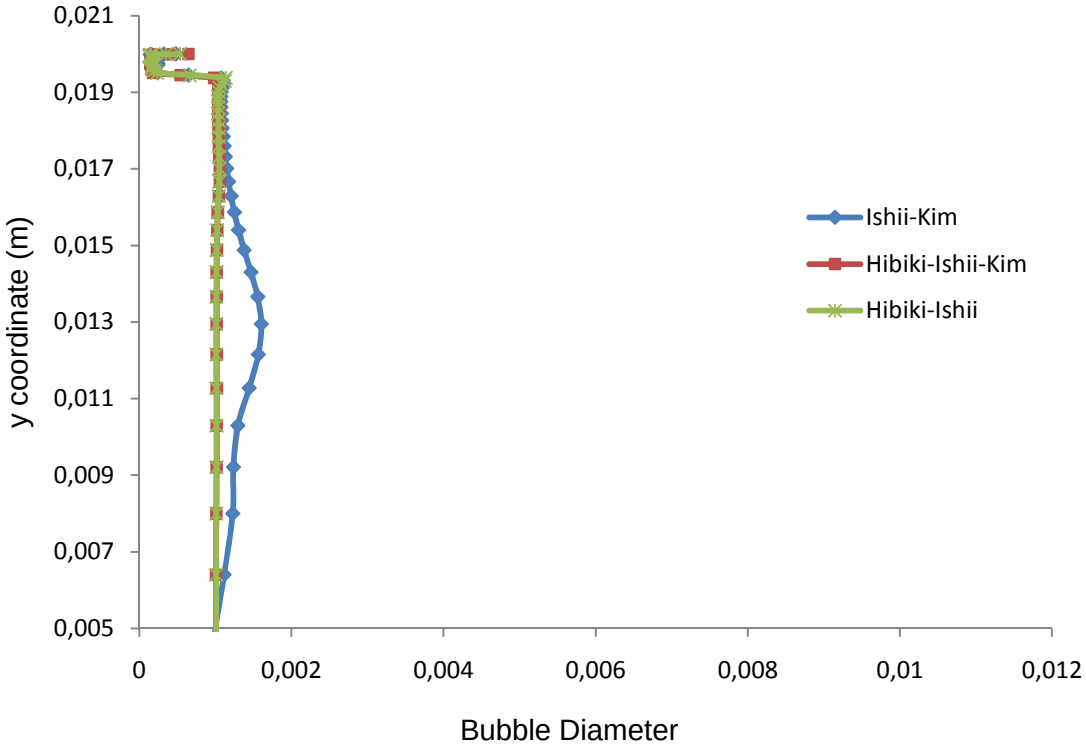

Figure 4.59. Comparison of bubble diameters at position 2

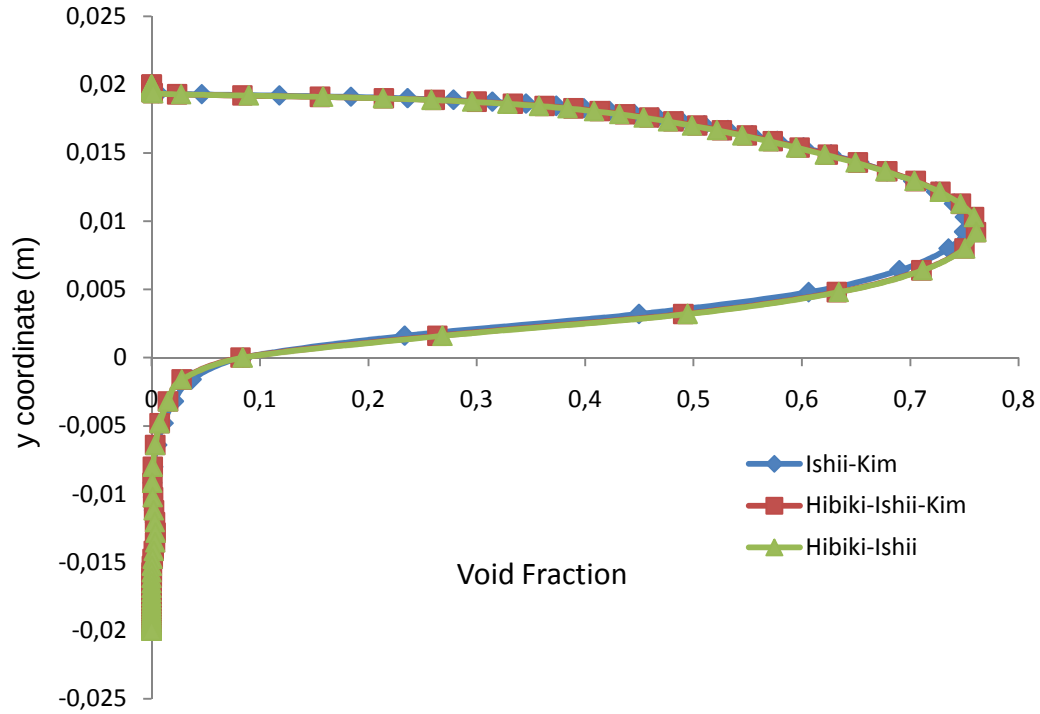

Figure 4.60. Comparison of void fraction profiles at position 2

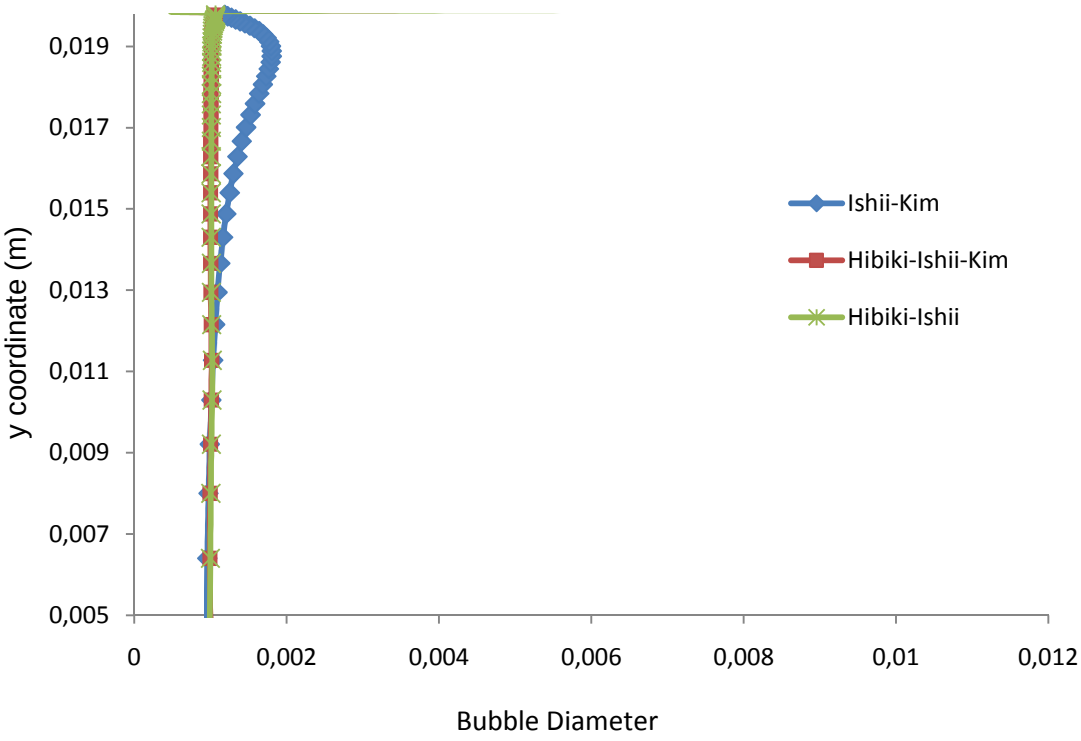

Figure 4.61. Comparison of bubble diameters at position 3

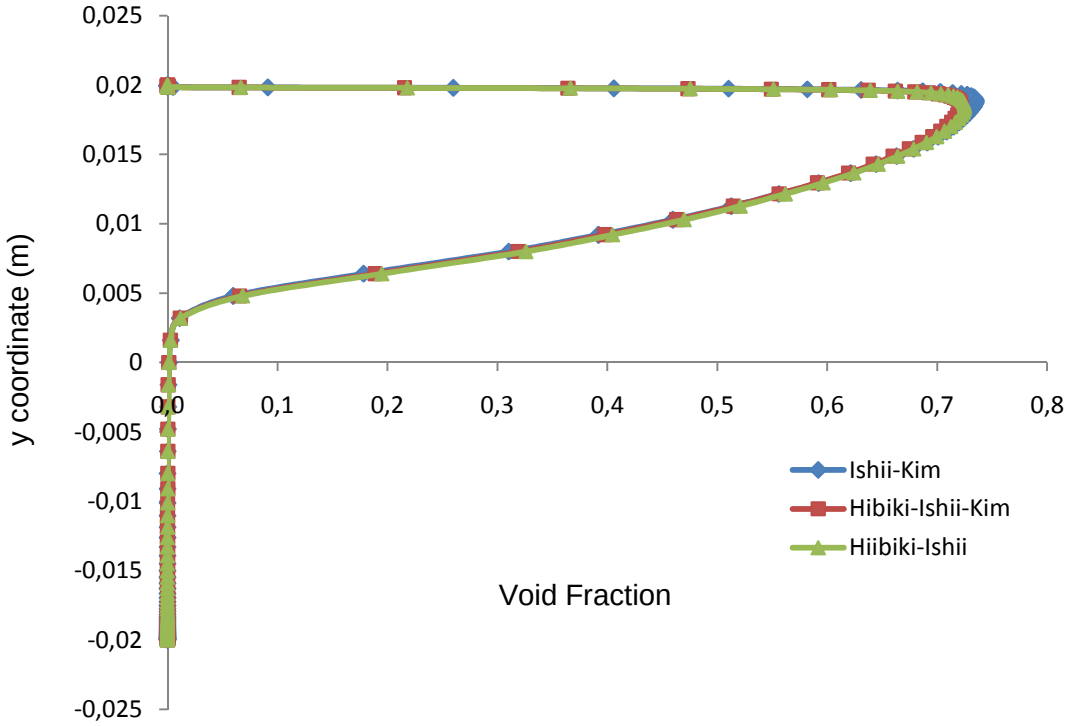

Figure 4.62. Comparison of void fraction profiles at position 3

There are not any differences in terms of void fractions. As we can see from Figures 4.60 and 4.62 there is no void below y-coordinate = 0.005.For this reason Figures 4.59 and 4.61 don't show this region. So there is only minor difference between "Ishii-Kim" and others.

4.6.3 Comparison of Different Bubble Diameters at the Inlet

During setting of IAC parameters, area concentration at the inlet boundary is an essential parameter which could manipulate bubble diameter in an indirect way. For this reason, this parameter was investigated as well. Two different concentrations were calculated in accordance with 2D and 3D analysis of the inlet boundary. "Hibiki and Ishii" model is used for both kernels. The only difference between them is a constant in front of bubble diameter in formulation. Some figures which are chosen to show the results are presented here;

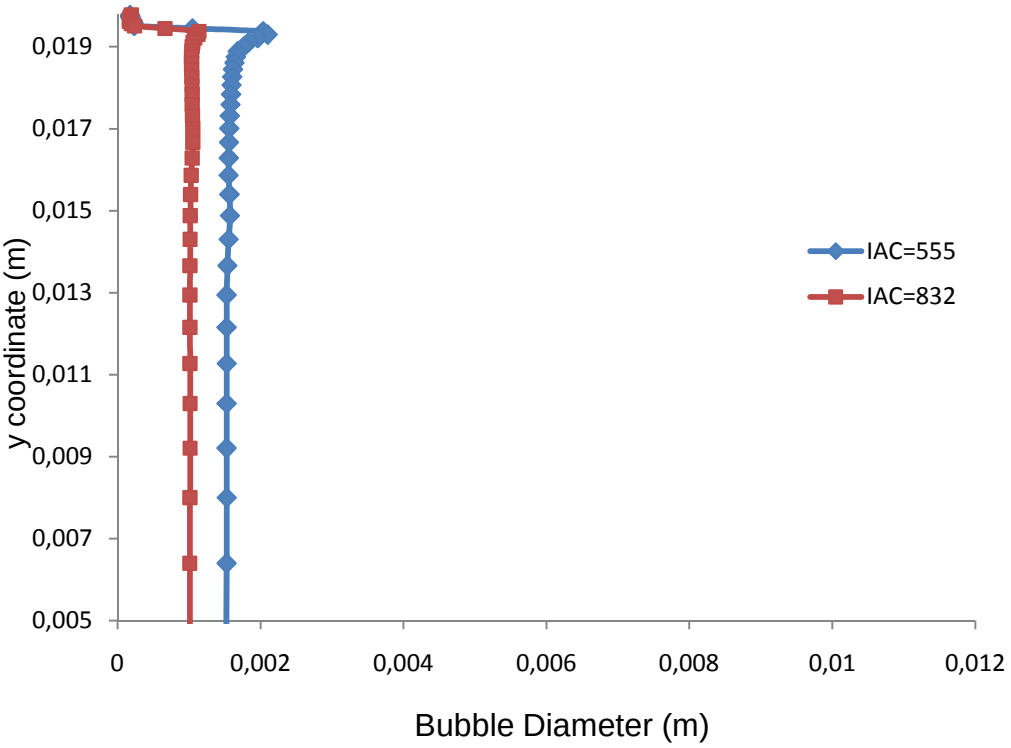

Figure 4.63. Comparison of bubble diameters for Hibiki- Ishii Model at position 2

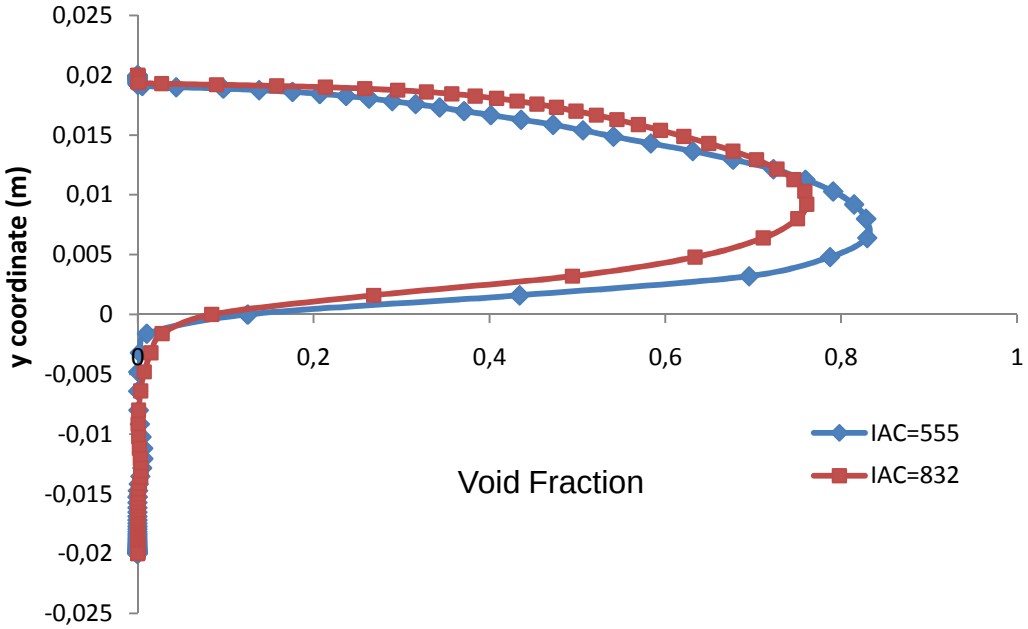

Figure 4.64. Comparison of void fraction profiles for Hibiki- Ishii Model at position 2

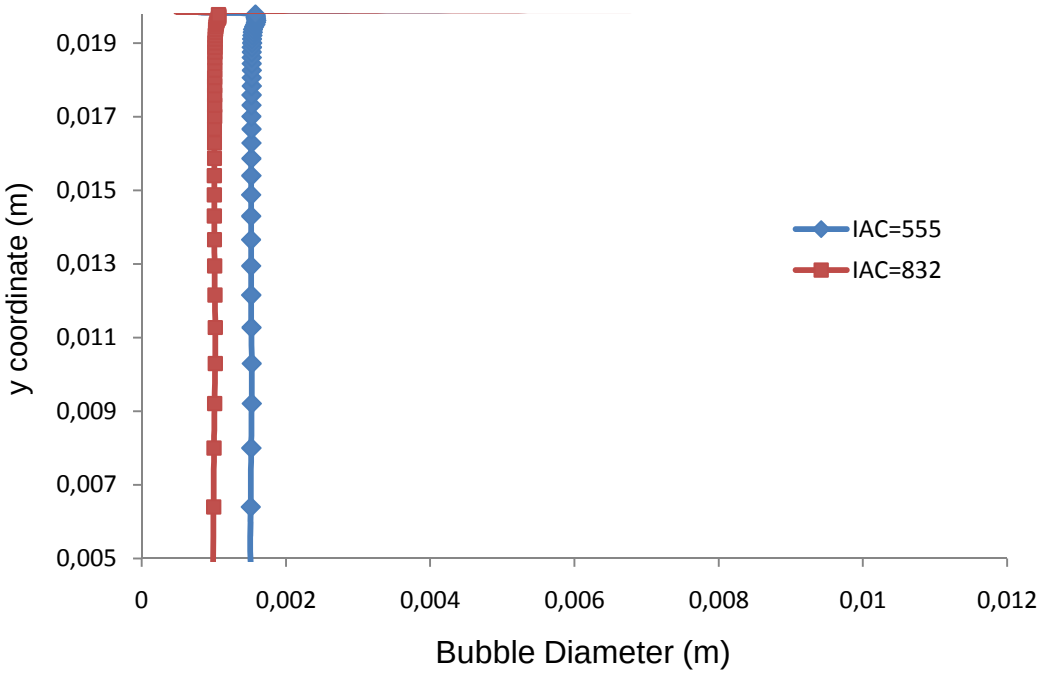

Figure 4.65. Comparison of bubble diameters for Hibiki- Ishii Model at position 3

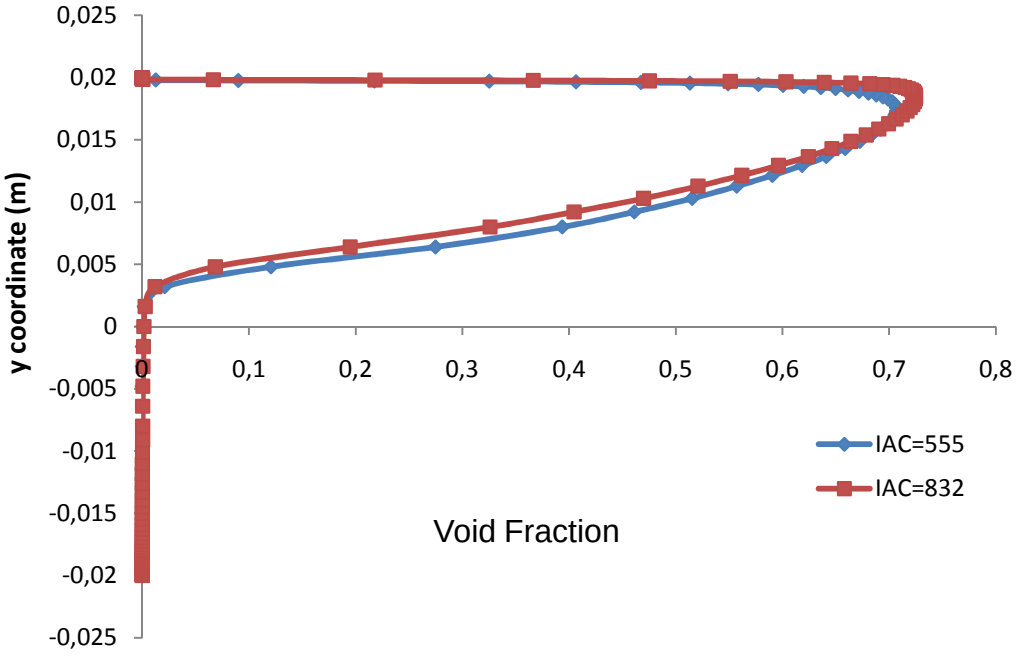

Figure 4.66. Comparison of void fraction profiles for Hibiki- Ishii Model at position 3

As it can be seen from figures, bubble diameter increased with same ratio as in decrease of IAC for the same void fraction at the inlet. Results are consistent with the previous results which were shown in Figure 4.43 and 4.46. Therefore it can be concluded that it is an important parameter to predict void fraction distribution as well.

5. CONCLUSION and FUTURE WORKS

Two-fluid model is the most complex numerical solution method for the two-phase flow modeling. There is nonlinear dependency between inter phase terms and slip velocity (as in the expansion zone). Therefore interfacial momentum transfer terms are used in coupling the balance equations. Drag and lift forces are two of these terms. Because of this complex and non-linear nature, convergence of the model is difficult when it is compared with other two phase models. This is the main disadvantage of the model in terms of computational effort and time management. However if realistic solutions are desired it is the only choice.

In the study, model is tested in several conditions using different flow parameters. An important flow parameter is diameter of the discrete phase. In this study, it is bubble diameter. Different bubble diameters have been studied and it is concluded that the bubble diameter effect on simulations is significant. There are different options of FLUENT for specification of bubble diameter in simulations. In the study, constant bubble diameter was chosen for this specification. Doing this, mechanism of bubble coalescence, grow up and break up were not taken into our account. It is important, since the mechanisms of diameter change were not simulated with proper models. Therefore, the real flow area especially for liquid phase and static pressure recovery inside of the expansion is not taken into account. As it can be seen from the results reported in sections 4.2.1 and 4.3, the static pressure recoveries depend on this parameter. However, still it can be concluded that if reasonable value is used for bubble diameter, the model can present good agreement with the experimental data even with constant bubble diameter.

The results presented in section 4.2.2 show the effect of low velocities in divergent channels. Low velocities lead the bubbles to escape more easily to the upper part of the channel. So this type of operation conditions and their bubble collection phenomena should be controlled before the design of these types of pipes. In many cases, these types of flow conditions are not desired.

For the analysis performed in this study to model turbulence, “Reynolds Stress Turbulence Model” was preferred. For the cases like investigated in this study, highly anisotropic flow conditions prevent using general “k – e “turbulence models. RSM is the only choice in reality. However, one simulation was carried out to see the ability of two-equation turbulence models like k - e. Results are consistent with theoretical expectations. Another way to try this could be using an unsteady solution and it can be subject of another study. On the other hand, there are examples of the modified “k – e” turbulence model in this type of flow conditions. In these modifications, proper source terms should be added to model equations. For this type of modification, reference [21] could be a simple example. In this way or with other options of ” RSM”, one may present the separation region after the expansion of pipe and get the good agreement between the experimental data and numerical results for the case of validation study with void fraction profiles. In literature there are some ways presented to use two equation models. One way is taking into account the bubble induced turbulence on the flow. Modification on turbulent viscosity or writing source terms for “k” and “e” equations are options to do that. In the future these could be tested.

Using “Pressure Outlet” boundary is an obligation when the simulations are performed using two-fluid approach. On the other hand, during early period of the study, time and computational opportunities did not give an opportunity to handle this problem. In addition “Outflow” boundary was chosen as the best alternative. Extension of the pipe made it possible to use “Pressure Outlet” in this study. This phenomenon was also investigated in the study. Results show consistency. It can be concluded that the “Outflow” boundary condition could be used as boundary condition in this type of two phase simulations.

Section 4.6 is the part of the study which investigated effects of “IAC” and “Dispersion on momentum”. IAC is an important parameter for two - phase flow modeling. Results show no big difference with IAC but it still needs more attention and future works. More studies can be carried out with different bubble diameters.

Last thing it should be mentioned is the “Lift force” in the momentum equation. Generally, its magnitude is smaller than the magnitude of the drag force. Because of this, it can be omitted. During the study, this term is neglected. However, it is important especially if phases separate from each other fast. Because of the fact that there is strong separation before and after the expansion of pipe, it is concluded that the contribution of this term should be taken into account. However the modeling this force causes problems in terms of convergence. Especially in the validation study with void fraction data, modeling of this force was tested using the existent models by using several lift coefficients. However simulation cases could not convergence. Therefore results are not presented here.

As a final conclusion, two-fluid approach can predict static pressure recovery in good agreement with the experimental data. Moreover, the capability of the model can be improved by modification over the turbulence model and changing mechanism of bubble diameter and also adding other interfacial terms. Present works on modeling of two phase flows are still generally experimental. However, with modeling improvements, commercial CFD codes could be used in the design of these types of pipe and singularities.

REFERENCES

[1] ”Numerical Simulation of Bubbly Flow in Singular Geometries” B.Kılınç – *DC Project Report 2009-15*

[2] http://www.flowserve.com

[3] M. L. Riethmuller J. M. Delhaye, M. Giot. “Thermohydralics of Two- Phase Systems for Industrial Design and Nuclear Engineering” Hemisphere Publishing Corporation and McGraw-Hill Book Company, New-York, *1981*

[4] N.E. Todreas M.S. Kazimi “Nuclear Systems I”

[5] G. E. Alves. Co-current liquid-gas flow in a pipeline contactor. *Chem.Eng. Prog., 50:449{456, 1954.*

[6] Y. Taitel and A. E. Dukler. A model of predicting flow regime transitions in horizontal and near horizontal gas-liquid flow. *AIChE J., 22:47{55,1976}*

[7] “Modeling of pressure drop in two-phase flow within expansion geometries” V.G. Kourakos, P.Ramboud, S.Chabane, J.M.Buchlin. *6th International Symposium on Multiphase Flow, Heat Mass Transfer and Energy Conversion Paper No. MN-30 Xi’an China, July 2009*

[8] B.R. Munson, D.F. Young, T. H. Okiishi “Fundamentals of Fluid Mechanics” 5th. Edition

[9] “Friction Factors for Pipe Flow” Lewis F. Moody, Transactions of the A.S.M.E., November 1944

[10] Theoretical Guide of Fluent 12.0

[11] “Evaluation of Computational Fluid Dynamic Methods for Reactor Safety Analysis / Review of two-phase modeling capabilities of CFD computer codes

and feasibility of transient simulations" *EUROPEAN COMMISSION, February-2004*

[12] "Application of General Constitutive Principles to the Derivation of Multidimensional Two-Phase Flow Equations" D.A. Drew, R.T. Lahey *Int. J. Multiphase Flow(1979), Vol. 5 pp. 243-264*

[13] "Micro Four-Sensor Probe Measurement of Interfacial Area Transport for Bubbly Flow in Round Pipes." M. Ishii and S. Kim.Nuclear Engineering and Design, 205:123-131, 2001.

[14] "One-group Interfacial Area Transport of Bubbly Flows in Vertical Round Tubes." T. Hibiki and M. Ishii. International Journal of Heat and Mass Transfer, 43:2711-2726, 2000.

[15] "One-group Interfacial Area Transport in Vertical Bubbly Flow." S.Kim Q.Wu and M.Ishii. International Journal of Heat and Mass Transfer, 41:1103-1112, 1997.

[16] "Micro Four-Sensor Probe Measurement of Interfacial Area Transport for Bubbly Flow in Round Pipes." M. Ishii and S. Kim. Nuclear Engineering and Design, 205:123-131, 2001.

[17] FLUENT 6.3. Documentation, User's Guide

[18]" Investigation of the void fraction, bubble size and velocities in divergence geometry" Vasilios Kourakos, Emrah Deniz, Patrick Rambaud, Said Chabane and Jean-Marie Buchlin. 7th International Conference on Multiphase Flow ICMF 2010, Tampa, FL USA, May 30-June 4, 2010

[19] " Modeling of pressure drop in two-phase flow within expansion geometries" V. G. Kourakos, P. Rambaud, S. Chabane J. M. Buchlin *6th International Symposium on Multiphase Flow, Heat Mass Transfer and Energy Conversion Xi'an, China, 11-15 July 2009* Paper No. MN-30

[20] “CFD Analysis of Two Phase Flow in a Horizontal Pipe-Prediction of Pressure Drop” P.Bhramara, V.D. Rao, K.V. Sharma, and T.K.K. Reddy. International Journal of Mechanical, Industrial and Aerospace Engineering 3:2 2009

[21] “Gas–liquid Flow in a 2D column: Comparison between experimental data and CFD modeling” Peter Spicka , Madalena M. Dias, Jose Carlos B. Lopes *Chemical Engineering Science – 2001.*

APPENDIX

An example of the “C” programming code for Inlet velocity profile:

```
#include "udf.h"

DEFINE_PROFILE(inlet_velocity, thread, index)
{
real x[ND_ND];
real z;
real y;
real U;
real R;

face_t f;

begin_f_loop(f, thread)
{
F_CENTROID(x,f,thread);
y=x[1];
z = x[2];
U = 5.119;
R = 0.016;
F_PROFILE(f, thread, index) = U*pow((1-(sqrt(y*y+z*z)/R)),0.14285);
}
end_f_loop(f, thread)
}
```

CURRICULUM VITAE

Surname, Name : KILINÇ Buğra

Place of Birth : ANKARA - TURKEY

Date of Birth : May 12, 1982

Marital Status : Single

Education

High School 199 - 1999

BS 2001 - 2006

Foreign Language : English

Work Experience

2007 – 2010 : Nuclear Engineer at Ministry of Energy and Natural Resources

2010 – Present : Nuclear Engineer at Turkish Atomic Energy Authority